RES | THE SCHOOL for RENEWABLE ENERGY SCIENCE

Hydraulic transient model developed and tested for Karahnjukar Hydroelectric Project with possible applications in Poland

Adam Narozniak

UNIVERSITY OF ICELAND

University of Akureyri

eea grants
iceland liechtenstein norway

PROJEKT PL0460

Hydraulic transient model developed and tested for Karahnjukar Hydroelectric Project with possible applications in Poland

Adam Narozniak

A 30 ECTS credit units Master´s thesis

Supervisors
Mr. Þorbergur S. Leifsson
Dr. Gunnar G. Tomasson

A Master´s thesis done at
RES | The School for Renewable Energy Science
in affiliation with
University of Iceland &
University of Akureyri

Akureyri, February 2011

Hydraulic transient model developed and tested for Karahnjukar Hydroelectric Project with possible applications in Poland

A 30 ECTS credit units Master´s thesis

RES | The School for Renewable Energy Science

Solborg at Nordurslod

IS600 Akureyri, Iceland

Telephone + 354 464 0100

www.res.is

Printed in 28.01.2011

at Stell Printing in Akureyri, Iceland

ABSTRACT

Karahnjukar Hydroelectric Project is an underground hydroelectric scheme in eastern Iceland. The characteristic feature of the powerplant is an extensive waterway system (total length of tunnels over 65 [km]) with complex flow phenomena including overspill and free surface flow.

Tunnel Element concept was introduced and tested on 4 representative powerplant trips showing good correlation between calculations and measurements. Next, various flow patterns were analyzed for a set of powerplant discharge profiles from design regime. The calculations were used for plotting Operating Curves, beneficial for safe HEP operation.

Introduced Tunnel Element concept turned out as a suitable way for complex waterway systems modeling. Although vast limitations, the method is promising and gives a base for further studies on leakage and dangerous operation regimes of powerplant.

Investigation showed that Polish Oil and Gas industry would be the most interested in Tunnel Element method development.

TABLE OF CONTENTS

Contents

Table of contents..... 6
List of figures..... 8
List of tables..... 11
Notation..... 12
1 Introduction..... 13
1.1 Research goals..... 16
1.2 State of the art..... 16
1.3 Research methodology..... 17
1.4 Anticipated research outcomes/results..... 17
2 Tunnel Element concept..... 18
2.1 Tunnel Element equations derivation..... 20
2.2 Linear interpolation between two known points..... 23
2.3 Integration – trapezoidal rule..... 23
2.4 Joints..... 24
2.5 Overspill..... 25
2.6 Throttle..... 26
2.7 Variable Surface Area tunnels modelling..... 26
2.8 Leakage..... 27
3 Karahnjukar Model details..... 28
3.1 Headrace Tunnel and Halslon Reservoir..... 29
3.2 Holsufs Surge Shaft..... 30
3.3 Midfell Surge Tunnel..... 32
3.4 Jokulsa Tunnel and Jokulsa Surge Tunnel..... 33
3.5 Energy Dissipater..... 36
3.6 Inverted Siphon..... 37
3.7 Jokulsa Intake Collector..... 38
4 Equations system..... 41
4.1 Model limitations due to simplifications……..... 45
5 Matlab solution method..... 46
5.1 Pre-processor..... 47
5.2 Solver..... 47
5.3 Post-processor..... 48
6

6 Comparison of calculations and measurements..... 49
6.1 Influence of leakage on the flow..... 53
6.2 The power plant trip at 18.12.2010..... 55
6.3 The power plant trip at 11.08.2009..... 60
6.4 The power plant trip at 09.04.2008..... 64
6.5 The power plant trip at 12.13.2007..... 67
7 Implementation of tunnel element method in Poland..... 71
8 Operating curves..... 74
8.1 Highest surge level in Holsufs Surge Shaft 75
8.2 Highest surge level in Midfell Surge Tunnel..... 78
8.3 Maximal discharge to Jokulsa Tunnel..... 80
8.4 Highest surge level in Jokulsa Tunnel/Jokulsa Surge Tunnel..... 82
8.5 Highest surge level in Ufsarlon Intake Collector..... 84
8.6 Maximal backflow to Ufsarlon Pond..... 85
9 Conclusions..... 86
10 Future development..... 86
11 Bibliography..... 87
Appendix 1 Model formulation scheme…… A-1
Appendix 2 Upper Joulsa Tunnel Surge development for Halslon Reservoir 600 [m a.s.l.] and Jokulsa Tunnel Discharge 80 [m3/s]……. A-2
Appendix 3 Upper Joulsa Tunnel Surge development for Halslon Reservoir 625 [m a.s.l.] and Jokulsa Tunnel Discharge 10 [m3/s]……. A-3

LIST OF FIGURES

Figure 1.1	Karahnjukar HEP, aluminium smelter and transmission lines.....	13
Figure 1.2	Schematic longitudinal section through the waterways, and a plan on the inserted picture (vertical scale extended 20 times).....	14
Figure 1.3	Longitudinal profile of the Jokulsa Tunnel (vertical scale enlarged 10 times).....	15
Figure 1.4	Comparison of water oscillations in Holsufs Surge Shaft calculated in AHYTRA [1] with measured and modelled by the basic version of Karahnjukar Transient Flow Model……	17
Figure 2.1	Tunnel Element scheme.....	19
Figure 2.2	Tunnel Element geometry functions.....	21
Figure 2.3	Tunnel Element head loss functions derivation.....	22
Figure 2.4	Linear Interpolation between two known points.....	23
Figure 2.5	The Trapezoidal Rule.....	24
Figure 2.6	Joint scheme.....	24
Figure 2.7	Spill function.....	25
Figure 2.8a	Flow through gate opening.....	25
Figure 2.8b	Flow over Spillway crest.....	25
Figure 2.9	Local Loss Coefficient Function.....	26
Figure 2.10	Variable area tunnel modelled by tunnel elements.....	26
Figure 2.11	Pressure and leakage distribution along TE.....	27
Figure 3.1a	Karahnjukar HEP Scheme……	28
Figure 3.1b	Karahnjukar Model Scheme…….....	28
Figure 3.2	Surface structure of Holsufs Surge Shaft and a section.....	30
Figure 3.3	profile along Surge Tunnel.....	32
Figure 3.4	Midfell Surge Tunnel cumulative volume and Effective Area.....	33
Figure 3.5	Jokulsa Tunnel Scheme.....	33
Figure 3.6	Jokulsa Surge Tunnel and canal plan view.....	34
Figure 3.7	Jokulsa Tunnel cumulative volume and Effective Area.....	34
Figure 3.8	Jokulsa Surge Tunnel cumulative volume and Effective Area.....	35
Figure 3.9	Plan and section through Energy Dissipater.....	36
Figure 3.10	Jokulsa Tunnel – Inverted Siphon Junction model (El.1 = 608 m a.s.l)..	37
Figure 3.11a	Definition sketch for Ufsarlon Intake with partly closed gate, ice skimming wall and trashracks.....	38
Figure 3.11b	Intake Collector and anti-vortex cross for flow straightening (four	39

	cross-beams are for structural purposes).....	
Figure 3.12	Effective area change for each element.....	39
Figure 3.13	Jokulsa Collector model and Spill function……..	40
Figure 4.1	Schematic to the system for different cases…….	41
Figure 5.1	Data flow between the subprograms; Colour key from table 5.1.....	46
Figure 6.1	Holsufs Surge Shaft and Midfell Surge Tunnel Pressure Meters……..	49
Figure 6.2	Jokulsa Valve Chamber.....	50
Figure 6.3	Holsufs Surge Shaft Pressure Meter.....	50
Figure 6.4	Ufsarlon Intake Pressure Meter localization.....	51
Figure 6.5	Jokulsa Surge Tunnel.....	51
Figure 6.6	Fitting evaluation for case 04.09.2008 – Penstock Valve Chamber.....	53
Figure 6.7	Outflow from the system due to leakage; case 09.04.2008…….	54
Figure 6.8	Penstock Valve Chamber pressure comparison; case 18.12.2010…….	55
Figure 6.9	Penstock Valve Chamber pressure comparison; case 18.12.2010.…	56
Figure 6.10	Plugs pressure comparison; case 18.12.2010…….…….	56
Figure 6.11	Plugs pressure comparison; case 18.12.2010……	57
Figure 6.12	Jokulsa Tunnel Discharge comparison; case 18.12.2010……	57
Figure 6.13	Air Vent pressure comparison; case 18.12.2010……..	58
Figure 6.14a	Water level comparison; case 18.12.2010……	58
Figure 6.14b	Water level comparison; case 18.12.2010…….	59
Figure 6.15	Outflow from the system due to leakage; case 18.12.2010…….	59
Figure 6.16a	Penstock Valve Chamber pressure comparison; case 11.08.2009…..	60
Figure 6.16b	Penstock Valve Chamber pressure comparison; case 11.08.2009….	61
Figure 6.17	Jokulsa Tunnel Discharge comparison; case 11.08.2009 ……	61
Figure 6.17	Jokulsa Tunnel Discharge comparison; case 11.08.2009…….	61
Figure 6.18	Air Vent pressure comparison; case 11.08.2009……	62
Figure 6.19	Water level comparison; case 11.08.2009……	62
Figure 6.20	Outflow from the system due to leakage; case 11.08.2009……	63
Figure 6.21a	Penstock Valve Chamber pressure comparison; case 09.04.2008…..	64
Figure 6.21b	Penstock Valve Chamber pressure comparison; case 09.04.2008…..	65
Figure 6.22	Air Vent pressure comparison; case 09.04.2008……..	65
Figure 6.23	Holsufs Surge Shaft water level comparison; case 09.04.2008……..	66
Figure 6.24	Outflow from the system due to leakage; case 09.04.2008…….	66
Figure 6.25a	Penstock Valve Chamber pressure comparison; case 13.12.2007…..	67
Figure 6.25a	Penstock Valve Chamber pressure comparison; case 13.12.2007…..	68

Figure 6.26	Air Vent pressure comparison; case 13.12.2007……	68
Figure 6.27	VSS and VST pressure comparison; case 13.12.2007……..	69
Figure 6.28	Outflow from the system due to leakage; case 13.12.2007……	70
Figure 7.1	Hydropowerplants localization in Poland.....	71
Figure 7.2	Examples of Hydroelectric projects in Poland…….	73
Figure 8.1	Powerplant discharge profile.....	74
Figure 8.2	Maximal water level in HSS; Halslon Reservoir 575[m a.s.l.] …….	75
Figure 8.3	Maximal water level in HSS; Halslon Reservoir 600 [m a.s.l.]…….	76
Figure 8.4	Maximal HSS Spill Volume; Halslon Reservoir 600 [m a.s.l.]…….	76
Figure 8.5	Maximal water level in HSS; Halslon Reservoir 625 [m a.s.l.]…….	77
Figure 8.6	Maximal HSS Spill Volume; Halslon Reservoir 625 [m a.s.l.]…….	77
Figure 8.7	Maximal water level in MST; Halslon Reservoir 575 [m a.s.l.]……	78
Figure 8.8	Maximal water level in MST; Halslon Reservoir 600 [m a.s.l.]……	78
Figure 8.9	Maximal water level in MST; Halslon Reservoir 625 [m a.s.l.]……	79
Figure 8.10	Maximal discharge to Jokulsa Tunnel; Halslon Reservoir 575 [m a.s.l.]	80
Figure 8.11	Maximal discharge to Jokulsa Tunnel; Halslon Reservoir 600 [m a.s.l.]	80
Figure 8.12	Maximal discharge to Jokulsa Tunnel; Halslon Reservoir 625 [m a.s.l.]	81
Figure 8.13	Maximal water level in JT/JST; Halslon Reservoir 575 [m a.s.l.]…….	82
Figure 8.14	Maximal water level in JT/JST; Halslon Reservoir 610 [m a.s.l.]……	82
Figure 8.15	Maximal water level in JT/JST; Halslon Reservoir 625 [m a.s.l.]…….	83
Figure 8.16	Maximal water level in UIC; Halslon Reservoir 600 [m a.s.l.]…….	84
Figure 8.17	Maximal water level in UIC; Halslon Reservoir 625 [m a.s.l.]…….	84
Figure 8.18	Maximal backflow to Ufsarlon Pond; Halslon Reservoir 625 [m a.s.l.]	85

LIST OF TABLES

Table 2.1	List of Tunnel Element parameters and variables.....	19
Table 3.1a	Headrace Tunnel data – Upstream of Jokulsa Tunnel.....	29
Table 3.1b	Headrace Tunnel data – Downstream of Jokulsa Tunnel.....	29
Table 3.3	Holsufs Surge Shaft data.....	31
Table 3.4	Midfell Surge Tunnel data.....	32
Table 3.5a	Jokulsa Tunnel data.....	35
Table 3.5b	Jokulsa Surge Tunnel data.....	35
Table 3.6	Energy Dissipater.....	36
Table 3.7	Inverted Siphon data.....	37
Table 3.8	Jokulsa Intake Collector data.....	39
Table. 4.1	Structure of equations system for each case.....	44
Table 5.1	KAR package.....	46
Table 5.2	ode15s solver settings.....	47
Table 6.1	Sensors characteristics.....	52
Table 6.2	Initial values for leakage test; 09.04.2008 case.....	53
Table 6.3	Initial values; 18.12.2010 case.....	55
Table 6.4	Initial values; 11.08.2009 case.....	60
Table 6.5	Initial values; 09.04.2008 case.....	64
Table 6.6	Initial values; 13.12.2007 case.....	67
Table 7.1	Largest hydroelectric projects in Poland.....	72
Table 8.1	Operating Curves Initial Vector parameters.....	74
Table 8.2	Jokulsa Discharge parameters.....	75

NOTATION

Abbreviation

HEP	Hydroelectric Project
HRT	Headrace Tunnel
HR	Halslon Reservoir
HSS	Holsufs Surge Shaft
MST	Midfell Surge Tunnel
JT	Jokulsa Tunnel
JST	Jokulsa Surge Tunnel
JIC	Jokulsa Intake Collector/ Ufsarlon Intake Collector
IS	Inverted Siphon
JVC	Jokulsa Valve Chamber
PVC	Penstock Valve Chamber
JSIJ	Jokulsa Tunnel – Jokulsa Surge Tunnel – Inverted Siphon Junction
TE	Tunnel Element
FTE	Free Surface Tunnel Element
PTE	Pressurized Tunnel Element

All symbols are stated in the text after their first use

1 INTRODUCTION

Karahnjukar Hydro Electric Project is a hydroelectric scheme in eastern Iceland (fig. 1.1) designed to produce 5 [TWh] annually for Alcoa's Fjardaal aluminium 75 [km] to the east in Reydarfjordur. The project, named after nearby Mount Karahnjukar, involves damming the Jokulsa a Dal River and the Jokulsa i Fljotsdal River with 6 dams, creating several reservoirs. Water from the reservoirs is then diverted through 53 [km] of underground water tunnels (fig 1.2) and down 420 [m] high vertical penstocks towards a single underground power station. The smelter became fully operational in 2008 and the hydro-power project was completed in 2009.

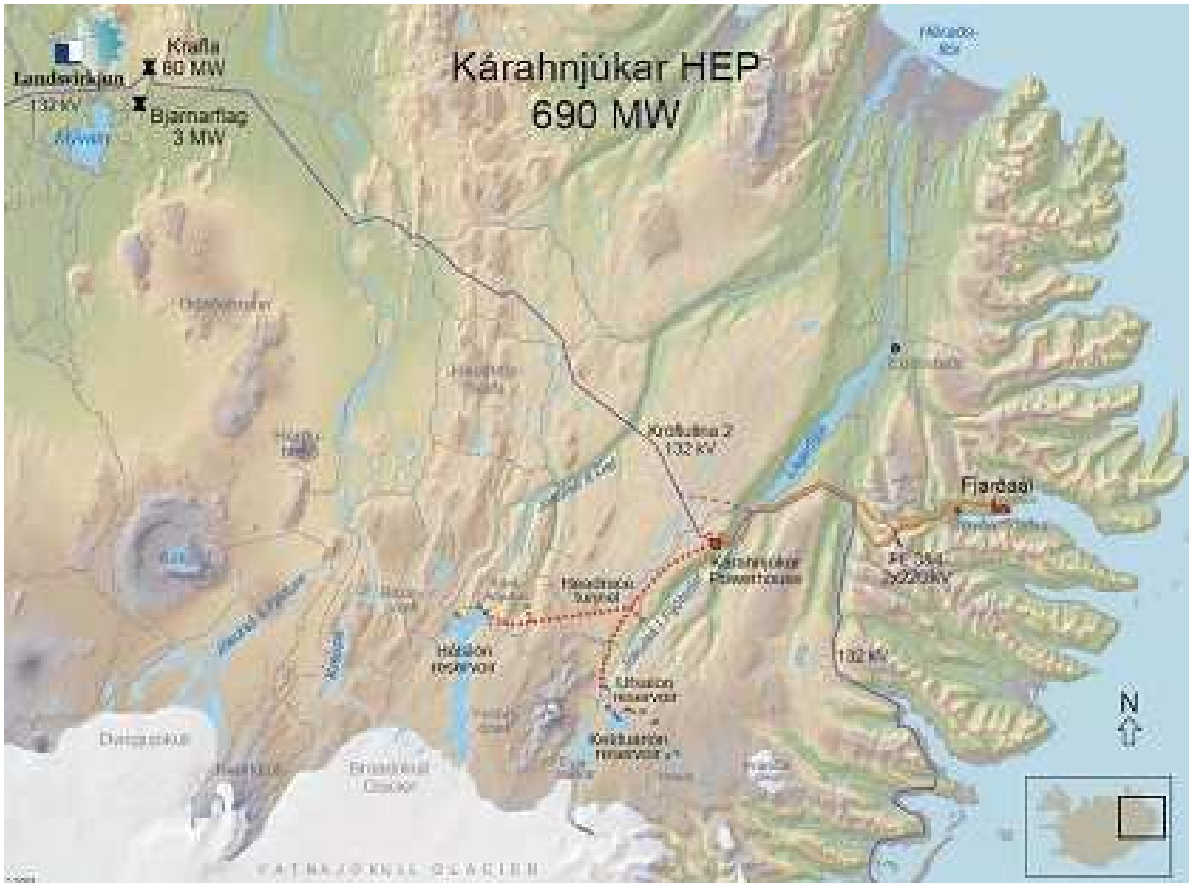

Figure 1.1 Karahnjukar HEP, aluminium smelter and transmission lines [5]

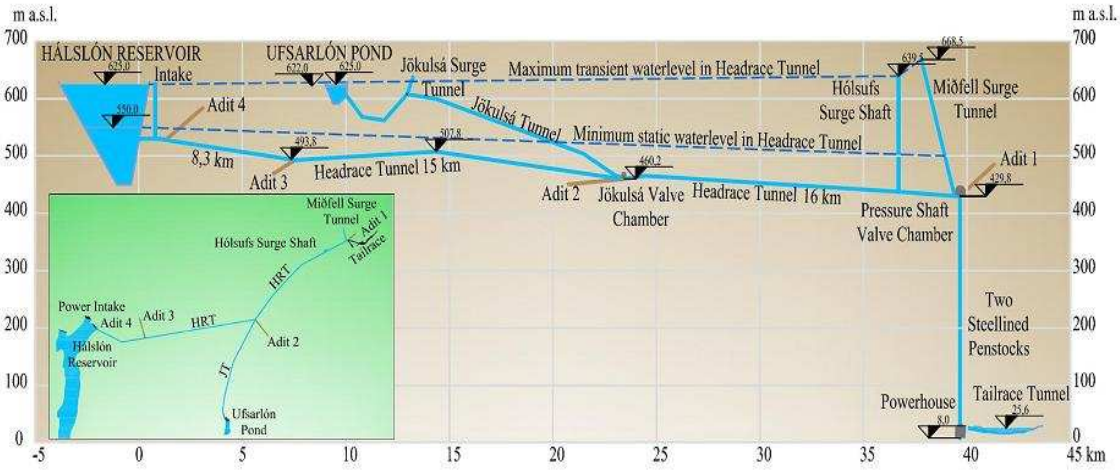

Figure 1.2 Schematic longitudinal section through the waterways, and a plan on the inserted picture (vertical scale extended 20 times)[5]

The Karahnjukar project has many uncommon features regarding transient flow.

Sloping Midfell Surge Tunnel

Due to topographical conditions the main surge facility is a 1650 [m] long tunnel sloping 12% to 16% from horizontal. In this exceptionally long surge tunnel the inertia and head loss cannot be neglected as is usually done for transient calculations of surge facilities in powerplants. Therefore, a standard commercial transient flow model cannot be used directly to accurately analyse this facility.

Additional Holsufs Surge Shaft

Due to the long surge tunnel a considerable part of the water hammer wave continues further up the headrace tunnel. A special vertical surge shaft was therefore added about 2.7 [km] upstream of the main surge tunnel, to protect the headrace tunnel upstream from the effect of a waterhammer wave. This surge shaft has an orifice inserted into it, allowing for extra dampening and water flows out of the system in case of a station trip. The maximum outflow discharge can be up to 70 [m^3/s].

Backflow in Jokulsa Tunnel

13.3 [km] long Jokulsa tunnel (fig. 1.3) is a diversion tunnel that connects, at about the midpoint, to the headrace tunnel . Due to complex hydraulic conditions, the tunnel can be both fully pressurised and have a free surface flow. During station trip a huge amount of water is pushed from the headrace tunnel into the Jokulsa Tunnel. In order to reduce the maximum backflow into the Jokulsa Tunnel a special asymmetric energy dissipater was installed close to the downstream end of the Jokulsa Tunnel. In some cases the backflow can fill up the free surface part of the Jokulsa tunnel up to the hydraulic control point, flow into the Jokulsa surge tunnel, and cause the water in the 3.0 [km] long inverted siphon to start to move backwards and fill up the Ufsarlon Intake Collector and eventually create flow out of the Ufsarlon Intake into the Ufsarlon pond. This normally happens long after

the trip has occurred typically during the second surge wave about 15 to 20 minutes after the trip. This special phenomena and the complex geometry associated with it, is not available in any commercially available surge modelling software and has to be specially built into a surge model.

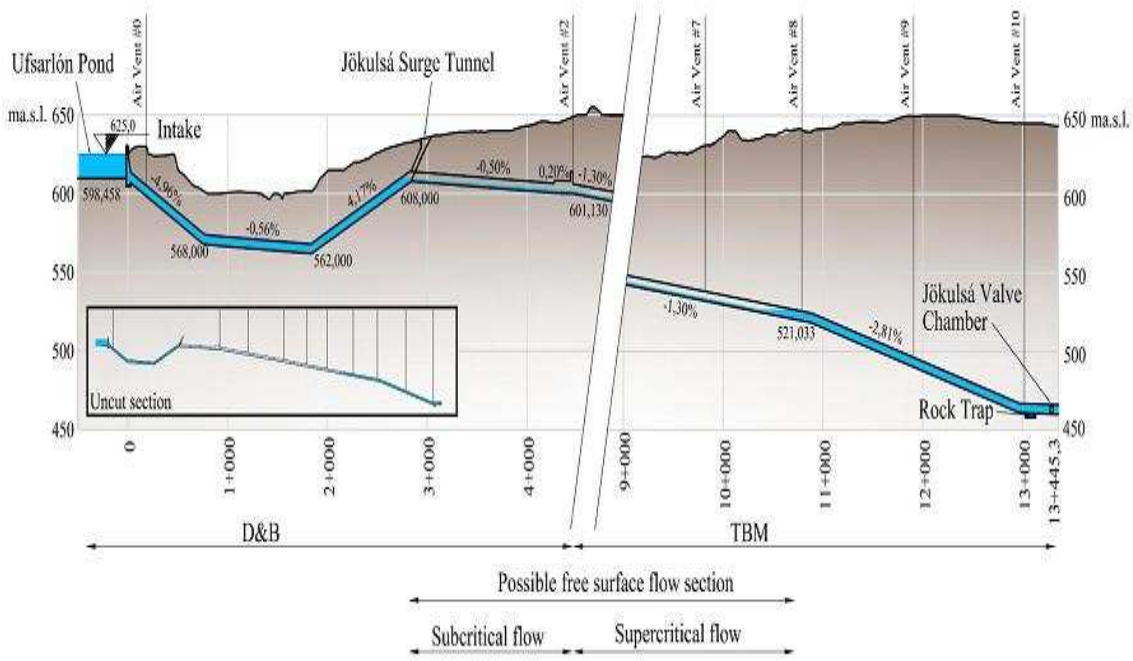

Figure 1.3 Longitudinal profile of the Jokulsa Tunnel (vertical scale enlarged 10 times) [5]

Large and leaky Headrace Tunnel system

The tunnel system in Karahnjukar is very long and large, dominated by unlined tunnels. The host rock is fractured and leakage in and out of the tunnel depends on the pressure differences between the water in the tunnel and the groundwater just around the tunnel. When the tunnel pressure increases more than 100 [m] within a few minutes the leakage can change significantly. This is generally not considered in transient calculations in HEP, but in Karahnjukar HEP this might significantly influence the transients.

When the transients in Karahnjukar were studied during design of the station with the aid of the AHYTRA[1] software, the model combined waterhammer, mass surge, turbine wicket gate manoeuvring and the rotational speed and inertia of the generator. This was necessary to evaluate the turbine design, closing speed of the wicket gates and the possible highest design pressure resulting from the waterhammering. Due to completeness of the model the setup, initializing and executing time of the model was rather long which resulted in a only limited number of cases that were simulated. The dominant and most commonly simulated cases were those for the most extreme cases.

The waterhammer and turbine characteristic do not significantly influence the mass surge after the first few seconds of a trip. To study all the special features of the HEP mentioned above, a model of only the mass surge upstream of the Penstock Valve Chamber.

1.1 Research goals

To build a mathematical model capable of simulating mass surges (without waterhammer) in the Karahnjukar HEP headrace tunnel system including fully the complex Jokulsa tunnel. The model will be tested with measured data from several station trips. Discrepancy between measured and calculated values will be investigated and explained and the model improved.

Finally the model will be used to develop several operating curves and information charts useful for operation of the station. Among others charts that show the following items during station trips as a function of station discharge and Halslon reservoir level.

1. Highest surge level in Holsufs Surge Shaft
2. Highest surge level in Midfell Surge Tunnel
3. Maximal backflow into Jokulsa Tunnel
4. Highest surge level in Jokulsa Tunnel and Jokulsa Surge Tunnel
5. Highest surge level in Ufsarlon Intake Collector
6. Maximal backflow to Ufsarlon Pond

1.2 State of the Art

The mathematical model and numerical tool AHYTRA [2] (Analysis of HYdraulic TRAnsients) developed by Electrowatt (now Pöyry), was used for the analysis of waterhammer and surges in the Karahnjukar HEP.

The program has been primarily designed to perform the numerical analysis for one-dimensional pressurized flow regimes in steady state and for transient conditions (ie. waterhammer, surges, column separation and other related occurrences). The program is based on a complete formulation of the momentum and continuity equations. It has been designed to handle a large variety of hydraulic networks characterized.

Computational procedures are based on the explicit Method of Characteristics for distributed system components using a specified space time grid and the use of a Newton-Raphson algorithm to solve a system of non-linear equations at nodes connecting 2 or more lumped and/or distributed elements at each computational time step. Further computations to determine other variables of component performance, in the form of numerical data, algebraic relations or differential equations are done separately within the component models at each computational time step.

Preliminary analysis of transients in a relatively simple case [1], where Jokulsa tunnel was closed, showed some discrepancy between measured and calculated values shown in figure 1.4

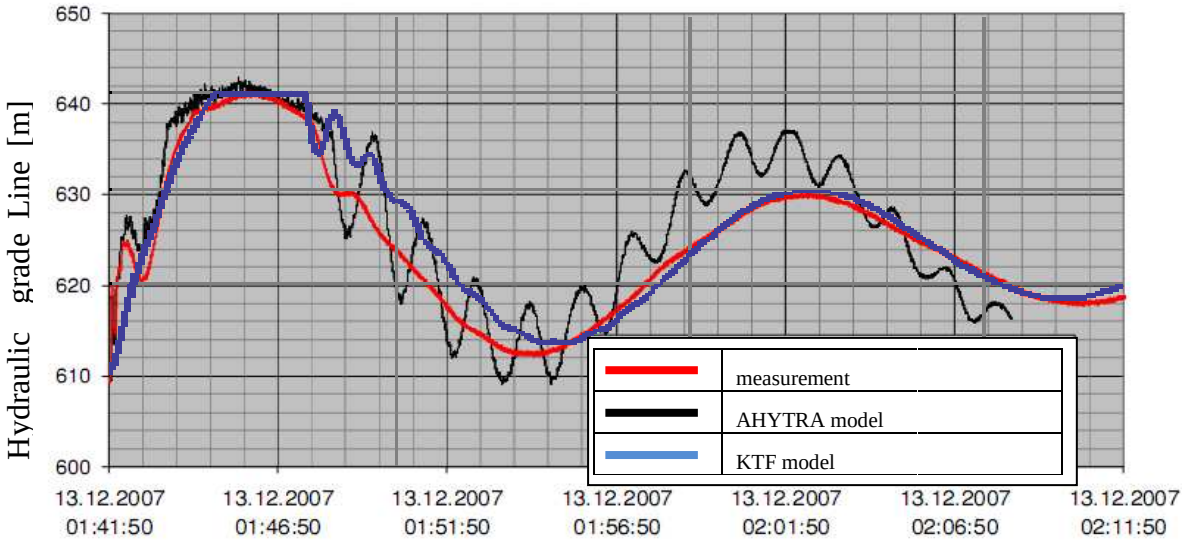

Figure 1.4 Comparison of water oscillations in Holsufs Surge Shaft calculated in AHYTRA [1] with measured and modelled by the basic version of Karahnjukar Transient Flow Model

Due to the complexity of the Karahnjukar tunnel system and abundance of flow phenomena, a particular model for the HEP mass surges needs to be set up. Preliminary calculations indicated that a simplified model may be successful in simulating the mass surges in the Karahnjukar system shown in figure 1.4.

1.3 Research Methodology

MATLAB is used for all calculations as the model requires formulating and solving a set of coupled, nonlinear, first order Differential Algebraic Equations (DAE). For simplification purposes, perfect fluid properties are applied and small terms are neglected.

Based on technical drawings of the Karahnjukar waterways, a geometric model is divided into characteristic sections (elements) where continuous flow parameters can be determined.

For each element a momentum and continuity equations, as well as boundary conditions (taking into account adjacent elements) are formulated and solved.

1.4 Anticipated Research Outcomes/Results

The research outcome is beneficial to understand better the physics of mass surges in the Karahnjukar headrace tunnel system and provide operation diagrams which are very valuable for the station operation. These results aid in knowing if it is safe to enter (for inspection or maintenance) the Ufsarlon intake, Jokulsa surge tunnel, the surge shaft without a chance of being reached by a surge.

Improved understanding through calculations of the surges within one of the most complicated waterway systems in the world is beneficial for the future modelling of transients within long ducts. This technique could also be applied to underground HEP, Oil and Gas and sewerage tunnels [3].

2 TUNNEL ELEMENT CONCEPT

Transient water flow

Changes in the discharge in waterways, caused by rapid valve closure, result in pressure surge which propagate along the pipeline from the source. If changes in the flow are gradual, the time variation of pressures and flow pattern can be achieved by assuming water incompressibility and neglecting the elastic properties of tunnels.

Since the origin of waterhammer and mass surge is different, it can be decoupled and consider separately [3].

The rapid deceleration of liquid column causes pressure surges having large pressure differences across the wave front. The speed of the pressure wave is dependent on the water compressibility and elasticity of tunnels. The speed of the wave is of order of magnitude 1000 [m/s] and is damped within several seconds after valve closure. Waterhammer is determined by geometry of the system. In general surge device should be as close to the source as possible to avoid propagation of the oscillations upstream the tunnel.

Mass surge is caused by change of inertia of the system and the life time of surge can last for several hours. Water oscillations period is determined by water mass within the system and the amplitude is determined by friction and the minor losses within tunnels. Number of surge devices has significant influence of surge pattern. Additional surge devices increase degrees of freedom of the system hence the general surge pattern becomes superposition of water oscillations from particular surge chambers.

Since the difference in life time of the waterhammer and mass surge is large, it is possible to neglect water compressibility for calculations of water oscillation within waterways.

Tunnel Element

The main idea of Tunnel Element (fig 2.1) is to create a set of simple equations describing water oscillation in a simplified 1D tunnel, which could be used for complex systems modelling.

The main tunnel element assumptions can be divided into:

physics

- Water incompressibility
- Ambient (atmospheric) pressure equals 0
- All physical variables are expressed in head pressure

geometry

- Each element has two nodes
- Circular cross section
- Constant cross section area normal to flow
- Fully turbulent flow within the element
- Uniform roughness distribution along each tunnel – specific head loss is constant

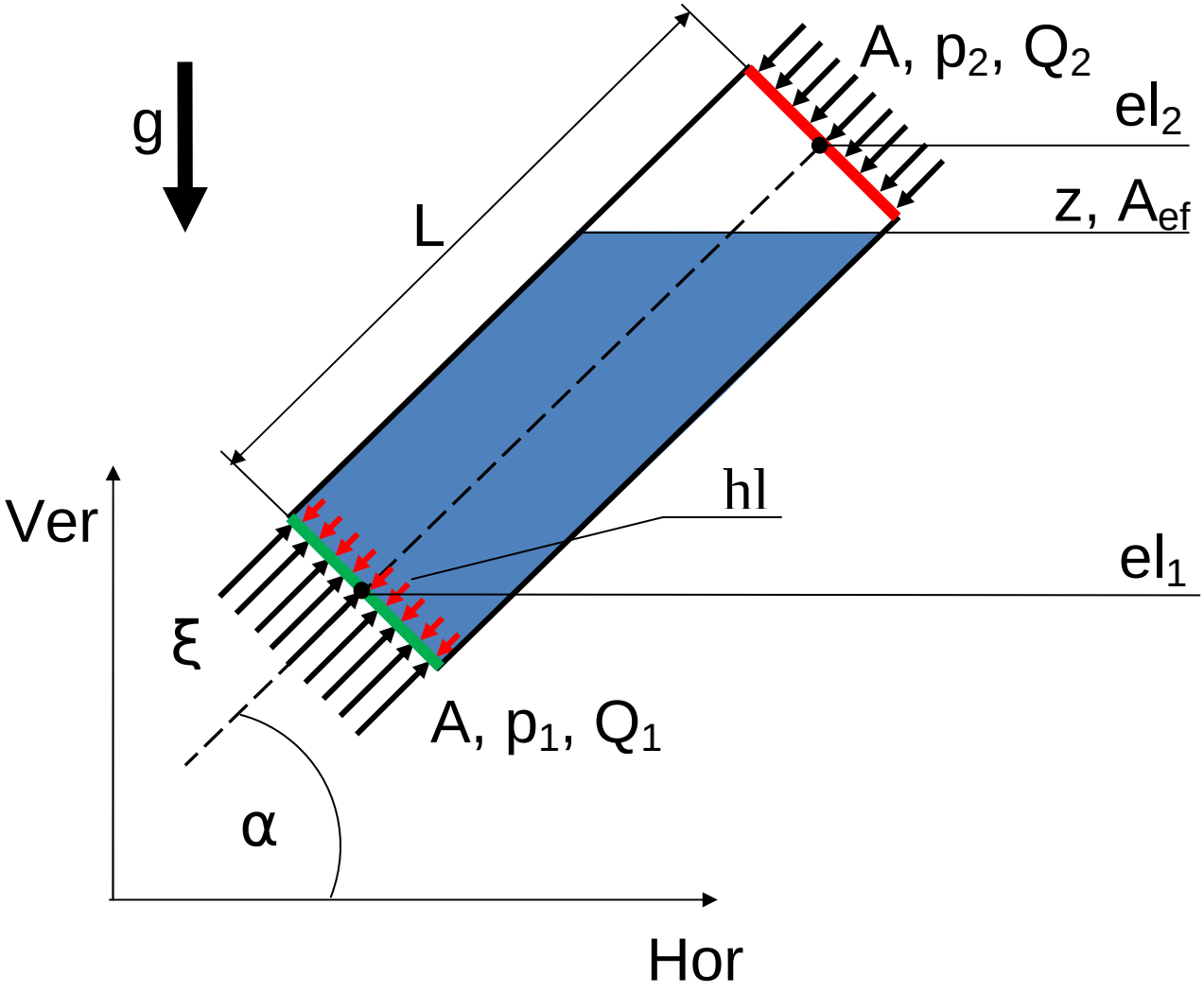

Figure 2.1 Tunnel Element scheme

Table 2.1 List of Tunnel Element parameters and variables	
Geometry	
Symbol	Description
ξ	local coordinate system along element centreline
α	element centreline angle
s	$s = \sin(\alpha)$
A	cross section area normal to flow
A_{ef}	effective (horizontal) cross section area; $A_{ef} = \frac{A}{s}$
L	length; $L = \frac{\lvert el2 - el1 \rvert}{s}$
hl	head loss due to friction and minor loss
g	gravitational constant g=9.8 $\left[\frac{m}{s^2}\right]$
Flow features	
p_1, p_2	Pressure
Q_1, Q_2	flow rate

2.1 Tunnel Element equations derivation

The element equations can be derived from continuity equation (eq. 2.1) and momentum equation (eq. 2.2).

$$\frac{A}{s}\frac{dz}{dt} = Q_1 + Q_2 \qquad 2.1$$

$$\frac{d}{dt}mU = \sum F \qquad 2.2$$

Here m is water mass in the element, U is flow speed and $\sum F$ is the sum of forces (pressure, gravity, friction loss) acting on the element in the direction along the element. Since uncompressible flow is considered (density (ρ) is constant), the mass (m) is constrained with volume (V) by equation: $m = \rho V$.

Thus, eq. 2.2 can be rewritten as:

$$\rho\frac{d}{dt}VU = F_{pressure} + F_{gravity} + F_{headloss} \qquad 2.3$$

Then it can be extended to form:

$$\rho\left(U\frac{dV}{dt} + V\frac{dU}{dt}\right) = Ap_1 - Ap_2 - g^{\xi}\rho V - F_{headloss} \qquad 2.4$$

Where g^{ξ} is a gravitational acceleration acting along element centreline which needs to be transformed to global coordinate system by relationship $g^{\xi} = gs$.

$$\rho\left(U\frac{dV}{dt} + V\frac{dU}{dt}\right) = Ap_1 - Ap_2 - gs\rho V - F_{headloss} \qquad 2.5$$

Since, tunnel element geometry is defined by the functions shown in figure 2.2, it is more convenient to use flow rate Q $\left[\frac{m^3}{s}\right]$ instead of U $\left[\frac{m}{s}\right]$, thus relation $U = \frac{Q}{A}$ is applied

a Sin function

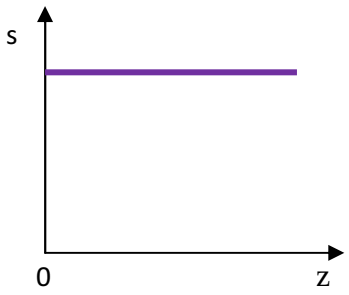

$s = s(z) = const$

b Area function

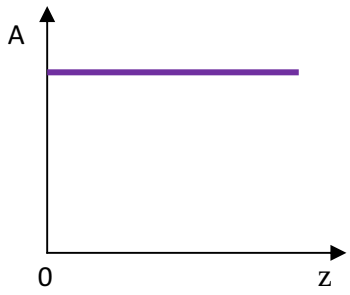

$A = A(z) = const$

c Volume function

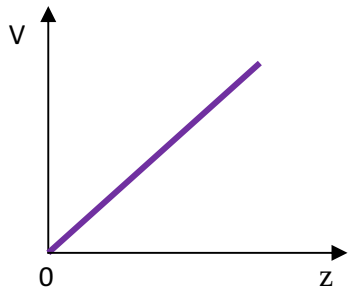

$$V = \int_{el_1}^{z} \frac{A}{s} dz = \frac{A}{s}(z - el_1)$$

$$\frac{dV}{dz} = \frac{A}{s}$$

Figure 2.2 Tunnel Element geometry functions

The unit of momentum equation can be transformed from force to pressure head by dividing both sides by $\rho g A$.

$$\frac{\rho}{\rho g A^2}\left(Q_1 \frac{dV}{dt} + V \frac{dQ_1}{dt}\right) = \frac{A}{\rho g A}(p_1 - p_2) - \frac{\rho g V s}{\rho g A} - \frac{F_{headloss}}{\rho g A} \qquad 2.6$$

After simplifications (fig 2.2c) the following formulation is obtained:

$$\frac{1}{gA^2}\left(Q_1 \frac{dz}{dt}\frac{d}{dz}V + V \frac{dQ_1}{dt}\right) = \frac{A}{\rho g A}(p_1 - p_2) - (z - el_1) - h_{headloss} \qquad 2.7$$

$$\frac{1}{gA^2}\left(\frac{A}{s} Q_1 \frac{dz}{dt} + V \frac{dQ_1}{dt}\right) = \frac{1}{\rho g}(p_1 - p_2) - (z - el_1) - h_{headloss} \qquad 2.8$$

Since $\frac{p}{\rho g}$ is pressure head it can be marked as P

$$\frac{Q_1}{gAs}\frac{dz}{dt} + \frac{V}{gA^2}\frac{dQ_1}{dt} = (P_1 - P_2) - (z - el_1) - h_{headloss} \qquad 2.9$$

Fully turbulent flow is assumed within TE, headloss (h_{loss}) is a sum of friction loss ($h_{friction}$) and local loss (h_{local}). Since the friction loss coefficient (k_f) is assumed to be

constant it will affect the model accuracy for low Reynolds number flow. Since headloss is square function of flow rate, poor damping is expected in long simulation time.

Headloss function can be derived as shown in figure 2.3.

Friction loss

$$h_{friction} = k_f \frac{L}{D}\frac{U^2}{2g} = k_f \frac{L}{D}\frac{Q^2}{2gA^2} = f_l(z)Q^2$$

Local loss

$$h_{local} = k_l \frac{U^2}{2g} = k_f \frac{Q^2}{2gA^2} = l_l Q^2$$

$$h_{loss} = h_{friction} + h_{local} = (f_l(z) + l_l)Q^2$$

Here:

k_f – Darcy friction factor
k_l – local loss factor
L – length
D – diameter
A – cross section area
f_l – friction loss function
l_l – local loss function

Figure 2.3 Tunnel Element head loss functions derivation

Equation 2.9 can be rewritten as follows

$$\frac{Q_1}{gAs}\frac{dz}{dt} + \frac{V}{gA^2}\frac{dQ_1}{dt} = (P_1 - P_2) - (z - el_1) - (l_l + f_l)Q_1|Q_1| \qquad 2.10$$

Considering Matlab formulation in form of $M(t,y)\frac{dy}{dt} = F(t,y)$, the final form of momentum equation is:

$$-\frac{V}{gA^2}\frac{dQ_1}{dt} = (P_2 - P_1) + (z - el_1) + (l_l + f_l)Q_1|Q_1| + \frac{Q_1}{gAs}\frac{dz}{dt} \qquad 2.11$$

Since $V = LA$, governing equations for pressurized flow can be written as

$$-\frac{L}{gA}\frac{dQ_1}{dt} = (P_2 - P_1) + (el_2 - el_1) + (l_l + f_l)Q_1|Q_1| \qquad 2.12$$

$$0 = Q_1 + Q_2 \qquad 2.13$$

Equations for tunnel element with free surface flow can be written as

$$-\frac{V}{gA^2}\frac{dQ_1}{dt} = (P_2 - P_1) + (z - el_1) + (l_l + f_l)Q_1|Q_1| + \frac{Q_1}{gAs}\frac{dz}{dt} \qquad 2.14$$

$$A_{ef}\frac{dz}{dt} = Q_1 + Q_2 \qquad 2.15$$

The term $\frac{Q_1}{gAs}\frac{dz}{dt}$ can be derived to other, more convenient, form for calculations

$$\frac{Q_1}{gAs}\frac{dz}{dt} = \frac{Q_1}{gAs}\frac{s(Q_1 + Q_2)}{A} = \frac{Q_1(Q_1 + Q_2)}{gA^2} \qquad 2.16$$

2.2 Linear interpolation between two known points

Since all model parameters are provided in discrete form e.g. area, volume, discharge profile; it is necessary to interpolate function values between known points. The linear interpolation method shown in figure 2.4 was chosen due efficiency and satisfactory accuracy.

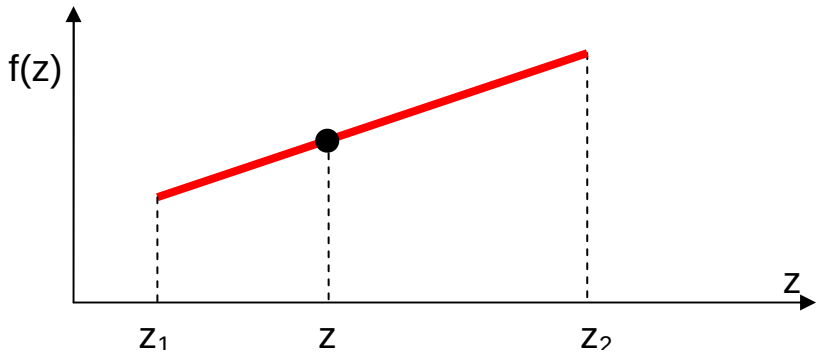

$$f(z) = \frac{(z - z_1)f(z_2) + (z_2 - z)f(z_1)}{z_2 - z_1}$$

Figure 2.4 Linear Interpolation between two known points

2.3 Integration – trapezoidal rule

Since the volume function (fig. 2.2) is an integral of the area function, the volume is calculated by rrapezoidal rule shown in figure 2.5. The rule works by approximating the region under the graph of the function $f(z)$ as a trapezoid and calculating its area.

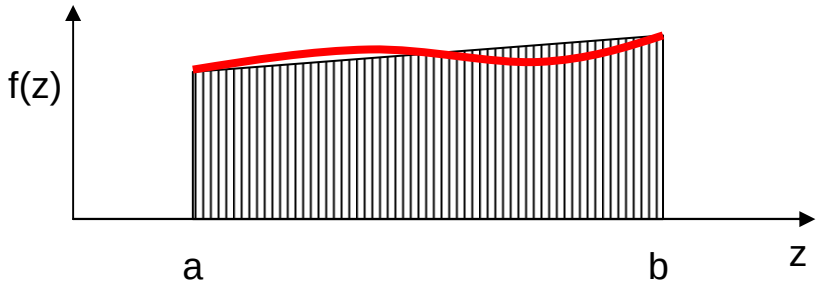

$$\int_a^b f(z)\,dz \approx (b-a)\frac{f(a)+f(b)}{2}$$

Figure 2.5 The Trapezoidal Rule

2.4 Joints

Tunnel Elements are connected by joints shown in figure 2.6, which satisfy continuity equation (eq. 2.17) and momentum equation (eq. 2.18).

$$0 = \sum Q_i \qquad 2.17$$

$$P = P_i \qquad 2.18$$

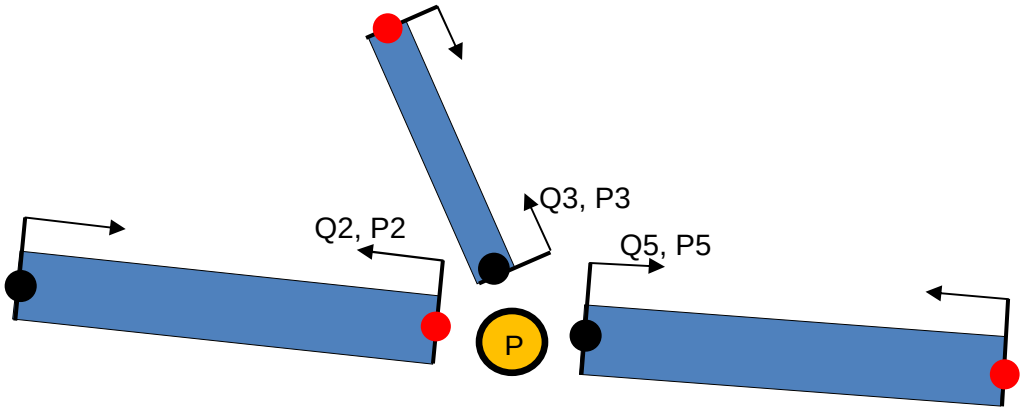

Figure 2.6 Joint scheme

2.5 Overspill

Overspill is modelled by Spill Function ($Q_{spill}(z)$) shown in figure 2.7, which modify continuity equation as follows:

$$\frac{A}{s}\frac{dz}{dt} = Q_1 + Q_2 - Q_{spill}(z) \qquad 2.19$$

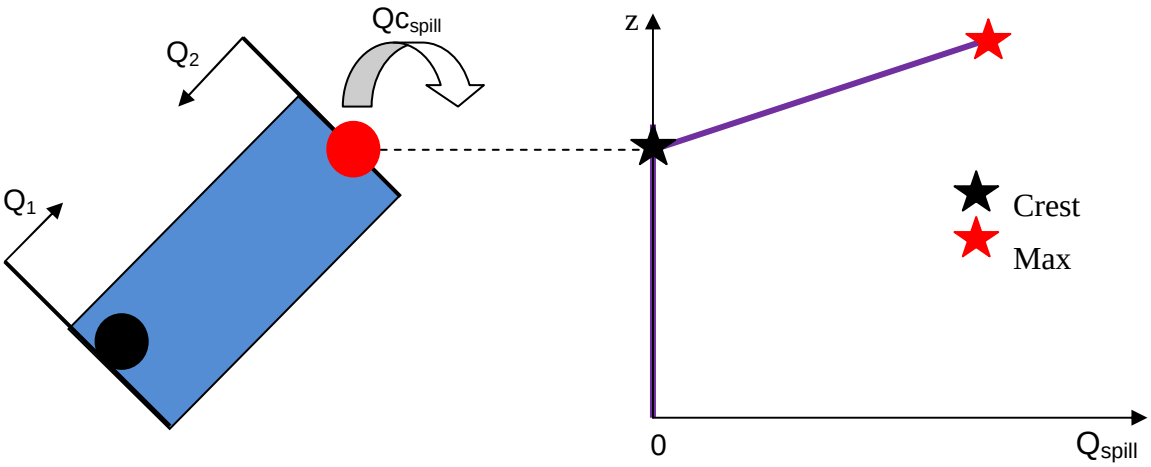

Figure 2.7 Spill function

Spill function is assumed to be a linear interpolation between characteristic points (crest and max value) shown in figure 2.7. Max value can be calculated for gated or crest spillway as shown in figure 2.8a and 2.8b

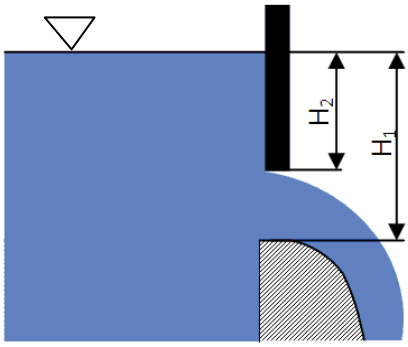

$$Qg_{spill} = C_0 L\,(H_1^{1.5} - H_2^{1.5})$$

Here:
C_0 – Gate coefficient
L – gate width
H_1 – water level above the crest
H_2 – gated water level

Figure 2.8a Flow through gate opening [7]

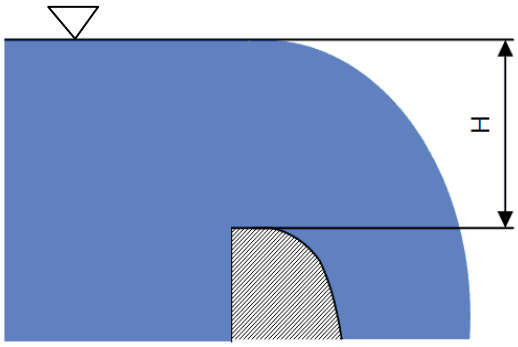

$$Qc_{spill} = C_0 L H^{1.5}$$

Here:
C_0 – Spillway coefficient
L – crest length
H – water level above the crest

Figure 2.8b Flow over Spillway crest [7]

2.6 Throttle

Asymmetrical throttling device (fig 2.9a) is modelled by a Local Loss Coefficient Function ($t_l(Q)$), as shown in figure 2.9b. LLCf is dependent on flow direction defined by equation 2.20.

$$t_l(Q) = \begin{cases} Q < 0; & k_{l1} \\ Q \geq 0; & k_{l2} \end{cases} \qquad 2.20$$

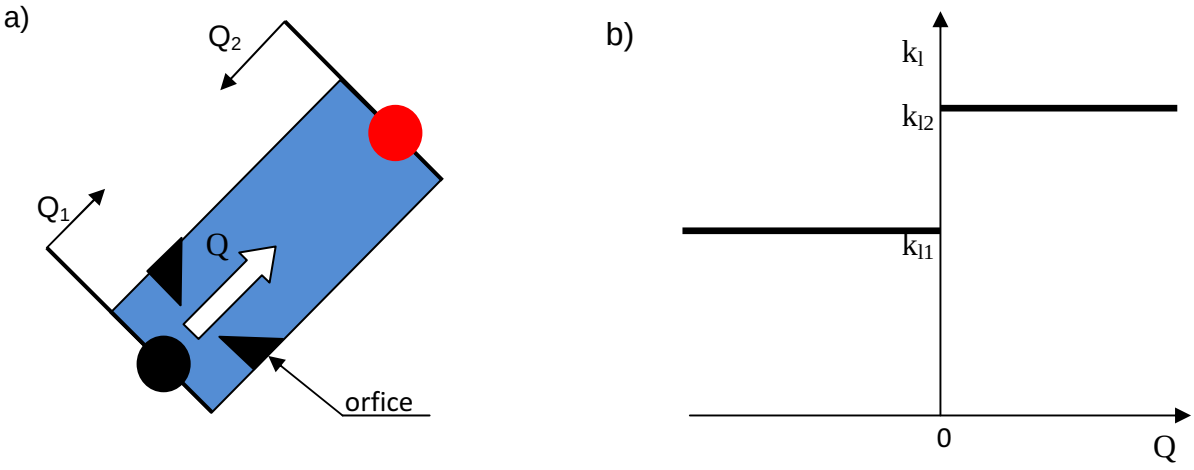

Figure 2.9 Local Loss Coefficient Function

2.7 Variable Surface Area tunnels modeling

According to TE assumptions it is not possible to model exactly free shape tunnels; equation 2.7 assumes $\frac{dA}{dz} = 0$. However, if the area variation along the centreline is close to 0, a complex geometry can be modelled as a stock of thin constant area elements as shown in figure 2.10. Since most of tunnels in Karahnjukar HEP have a regular shape, introduced error would not affect significantly the global solution.

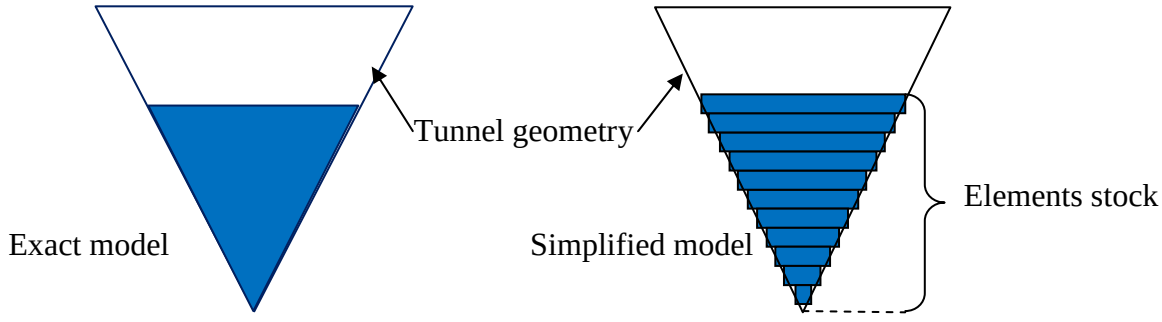

Figure 2.10. Variable area tunnel modelled by tunnel elements

2.8 Leakage

Leakage out of the Tunnel Element can be applied to each element as an additional discharge term Leakage Function Q_{leak} modifying continuity equation (eq. 2.1) to form:

$$A_{ef}\frac{dz}{dt} = Q_1 + Q_2 - Q_{leak} \qquad 2.21$$

The leakage Function is defined in figure 2.11 on basis of the following assumptions:

- No flow to aquifer for initial state due to full saturation and equilibrium between pressure inside the tunnel and in the surrounding aquifer
- Any pressure variation from initial state causes water flow to/from aquifer
- Leakage coefficient is constant
- Water pressure has trapezoidal distribution along element centerline

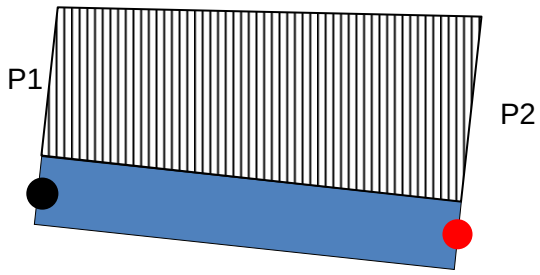

$$Q_{leak} = 0.5k_{leak}A_{wet}((P0_2 + P0_1) - (P_1 + P_2))$$

$$A_{wet} = \int_{el}^{z} \frac{O}{s}dz = O\frac{z - el}{s} = OL$$

Here:

Symbol	Description	Unit
k_{leak}	Leakage coefficient	$\left[\frac{m^3}{s}\frac{1}{m^3}\right]$
L	Length	[m]
O	Circumference	[m]
s	sin(α)	[-]
A_{wet}	Wetted Area	$[m^2]$
P0	Initial pressure	[m]
P	Current pressure	[m]

Figure 2.11 Pressure and leakage distribution along TE

3 RAHNJUKAR MODEL DETAILS

Karahnjukar waterways system is described on basis of “Waterways Operation Manual, Revision 1”. Detailed Karahnjukar Model Scheme is shown in Appendix A.

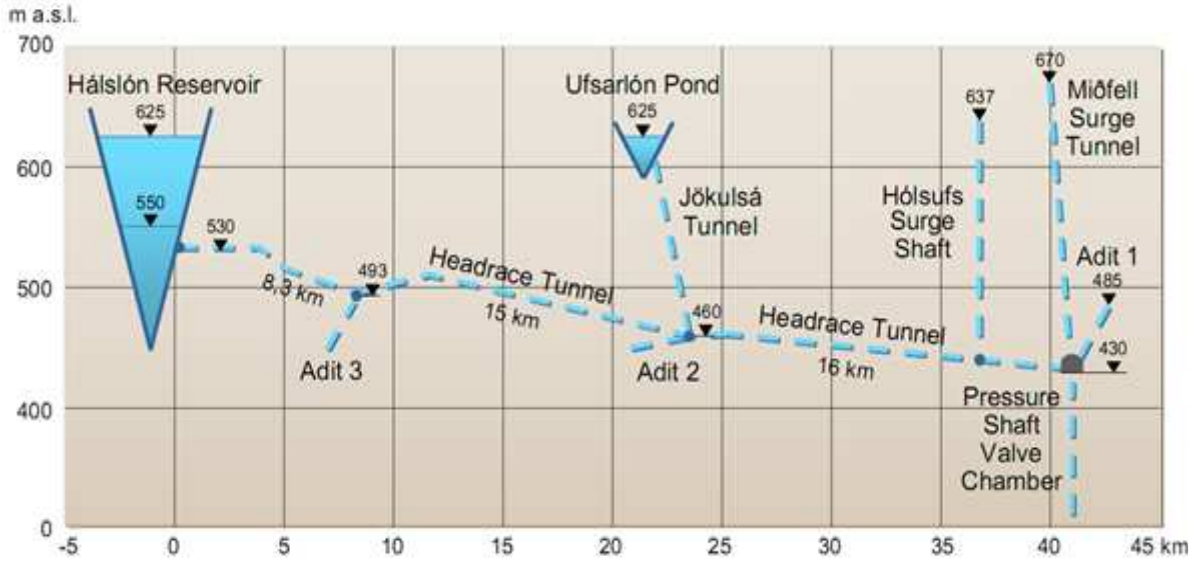

Figure 3.1a Karahnjukar HEP Scheme [5]

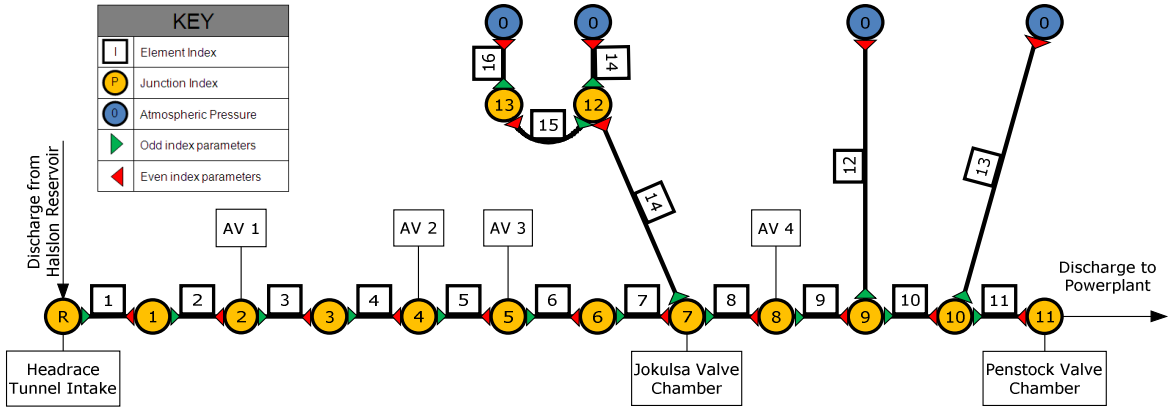

Figure 3.1b Karahnjukar Model Scheme

3.1 Headrace Tunnel and Halslon Reservoir

The 39.7 [km] long Headrace Tunnel conveys water, in a generally unlined pressure tunnel, from the Power Intake at Halslon Reservoir to the Pressure Shafts and through these to the Powerhouse. The vertical alignment of the tunnel was selected to ensure full pressurization during all operating conditions. Static pressure head within the Headrace Tunnel downstream of the Power Intake varies between approximately 20 and 100 [m], and in the manifolds leading to the Pressure Shafts Valve Chamber between 120 and 195 [m]. Approximately 35.5 [km] of the tunnel were excavated using a TBM with diam. 7.2 [m] upstream of the junction with the Jokulsa Tunnel and diam. 7.6 [m] downstream of the junction. The remainder of the Headrace Tunnel was excavated with D&B, horseshoe shaped with the diameter varying between 7.2 and 8.4 [m].

Model

Headrace Tunnel, from Power Intake to Penstock Valve Chamber is modelled by 11 fully pressurized elements defined by equations 2.12 and 2.13 shown in table 3.1a and 3.1b. The elevation presented in the tables are defined for the tunnel invert, hence to transform elevation values to TE centreline coordinates, a half of corresponding tunnel diameter should be added.

Table 3.1a Headrace Tunnel data – Upstream of Jokulsa Tunnel [9]

TE	El 1	El 2	L	A	k_f	k_l	hl*	D	Section
	[m a.s.l]	[m a.s.l]	[m]	[m^2]	$\left[\frac{m}{m}\left(\frac{m^3}{s}\right)^{-2}\right]$	$\left[m\left(\frac{m^3}{s}\right)^{-2}\right]$	[m]	[m]	
1	528.1	529.6	1011.1	36.30	8.62E-08	0	1.81	6.5	D&B 7.2 H.1-H.14 Concrete lined
2	529.6	523.3	1119.0	52.40	1.08E-07	0	2.50	8.17	D&B 7.2 H.14-H.14-9
3	523.3	493.8	5198.0	40.36	1.01E-07	0	10.89	7.17	TBM3 7.2 H.14.9-H.16
4	493.8	492.9	159.0	57.52	8.53E-08	0	0.28	8.56	D&B 7.2 H.16-H.16-9
5	492.9	507.9	6733.0	40.36	8.85E-08	0	12.35	7.17	TBM3 7.2 H.16-9 H.21-9
6	507.9	461.0	8946.0	40.36	9.21E-08	0	17.08	7.17	TBM2 7.2 H.21-HA.2.9-0
7	461.0	460.2	254.0	49.24	1.31E-07	0	0.69	7.92	D&B 7.2 HA.2.9-0-H.J
TOTAL			23420	[m]			45.6	[m]	

Table 3.1b Headrace Tunnel data – Downstream of Jokulsa Tunnel [9]

TE	El 1	El 2	L	A	k_f	k_l	hl*	D	Section
	[m a.s.l]	[m a.s.l]	[m]	[m^2]	$\left[\frac{m}{m}\left(\frac{m^3}{s}\right)^{-2}\right]$	$\left[m\left(\frac{m^3}{s}\right)^{-2}\right]$	[m]	[m]	
8	460.2	465.6	1075.0	57.52	7.90E-08	0	1.76	8.56	D&B 7.6 H.J-H.30-1
9	465.6	437.6	12161	44.98	5.91E-08	0	14.89	7.57	TBM1 7.6 H.30-1-HSS 1.9
10	437.6	430.2	2712.5	50.74	8.40E-08	0	4.73	8.04	D&B 8 HSS 1.9 HS1.9-9
11	430.2	429.8	182.45	41.83	8.40E-08	0	1.32	7.3	D&B 8 HS1.9-9 - av(H.34, H.35)
	TOTAL		16130	[m]			22.7	[m]	

*Head loss calculated for flowrate Q=144 $\left[\frac{m^3}{s}\right]$

Halslon Reservoir wl. is modelled as a pressure head equivalent applied to element no.1 simply as pressure (P_1), which is a difference between HR wl. and the first element TE1.

$$-\frac{L}{gA}\frac{dQ_1}{dt} = (P_2 - P_1) + (el_2 - el_1) + (k_f L + k_l)Q_1|Q_1| \qquad 3.1$$

The total HRT volume according to the tables 3.1a and 3.1b is 1 713 658 [m^3].

3.2 Holsufs Surge Shaft

The Holsufs Surge Shaft (fig 3.2) is a 200 [m] long vertical shaft, excavated 5 [m] in diameter, branching off from the Headrace Tunnel and open to the surface at elevation 639.5 [m a.s.l.]. The shaft is shotcrete lined (4.8 [m] effective diameter) and has a damping throttle close to the bottom where the diameter is reduced to 2.25 [m] over a 5 [m] length of steel pipe. The surface structure is a steel cylinder structure protruding above ground level by approximately 4 [m].

Up to 10 000 [m^3] volume of water can be discharged up through the Surge Shaft, but is only expected a few times every year when a full turbine trip occurs depending on Halslon Reservoir wl., Jokulsa Tunnel discharge and the powerplant discharge.

Figure 3.2 Surface structure of Holsufs Surge Shaft and a section [5]

Model

Holsufs Surge Shaft is modelled by a free surface element with constant area, an orifice and spill function defined by equation 3.6. Since orifice loss does not depend on flow direction, it is modelled as a local head loss defined by equation 3.3.

Orifice head loss can be calculated as a sum of sudden enlargement and contraction head loss [3]:

$$h_{l\,orifice} = h_{l\,enlargment} + h_{l\,contraction} \tag{3.2}$$

$$h_{l\,orifice} = \left(\frac{\left(\frac{1}{A_{orifice}} - \frac{1}{A_{HSS}}\right)^2}{2g} + \frac{C}{2gA_{orifice}^2} \right) Q^2 \tag{3.3}$$

Here $A_{orifice}$ is the orifice cross section area; A_{HSS} is Surge Shaft area and C is an empirical coefficient dependent on orifice geometry. Since A_{HSS} =18.09 [m^2], $A_{orifice}$=3.97 [m^2], C=0.5, thus the orifice head loss can be calculated as follows:

$$h_{l\,orifice} = 0.00358\, Q^2 \tag{3.4}$$

Table 3.3 Holsufs Surge Shaft data [9]

TE	El 1	s	L	A	A_{eff}	k_f	k_l	hl^*	D	section
	[m a.s.l]	[/]	[m]	[m^2]	[m^2]	$\left[\frac{m}{m\left(\frac{m^3}{s}\right)^{-2}}\right]$	$\left[m\left(\frac{m^3}{s}\right)^{-2}\right]$	[m]	[m]	
12	437.58	1	0.00	18.09	18.09	0	3.58E-03	74.27	4.8	HSS
	640	1	202.42	18.09	18.09	0	0	0	4.8	HSS

*Head loss calculated for flowrate Q=144 $\left[\frac{m^3}{s}\right]$

The Surge Shaft Spill Function is modelled as discharge through crest spillway (fig. 2.8b). The C_0 coefficient equals 1.7; a crest length can be calculated:

$$L = \pi D = 15.07 \tag{3.5}$$

The max spill value is assumed for water level 4 [m] above the average crest elevation 639.5 [m a.s.l.]

$$Qc_{spill} = 204.96 \left[\frac{\mathrm{m}^3}{\mathrm{s}}\right] \tag{3.6}$$

3.3 Midfell Surge Tunnel

The Midfell Surge Tunnel (fig 3.3) is located 2.7 [km] downstream of the Holsufs Surge Shaft, just upstream of the Manifolds. The surge tunnel is a mildly sloped (12 % - 16 %), shotcrete lined tunnel with a horseshoe section excavated by D&B, with total length of 1700 [m]. The upper portal elevation is 668.5 [m a.s.l.] The lower part, below an invert elevation of 592 [m a.s.l.], has a design diameter of 5 [m] and a longitudinal slope of 16 %. The upper part has a design diameter of 4.5 [m] and a slope of 12 %. The average effective cross-sectional area is 26.7 [m^2] and 22 [m^2] for the lower and upper part respectively (based on measured tunnel profiles). This provides an effective horizontal area of free water surface of about 169.9 [m^2] in the lower section and 183.6 [m^2] in the upper section.

The highest water surface level is estimated to be 659 [m a.s.l.] during sudden turbine shutdown (full turbine trip) at full discharge and full Halslon Reservoir level. The highest possible level during a worst possible combination of opening and closing operation is 661.6 [m a.s.l.] [5].

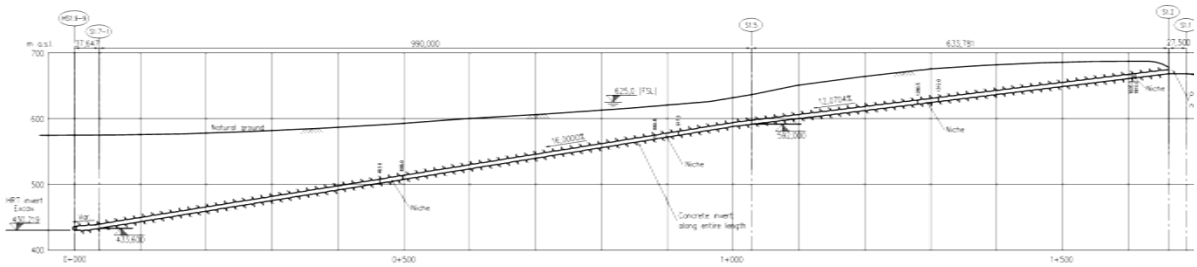

Figure 3.3 profile along Surge Tunnel [5]

Midfell Surge Tunnel is modelled by free surface element with variable area coefficient.

Table 3.4 Midfell Surge Tunnel data [4]

TE	El 1	s	L	A	Aef	k_f	k_l	hl*	D	Section
	[m a.s.l]	[/]	[m]	[m^2]	[m^2]	$\left[\frac{m}{m}\left(\frac{m^3}{s}\right)^{-2}\right]$	$\left[m\left(\frac{m^3}{s}\right)^{-2}\right]$	[m]	[m]	
13	430.22	0.157	0.00	26.7	169.9	5.97E-07	7.23E-05	1.50	5.83	D&B 5 HS 1.9-9
	592.00	0.157	1030.27	26.7	169.9	5.97E-07	0	13.7	5.83	D&B 5 S 1.5-tran
	597.44	0.12	45.42	22.1	183.6	1.13E-06	0	1.18	5.44	D&B 4.5 S1.5-tran
	668.00	0.12	588.81	22.1	183.6	1.13E-06	0	15.3	5.44	D&B 4.5 S1.2
	TOTAL		1668.4	[m]				31.6	[m]	

*Head loss calculated for flowrate Q=144 $\left[\frac{m^3}{s}\right]$

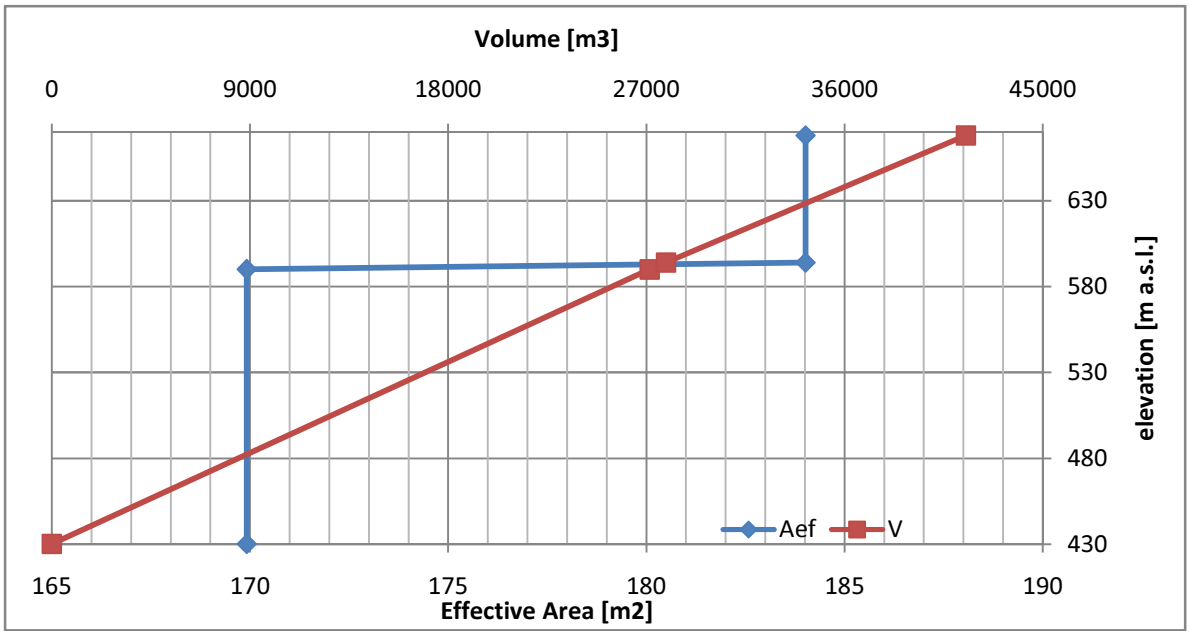

Figure 3.4 Midfell Surge Tunnel cumulative volume and Effective Area

3.4 Jokulsa Tunnel and Jokulsa Surge Tunnel

The Jokulsa Tunnel (fig 3.5) is 13.5 [km] long, connecting the Ufsarlon Intake at Ufsarlon Pond with the Headrace Tunnel. The vertical alignment of the JT in the first 3 km forms an inverted siphon whereas the remaining 10,5 km descend at between 0,5 % and 2,8 % slope towards the HRT. While the 4,5 km upper portion of the JT upstream of the TBM disassembly chamber was excavated with a D-shape profile by D&B (mostly with D = 6 m), the lower portion was bored by TBM (D = 7,2 m).

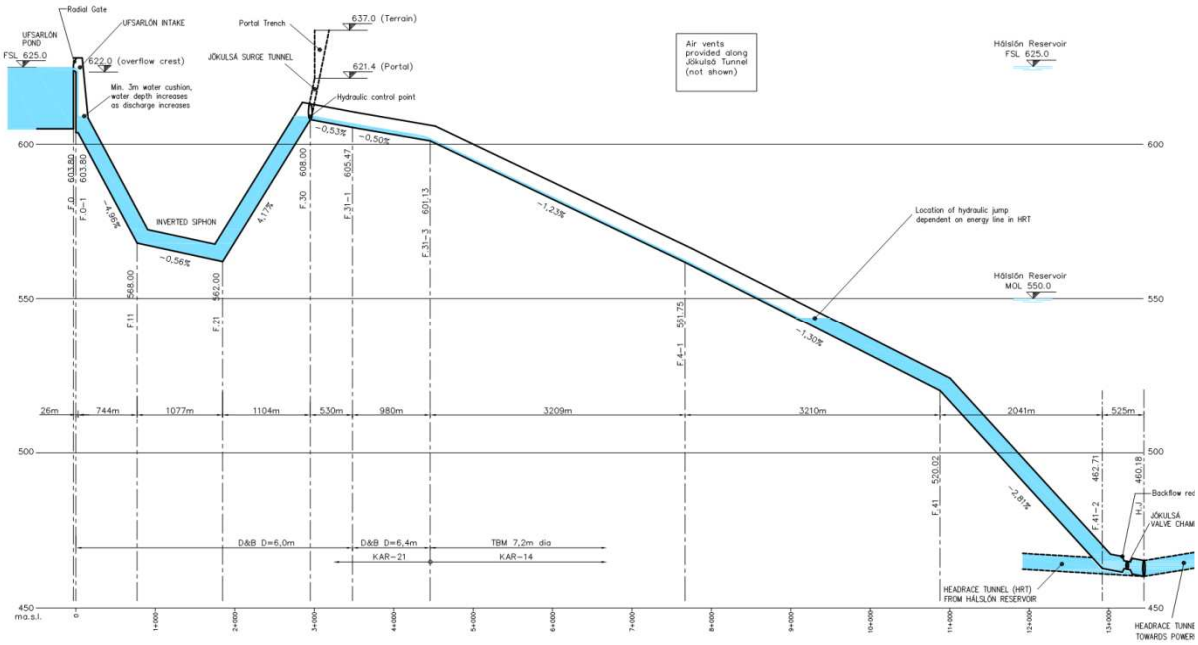

Figure 3.5 Jokulsa Tunnel Scheme [5]

Jokulsa Surge Tunnel (fig 3.6) branches off the Jokulsa Tunnel adjacent to the downstream end of the Inverted Siphon. JST ascends at 12 % for 110 [m] and continuous another 130 [m] at the same slope as an open trench to the ground surface. The surge tunnel is excavated by D&B (D = 8 m), shotcrete lined to the extent required by rock conditions and is provided throughout with invert concrete. The invert of the portal trench is protected by rock cobble.

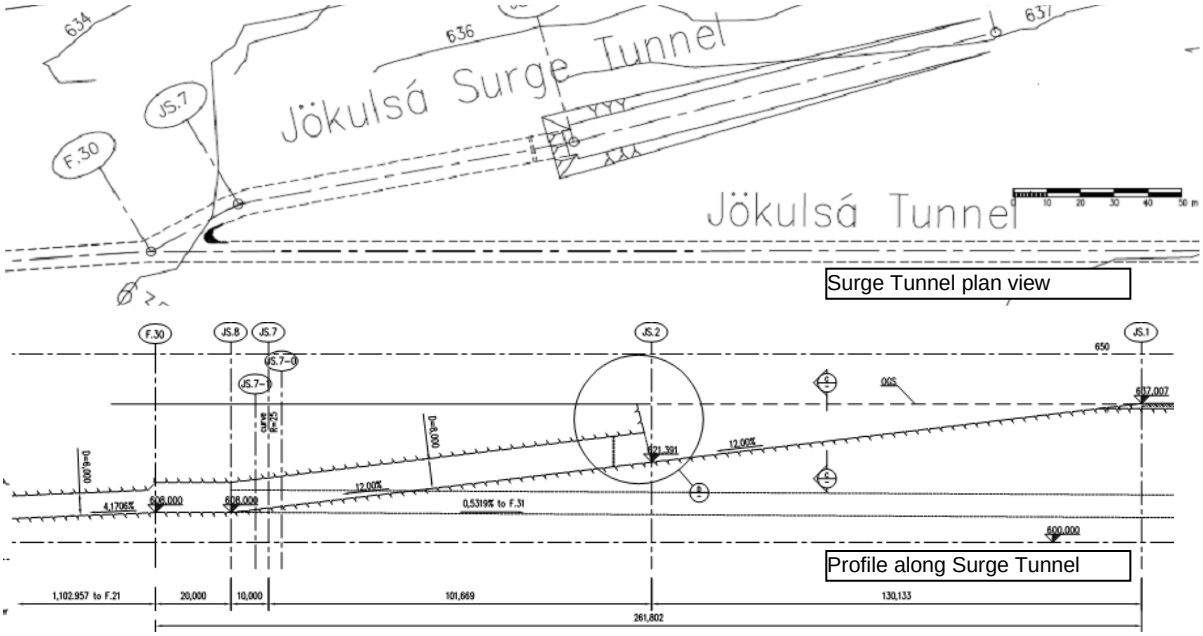

Figure 3.6 Jokulsa Surge Tunnel and the canal plan view [5]

Model

Jokulsa Tunnel (downstream of the inverted siphon) and Jokulsa Surge Tunnel are modelled by one FTE with variable area coefficient. Volume and Area functions are a sum of 2 elementary functions shown in figure 3.7 and 3.8. Since JST volume is small comparing to JT volume, the inertia of JST is neglected.

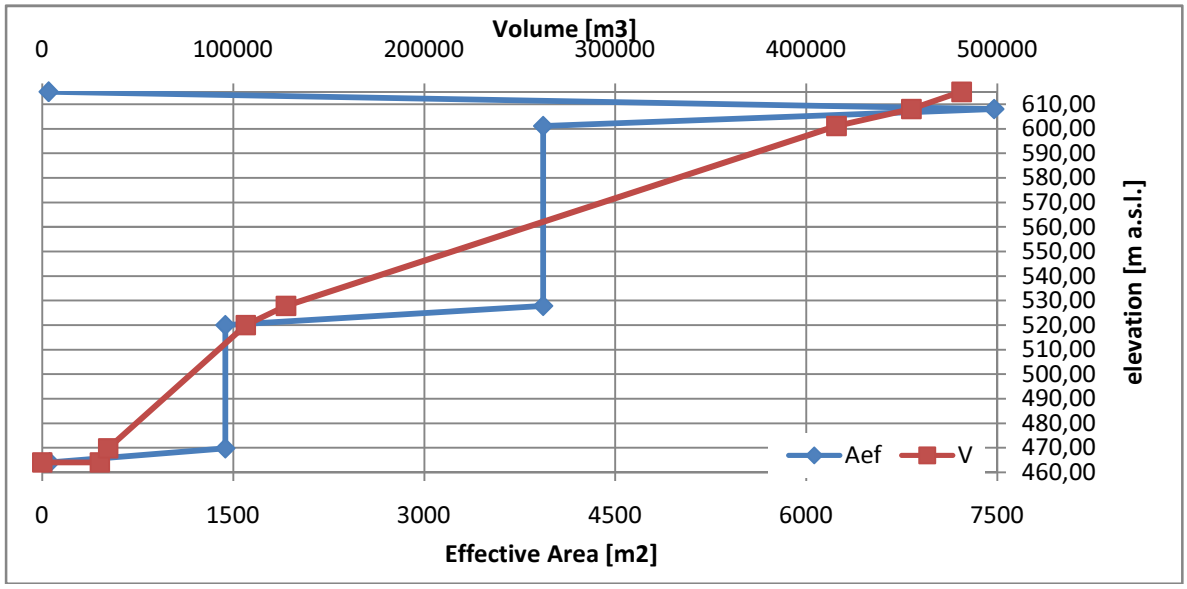

Figure 3.7 Jokulsa Tunnel cumulative volume and Effective Area

Table 3.5a Jokulsa Tunnel data [9]										
TE	El 1	s	Length	Area	Effective Area	k_f	k_l	hl^*	D	Section
	[m a.s.l]	[/]	[m]	[m^2]	[m^2]	$\left[\frac{m}{m}\left(\frac{m^3}{s}\right)^{-2}\right]$	$\left[m\left(\frac{m^3}{s}\right)^{-2}\right]$	[m]	[m]	
14	460.18	1.000	0.00	57.52	57.5	8.63E-08	0	0.00	8.56	D&B 7.2 H.J
	462.71	1.000	525.00	57.52	57.5	8.63E-08	0	0.37	8.56	D&B 7.2 F.41-2
	469.88	0.028	255.1	40.36	1436.7	9.21E-08	0	0.19	7.17	TBM2 7.2 F.41-4
	520.02	0.028	1785.1	40.36	1436.7	9.21E-08	0	1.33	7.17	TBM2 7.2 F.41
	527.87	0.012	638.21	48.37	3933.1	1.15E-07	0	0.60	7.85	TBM 7.2 F.41
	601.13	0.012	5956.6	48.37	3933.1	1.15E-07	0	5.55	7.85	TBM 7.2 F.31-3
	608.00	0.005	1374.0	37.37	7474.9	2.30E-07	0	2.56	6.9	D&B 6.2 F.31-3
	615.00	1.000	7.00	50	50	0	0	0.00	8	JST
	TOTAL		10541.1	[m]				10,6	[m]	

*Head loss calculated for flowrate Q=90 $\left[\frac{m^3}{s}\right]$

Note: Tunnel from section D&B 7.2 to D&B 7.2 F.41 is always pressurized, thus s can be set 1.

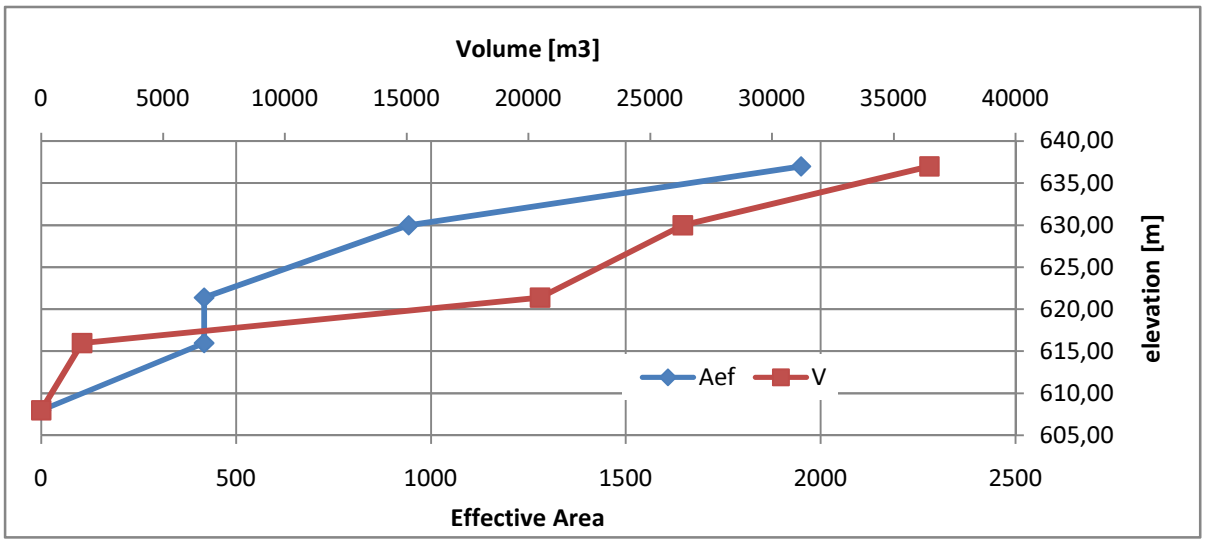

Figure 3.8 Jokulsa Surge Tunnel cumulative volume and Effective Area

Table 3.5b Jokulsa Surge Tunnel data[5]										
Element Index	El 1	s	Length	Area	Effective Area	kf	kl	hl*	D	section
	[m a.s.l]	[/]	[m]	[m^2]	[m^2]	$\left[\frac{m}{m}\left(\frac{m^3}{s}\right)^{-2}\right]$	$\left[m\left(\frac{m^3}{s}\right)^{-}\right.$	[m]	[m]	
14	608	1	0.00	0	0	0	0	0	0	JST
	616	0.12	8	50.24	418.7	0	0	0	8	JST
	621.39	0.12	44.92	50.24	418.7	0	0	0	8	JST
	630	1	8.61	943	943	0	0	0	-	JST
	637	1	7.00	1950.00	1950	0	0	0	-	JST

3.5 Energy Dissipater

In normal operation conditions the Jokulsa Tunnel acts as an extra surge tunnel to the Headrace Tunnel system. Reverse flow is obtained in the tunnel when the station trips and water is pushed from the HRT back into the JT and in some cases all the way up to the Ufsarlon Pond. The reverse flow could have become extensive and in many cases could have exceeded the maximum normal design flow of the tunnel by up to 170 [m^3/s]. The reverse flow maximum also has to be limited to permissible values for the butterfly valve of 100 [m^3/s] [6], hence an Energy Dissipater (fig. 3.9) is implemented as sudden enlargement in a discharge conduit. The shape was optimized to give a little head loss in the normal flow direction and high for backflow.

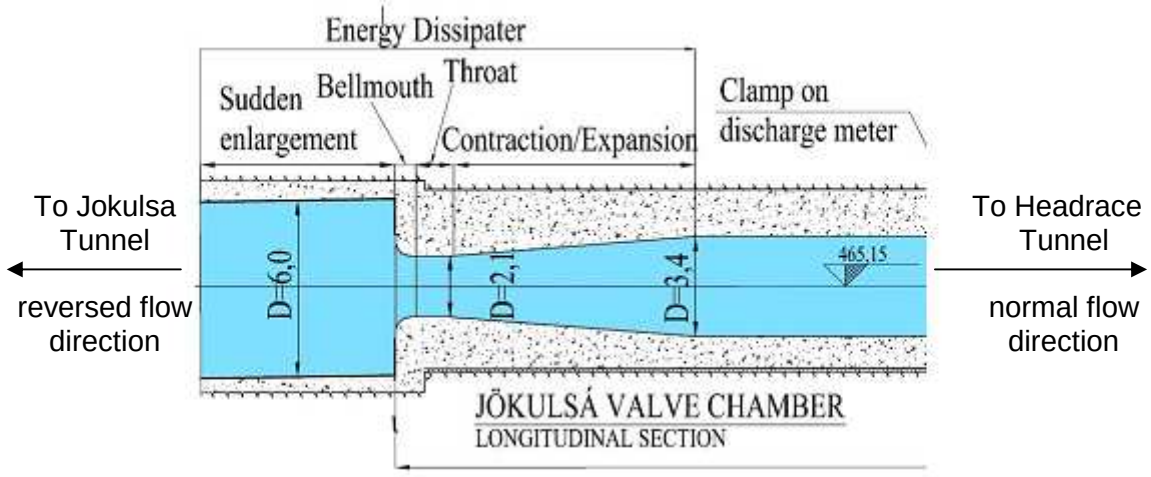

Figure 3.9 Plan and section through Energy Dissipater [6]

Energy dissipater is modelled as additional headloss function t_l modifying momentum equation 3.7.

$$-\frac{V}{gA^2}\frac{dQ_1}{dt} = (P_2 - P_1) + (z - el_1) + (l_l + f_l + t_l)Q_1|Q_1| + \frac{Q_1}{gAs}\frac{dz}{dt} \qquad 3.7$$

Table 3.6 Energy Dissipater [6]			
Index	Direction	kl $\left[m\left(\frac{m^3}{s}\right)^{-2}\right]$	hl* [m]
1	Normal Q>0	0.00061	4.94
2	Reversed Q<0	0.00333	26.97

*Head loss calculated for flowrate Q=90 $\left[\frac{m^3}{s}\right]$

3.6 Inverted Siphon

The Inverted Siphon is a shotcrete lined tunnel with a horseshoe section excavated by D&B, with total length of 2950 [m], always filled with water. The minimum water elevation of 608 [m a.s.l.] is maintained upstream of the high point where the Jokulsa Surge Tunnel meets the Jokulsa Tunnel. The maximum water elevation during normal operation is approximately 624.6 [m a.s.l.] at the upstream end. When JT is emptied the IS will remain full with wl. at 608 [m a.s.l.]. Mobile pumps are necessary to empty the siphon by pumping water out through the JST. IS control point at its downstream end at elevation 608 [m a.s.l.] limits the flow capacity of Ufsarveita Diversion when JT is not flowing full. The maximum discharge that is possible to get through the siphon is about 110 [m^3/s].

Model

Inverted Siphon is modelled by one PTE (tab. 3.10). If JT wl. is higher than IS critical wl. El.1', JT flow influences IS discharge. El.1' can be calculated by formula 3.8 derived from figure 2.8b.

If JT wl. is higher than El.1', IS and JT is treated as fully pressurized tunnel modelled by PTE. The residue volume from El.1' to 615 [m a.s.l.] is treated as a part of Jokulsa Surge Tunnel and the effective JT area function is added to effective JST area.

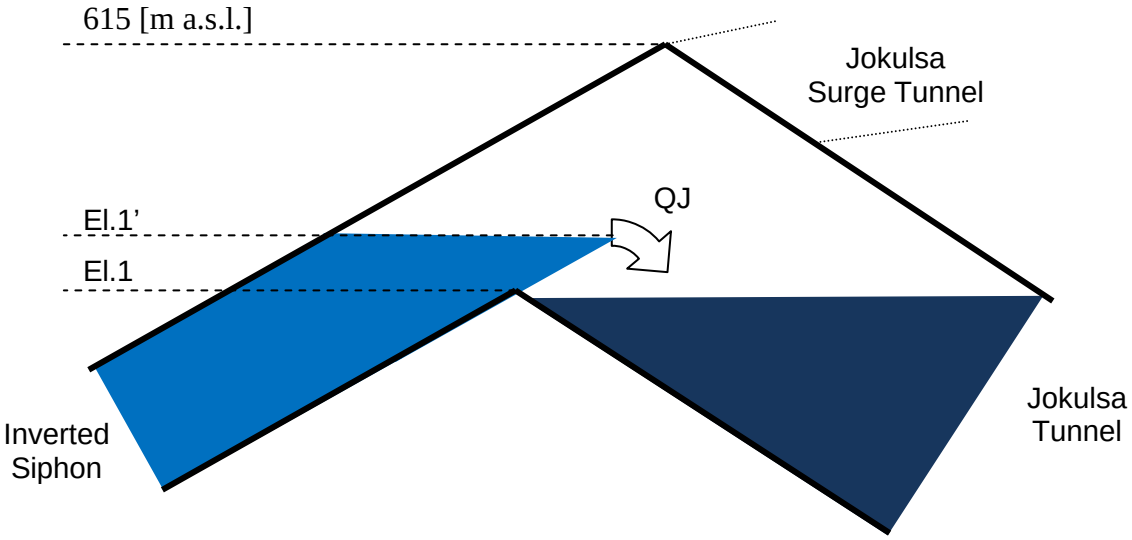

Figure 3.10 Jokulsa Tunnel – Inverted Siphon Junction model (El.1 = 608 m a.s.l)

$$El.1' = El.1 + \left(\frac{QJ}{C_0 L}\right)^{\frac{2}{3}} \qquad 3.8$$

Here Spillway coefficient (C_0) is equal 1.6 and the crest length (L) is 6 [m].

Table 3.7 Inverted Siphon data [9]

TE	El 1	El 2	L	A	k_f	k_l	hl*	D	Section
	[m a.s.l]	[m a.s.l]	[m]	[m^2]	$\left[\frac{m}{m}\left(\frac{m^3}{s}\right)^{-2}\right]$	$\left[m\left(\frac{m^3}{s}\right)^{-2}\right]$	[m]	[m]	
15	608	607.85	2950.00	36.51	3.26E-07	0	7.8	6.82	D&B 6 F.1 - F.30

*Head loss calculated for flowrate Q=90 $\left[\frac{m^3}{s}\right]$

3.7 Ufsarlon Intake Collector

Ufsarlon Intake Collector follows the concept of a side channel spillway consisting of a 10.6 [m] long gated overflow weir with a crest elevation at 622 [m a.s.l.], to maintain a minimum operating level of 622 [m a.s.l.] in the reservoir. Water flowing over the crest falls into a collector channel with a bottom invert at elevation 605 [m a.s.l.]. Opening above the overflow crest is furnished with a 10,6 m long radial gate. The purpose of the gate is to limit maximum flow to the design discharge of the diversion and for isolation of the Jokulsa Tunnel during inspection and maintenance. If the Intake gate is closed the water level during backflow resulting from trip could reach elevations higher than the roof of the intake collector (629.5 [m a.s.l.]) [5]. Therefore three overflow spill openings are provided at the south wall of the collector. If water level in the collector is higher 629.5 [m] [a.s.l.] the openings can discharge up to 50 [m^3/s].

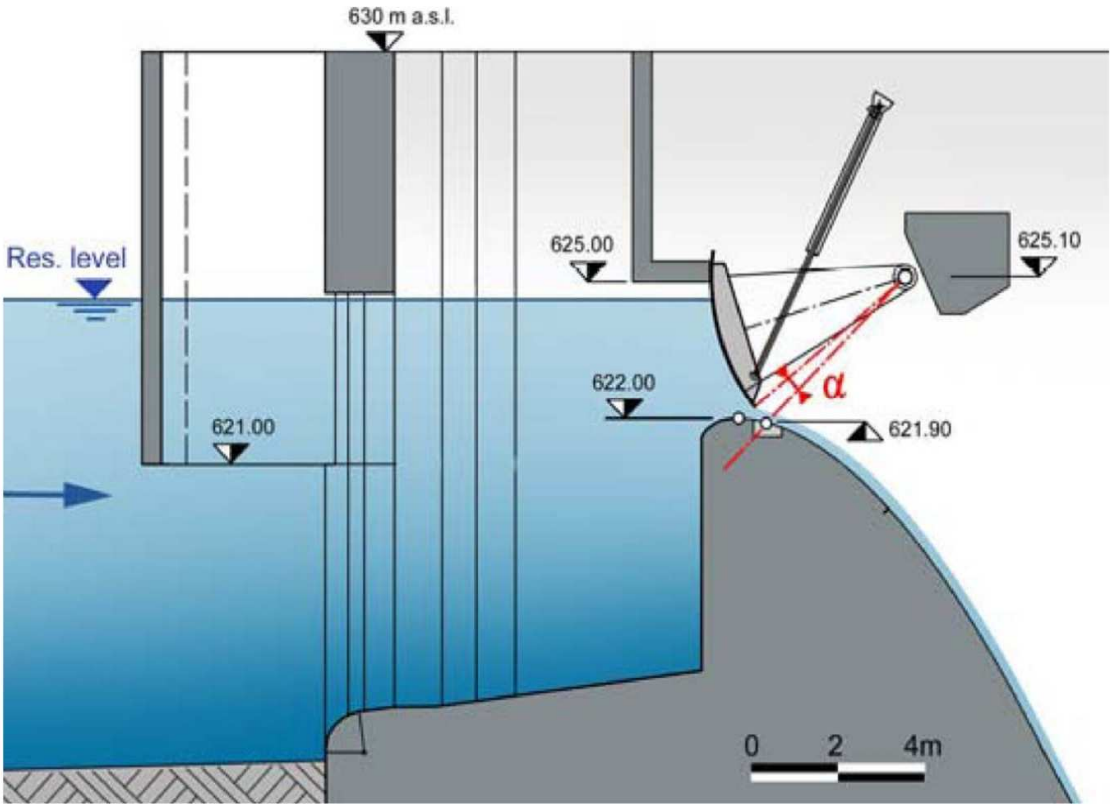

Figure 3.11a Definition sketch for Ufsarlon Intake with partly closed gate, ice skimming wall and trashracks [5]

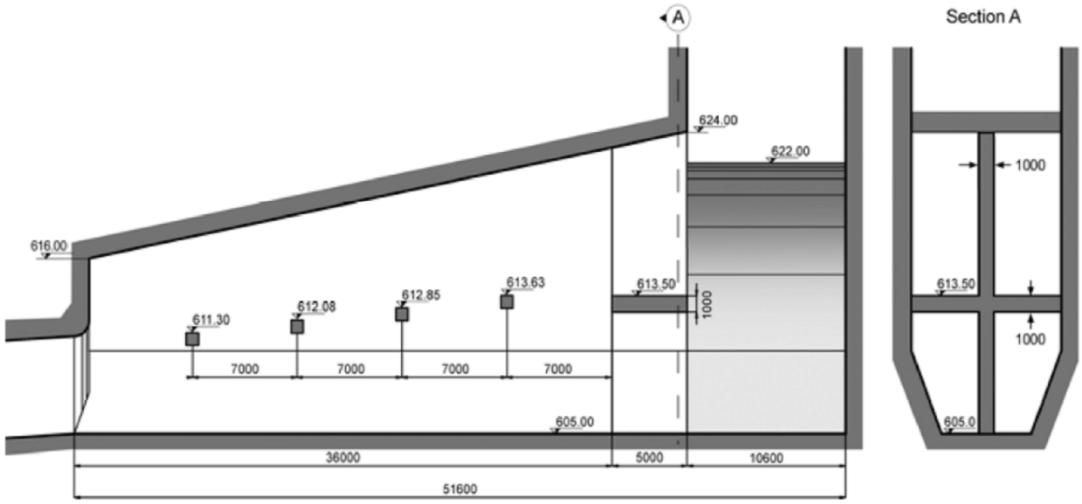

Figure 3.11b Intake Collector and anti-vortex cross for flow straightening (four cross-beams are for structural purposes)[5]

Model

Jokulsa Intake Collector is modelled by FSE with variable area coefficient (fig. 3.12) and additional spill function, which can be derived on the basis of formulas for flow past crest and gated spillway shown in figure 2.8a and 2.8b.

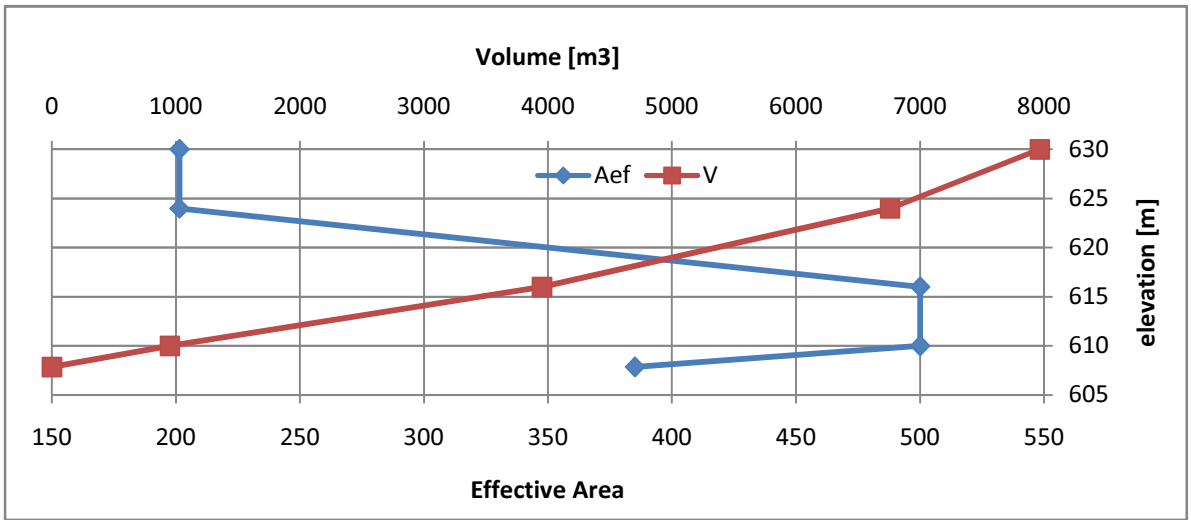

Figure 3.12 UIC Effective area change

Table 3.8 Jokulsa Intake Collector data[5]

TE	El 1	s	L	A	k_f	k_l	hl*	section
	[m a.s.l]	[/]	[m]	[m2]	$\left[\frac{m}{m}\left(\frac{m^3}{s}\right)^{-2}\right]$	$\left[m\left(\frac{m^3}{s}\right)^{-2}\right]$	[m]	
16	607.85	1	0	385	0	0.00	0.00	JIC
	610	1	2.15	500	0	0.00	0.00	JIC
	616	1	6.00	500	0	0.00	0.00	JIC
	624	1	8.00	201.4	0	0.00	0.00	JIC
	630	1	6.00	201.4	0	0.00	0.00	JIC

Jokulsa Collector Spill Function is a linear interpolation between characteristic points calculated on flow past gated spillway and crest spillway shown in figure 3.13.

UIC spill function can be defined by following characteristic points:

1. Due to supercritical flow from Ufsarlon Pond, the spill function has no influence of the flow within UIC until water level reach 80% of head between crest (gt_1) and UP wl. (H_2):

$$gt_1 + 0.8(H_2 - gt_1)$$

2. No water flow between UIC and UP is assumed for UIC wl. equal UP wl. (H_2). Hence, the spill function value is equal to initial discharge from UP (-QJ).
3. As UIC wl. increases, the gate starts to affect the backflow to UP. The maximal discharge at the emergency opening bottom (gt_3) can be calculated from figure 2.8a.
4. Emergency opening and the gate affect backflow to UP. The maximum value of the spill function for UIC ceiling (gt_4) is calculated as sum of maximal discharges from the gated spillway and crest spillway shown in figure 2.8a and 2.8b.

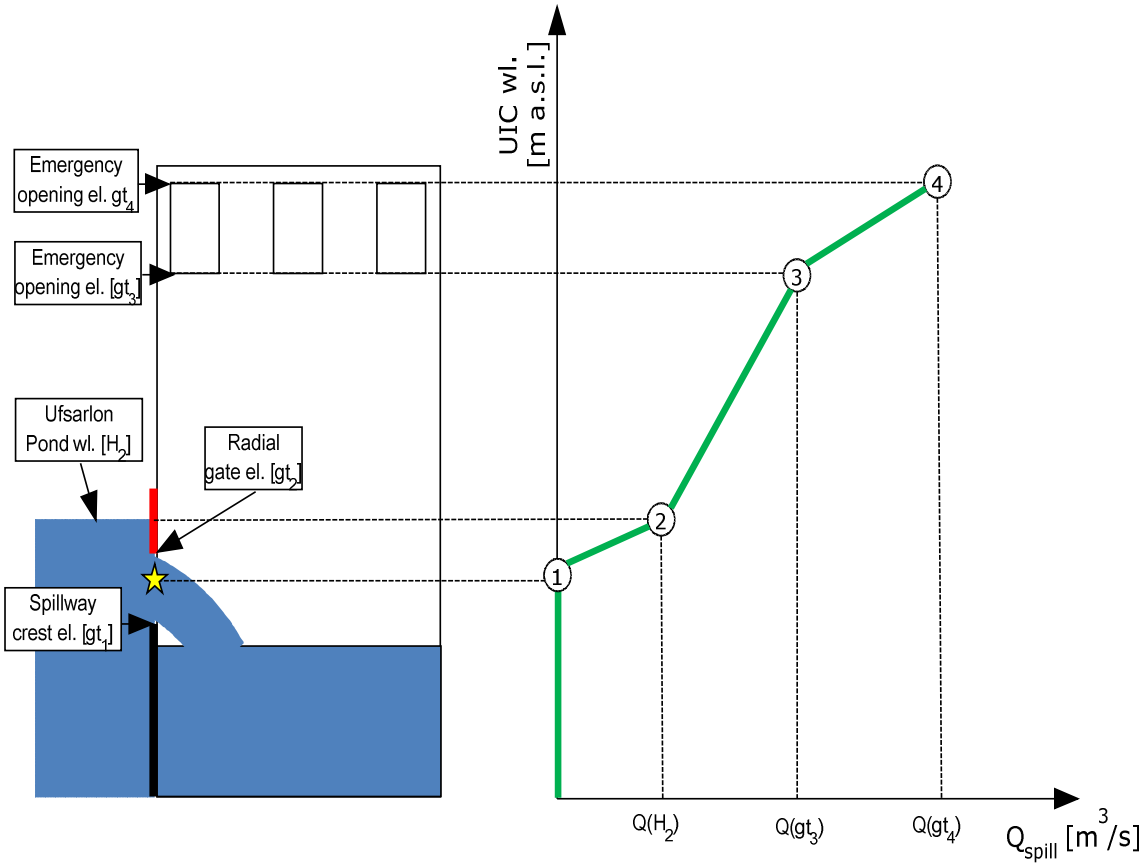

Figure 3.13 Jokulsa Collector model and Spill function

4 EQUATIONS SYSTEM

The mathematical model scheme is shown in appendix A. System of equations defining the model can be written for the following cases shown in figure 4.1:

1. Jokulsa Tunnel closed
2. Jokulsa Tunnel open – free surface flow
3. Jokulsa Tunnel open – pressurized flow

Case 1 can be considered as a particular case of Free/Pressurized Jokulsa Tunnel (dependent on initial state) with no discharge to JT, thus the number of cases is reduced to 2. Cases 2 and 3 have different equations system, hence they need to be solved separately. Switching between cases 2 and 3 can be done automatically with respect to flow development during computations. According to surge development the model can be switched several times between the cases.

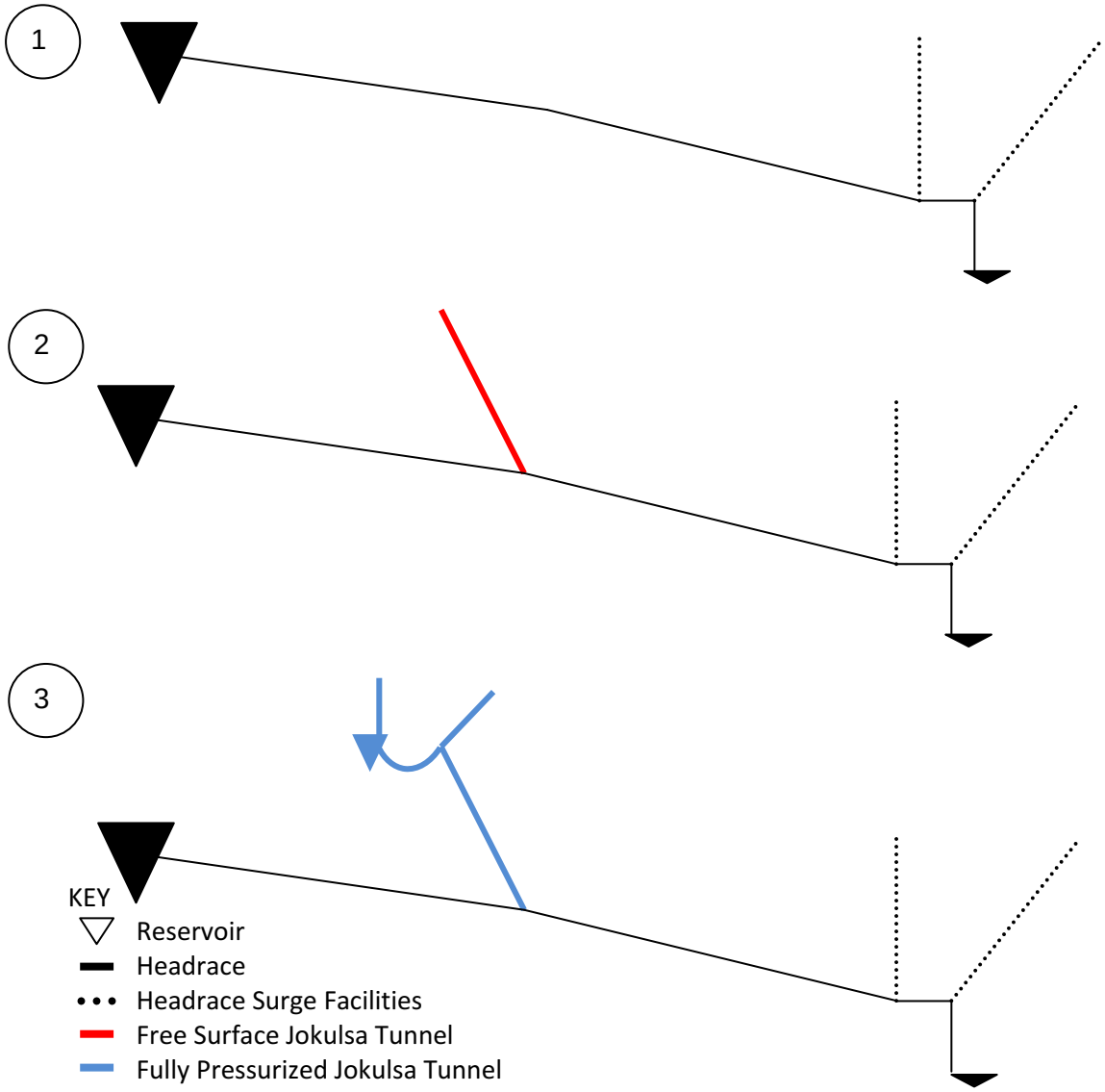

Figure 4.1 Schematic to the system for different cases

The model for closed Jokulsa Tunnel is described by the following equations

Headrace Tunnel

$$-\frac{L_i}{gA_i}\frac{dQ_{i,1}}{dt} = \left(P_{i,2} - P_{i,1}\right) + \left(el_{i,2} - el_{i,1}\right) + (l_l + f_l)Q_{i,1}|Q_{i,1}| \quad 4.1$$

$$0 = Q_{i,1} + Q_{i,2} \quad 4.2$$

Where 'i' is an element index from 1 to 11

Holsufs Surge Shaft

$$-\frac{V_{12}}{gA_{12}^2}\frac{dQ_{12,1}}{dt} = \left(0 - P_{12,1}\right) + \left(z_{12} - el_{12,1}\right) + l_l Q_{12,1}\left|Q_{12,1}\right| + \frac{Q_{12,1}}{gA_{12}s_{12}}\frac{dz_{12}}{dt} \quad 4.3$$

$$A_{ef\,12}\frac{dz_{12}}{dt} = Q_{12,1} + Q_{spill} \quad 4.4$$

Midfell Surge Tunnel

$$-\frac{V_{13}}{gA_{13}^2}\frac{dQ_{13,1}}{dt} = \left(0 - P_{13,1}\right) + \left(z_{13} - el_{13,1}\right) + (l_l + f_l)Q_{13,1}\left|Q_{13,1}\right| + \frac{Q_{13,1}}{gA_{13}s_{13}}\frac{dz_{13}}{dt} \quad 4.5$$

$$A_{ef\,13}\frac{dz_{13}}{dt} = Q_{13,1} \quad 4.6$$

Headrace Tunnel Junctions

$$0 = Q_i + Q_{i+1} \quad 4.7$$

$$P_{i,2} = P_{i+1,1} \quad 4.8$$

Where 'i' is from 1 to 8

Holsufs Surge Shaft - Headrace Tunnel Junction

$$P_{13,1} = P_{9,2} = P_{10,1} \quad 4.9$$

$$0 = Q_{13,1} + Q_{9,2} + Q_{10,1} \quad 4.10$$

Midfell Surge Tunnel – Headrace Tunnel Junction

$$P_{14,1} = P_{10,2} = P_{11,1} \quad 4.11$$

$$0 = Q_{14,1} + Q_{10,2} + Q_{11,1} \quad 4.12$$

The system has 56 unknowns and 56 coupled, nonlinear equations which can be solved using an appropriate numerical method. When Jokulsa Tunnel is added to the system it is necessary to modify JVC equations (eq. 4.7, 4.8) to following form:

Jokulsa Tunnel – Headrace Tunnel Junction

$$P_{14,1} = P_{8,2} = P_{9,1} \tag{4.13}$$

$$0 = Q_{14,1} + Q_{7,2} + Q_{8,1} \tag{4.14}$$

Free Surface Jokulsa Tunnel

$$-\frac{V_{14}}{gA_{14}^2}\frac{dQ_{14,1}}{dt} = \left(0 - P_{14,1}\right) + \left(z_{14} - el_{14,1}\right) + (l_l + f_l + t_l)Q_{14,1}\left|Q_{14,1}\right| + \frac{Q_{14,1}}{gA_{14}s_{14}}\frac{dz_{14}}{dt} \tag{4.15}$$

$$A_{ef\,14}\frac{dz_{14}}{dt} = Q_{14,1} + QJ \tag{4.16}$$

Pressurized Jokulsa Tunnel

When the water surface starts to influence flow within Inverted Siphon, Jokulsa Tunnel has to be treated as pressurized tunnel, thus equations (eq. 4.15, 4.16) have to be modified to form:

$$-\frac{V_{14}}{gA_{14}^2}\frac{dQ_{14,1}}{dt} = \left(P_{14,2} - P_{14,1}\right) + \left(el_{16,1} - el_{14,1}\right) + (l_l + f_l + t_l)Q_{14,1}\left|Q_{14,1}\right| \tag{4.17}$$

$$0 = Q_{14,1} + Q_{14,2} \tag{4.18}$$

Moreover, additional equations for Jokulsa Surge Tunnel, Inverted Siphon and Jokulsa Intake Collector are introduced:

Inverted Siphon

$$-\frac{L_{15}}{gA_{15}}\frac{dQ_{15,1}}{dt} = \left(P_{15,2} - P_{15,1}\right) + \left(el_{15,2} - el_{15,1}\right) + (l_l + f_l)Q_{15,1}|Q_{15,1}| \tag{4.19}$$

$$0 = Q_{15,1} + Q_{15,2} \tag{4.20}$$

Jokulsa Intake Collector

$$0 = \left(0 - P_{16,1}\right) + \left(z_{16} - el_{16,1}\right) + (l_l + f_l)Q_{16,1}\left|Q_{16,1}\right| + \frac{Q_{16,1}}{gA_{16}s_{16}}\frac{dz_{16}}{dt} \tag{4.21}$$

$$A_{ef\,16}\frac{dz_{16}}{dt} = Q_{16,1} + QJ + Q_{spill} \tag{4.22}$$

Jokulsa Surge Tunnel

$$0 = \left(0 - P_{17,1}\right) + \left(z_{17} - el_{17,1}\right) + (l_l + f_l)Q_{17,1}\left|Q_{17,1}\right| + \frac{Q_{17,1}}{gA_{17}s_{17}}\frac{dz_{17}}{dt} \quad 4.23$$

$$(A_{ef\,17} + A_{ef\,15})\frac{dz_{17}}{dt} = Q_{17,1} \quad 4.24$$

Inverted Siphon – Jokulsa Intake Collector Junction

$$P_{16,1} = P_{15,2} \quad 4.25$$

$$0 = Q_{16,1} + Q_{15,2} \quad 4.26$$

Jokulsa Tunnel – Jokulsa Surge Tunnel – Inverted Siphon Junction

$$P_{14,1} = P_{17,2} = P_{15,1} \quad 4.27$$

$$0 = Q_{15,1} + Q_{14,2} + Q_{17,1} \quad 4.28$$

Jokulsa Tunnel modifies the main equation system (fig. 4.1 cas.1) by additional 4 equations for free surface (fig. 4.1 case 2) and 16 equations for pressurized case (fig. 4.1 case 3). Table 4.1 shows structure of equations system for each case.

Table. 4.1 Structure of equations system for each case

Case No	Case Name	Equations system	Equations
1	Jokulsa Tunnel closed	$\{Headrace\ Eq.$	56
2	Jokulsa Tunnel Free Surface	$\begin{cases} Headrace\ Eq.^{*} \\ Jokusla\ Free\ Surface\ Eq. \end{cases}$	60
3	Jokulsa Tunnel Fully Pressurized	$\begin{cases} Headrace\ Eq.^{*} \\ Jokusla\ Fully\ Pressurized\ Eq. \\ Jokulsa\ Surge\ Tunnel\ Eq. \\ Inverted\ Siphon\ Eq. \\ Jokulsa\ Intake\ Collector\ Eq. \end{cases}$	72

*Jokulsa Tunnel - Headrace Tunnel junction applied (eq. 5.13, 5.14)

The introduced equations system can be solved by any capable commercial software like: Matlab, Mathematica, Excel, Mathcad etc. or any capable numerical algorithm coded in a programming language.

4.1 Model limitations due to simplifications

Introduced mathematical model has many limitations and poor defined regions. The most important and significant errors are introduced by:

1. Poor definition of Free Surface / Pressurized transient within upper JT. Inertia discontinuity during transient causes uncertain nonlinear characteristics. The transient region has the strongest influence on surge development in wl. range from 608 [m a.s.l.] to 616 [m a.s.l.].
2. Poor definition of variable geometry tunnels, simplifications of JST, UIC and MST geometry. The tunnels have complicated geometry which had to be simplified. MST overbreak order of magnitude is 20% [4] moreover the tunnel has additional niches which have significant volume and are not modeled. Large and rapid variation of geometry causes errors in particular surge cases.
3. Constant friction loss coefficient which causes undamped oscillations in long simulation time.
4. Constant leakage coefficient. The leakage depends on waterways hydraulic history. The value of coefficient should decrease with time reducing damping effect.
5. Coarse Tunnel Elements distribution. It is impossible to read all results corresponding to powerplant sensors. The additional calculations are necessary to obtain particular data.
6. No waterhammer delay effect. Pressure information about valve closure instantaneously reach Jokulsa Tunnel and Halslon Reservoir. Lack of the delay introduce initial time shift (order of 20 [s]) and modifies the flow pattern by incorrect pressure distribution within waterways just after trip.

5 MATLAB SOLUTION METHOD

Matlab R2008a package has been chosen to solve the Karahnjukar mathematical model due to accessibility and simple language structure. The package contains vast amount of tools which can be used for obtaining the solution [11]:

- Linear interpolation
- Trapezoidal integration
- Linear Equations Solver
- Differential Algebraic Equations Solver

Calculations are carried out in 3 sub-programs as shown in table 5.1

Table 5.1 KAR package

Sub-program	Name	Function
1	Pre-processor	• input data load • calculation of Initial Conditions Vector
2	Solver	• calculation of Solution Vector • save solution vector
3	Post-processor	• calculate statistics • plot graphs

Data flow between each sub-program is shown in figure 5.1

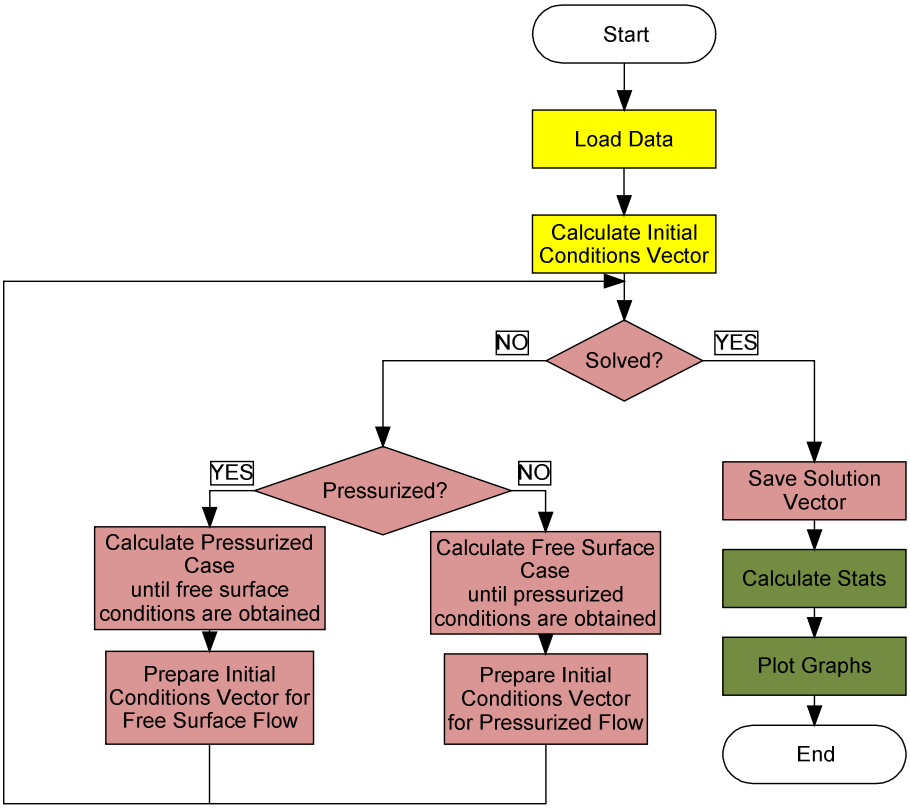

Figure 5.1 Data flow between the subprograms; Colour key from table 5.1

5.1 Pre-processor

Karahnjukar HEP and Case data are loaded from 2 external files and transferred into matrices for further functions defining:

1. Powerplant discharge function
2. Jokulsa Tunnel discharge
3. Reservoirs water level
4. Gates position
5. Simulation time

Case data, variable

6. Area functions
7. Volume functions
8. Head loss functions
9. Spill functions

Powerplant data, constant

Initial conditions vector is a set of initial values for each equation defining Karahnjukar mathematical model. Since the initial state is assumed to be steady, all differential terms are neglected and the equations can be simplified to a linear system.

5.2 Solver

Since presented Karahnjukar HEP mathematical model is a system of stiff, Differential Algebraic Equations, the "ode15s" solver is used. The solver is based on the Numerical Differentiation Formulas [12, 13]. Ode15s settings are shown in table 5.2.

Table 5.2 ode15s solver settings

Parameter	Value	Description
Maximal Timestep	0.5 [s]	Upper bound on solver step size
Relative Tolerance	1%	Measure of the error relative to the size of each solution component
Absolute Tolerance	0.1%	Threshold below which the value of the solution component is unimportant

If an event: Jokulsa Tunnel water level – Inverted Siphon impact; is detected during the computations, solver stops and the case switch occurs. The solution vector from the current solution is transferred as initial vector for the next case. The computation is finished when current time reaches the given time boundary. The solution vector is saved to Excel file for further processing.

Tolerances and timestep are chosen empirically during program tests. Smaller values would negligible influence on the solution but they would significantly increase computation time.

5.3 Post-processor

Post-processor bases on Matlab functions and is responsible for graphical representation of calculated data and calculation of surge statistics. Since solver results are saved into Excel file, data can be processed manually in any spreadsheet editor.

6 COMPARISON OF CALCULATIONS AND MEASUREMENTS

Several water pressure gauges and flow discharge meters are installed in the reservoirs, ponds and the waterways of the project. The most important meters can be read online from the powerstation control and monitoring system. Location of each meter is also shown in figures below and considered meters are listed in Table 6.1. The calibration is shown in the last column and has to be added to the readings to obtain the correct results.

Water pressure sensors were used for initial monitoring and evaluation of head losses and transients along the Headrace Tunnel. Some of these water pressure meters is operated by off grid solar cell or wind propeller and collects the data to data loggers, which can be downloaded by wireless communication.

Since the model provides only nodal solution, in some cases it is necessary to interpolate parameters between the nodes using formulation 2.4. Arbitrary parameters close to the joints are assumed to be similar to parameters at corresponding nodes and can be taken directly from the solution and modified by appropriate calibration.

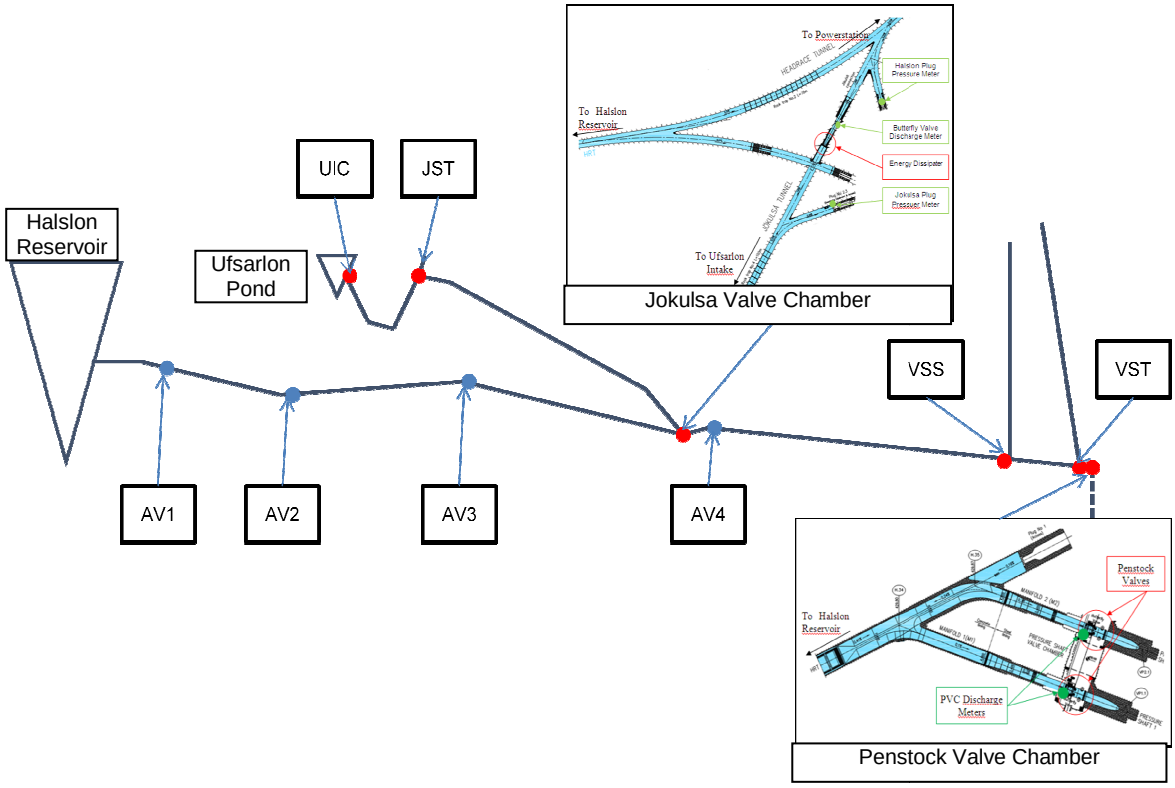

Figure 6.1 Holsufs Surge Shaft and Midfell Surge Tunnel Pressure Meters

VSS1, VSS2, VST1 and VST2 are 4 identical (for safety reason) high frequency pressure meters (fig. 6.2), capable of registering waterhammer. VST sensors were mounted in Midfell Surge Tunnel. The sensors were destroyed in April 2008. VSS sensors are mounted in Headrace Tunnel about 100 [m] upstream of Holsufs Surge Shaft.

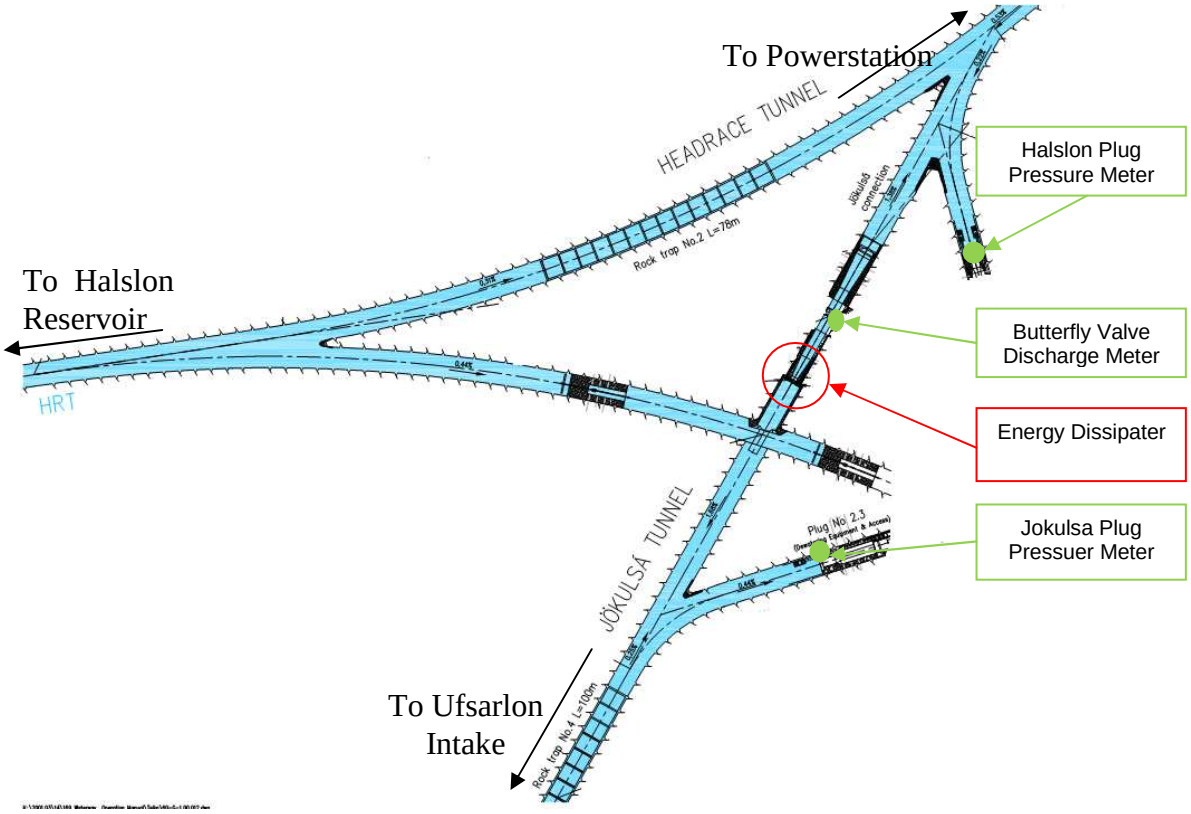

Figure 6.2 Jokulsa Valve Chamber [5]

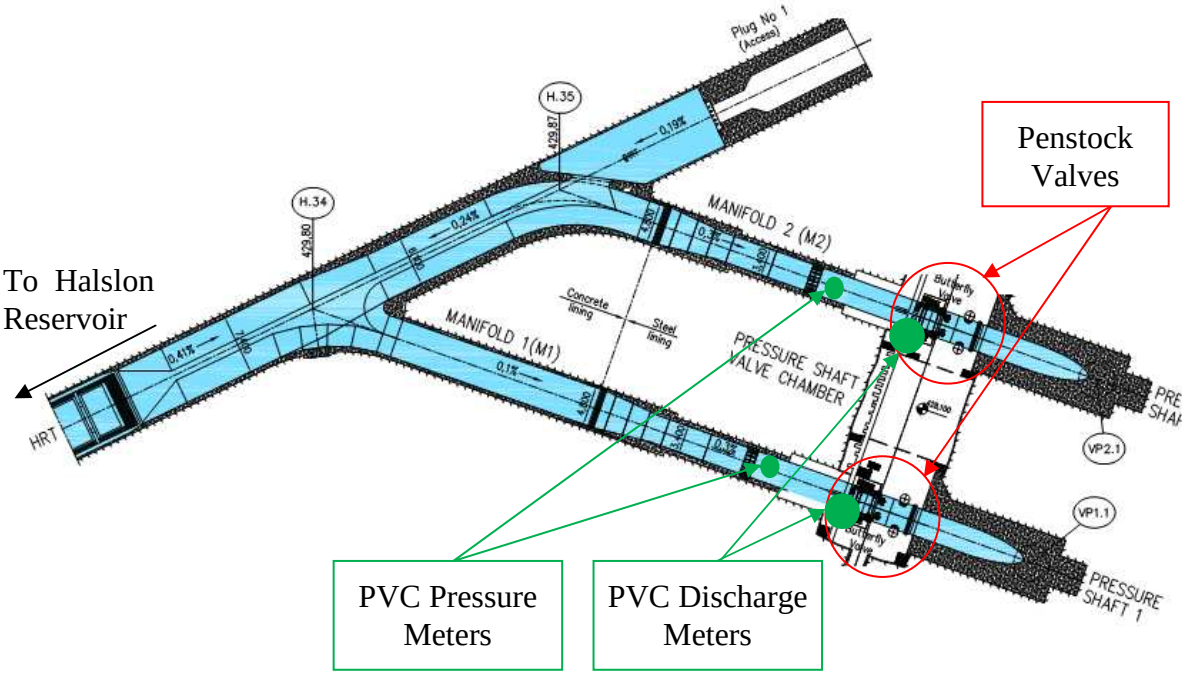

Figure 6.3 Penstock Valve Chamber Pressure and Discharge meters [5]

An ultrasonic flow meter is installed in the Jokulsa Valve Chamber on the steel pipe, just upstream of the Butterfly Valve. The system is a two planes, eight path system, with

an accuracy of ± 2,5 %. The flow meter system provides continuous information on velocity and discharge to the control system.

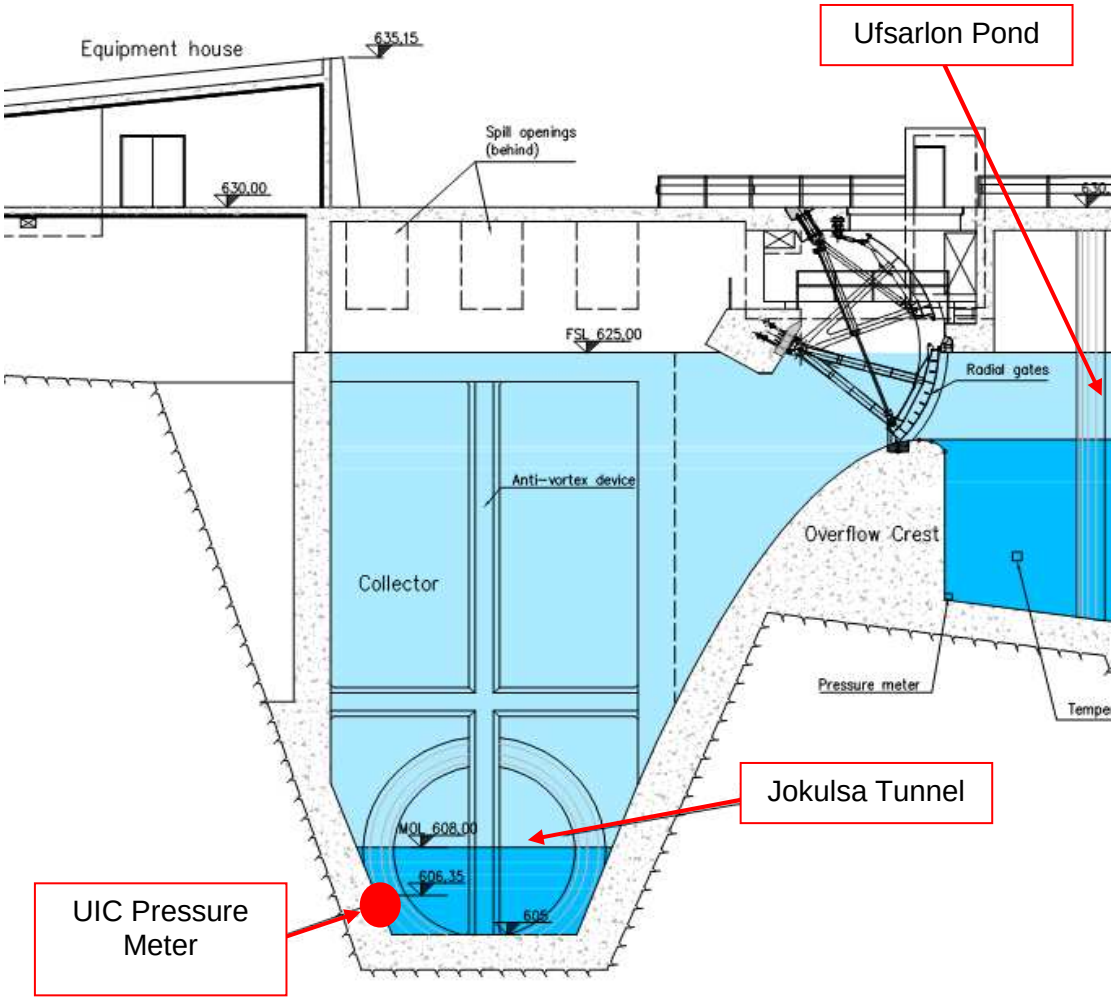

Figure 6.4 Ufsarlon Intake Pressure Meter localization [5]

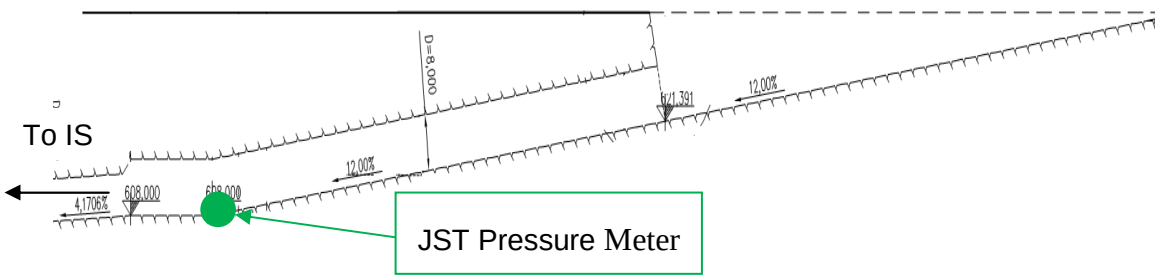

Figure 6.5 Jokulsa Surge Tunnel Pressure Meter [5]

Jokulsa Surge Tunnel Pressure Meter has sampling time 5 [min] and provides average pressure from 5 [min] intervals.

Table 6.1 Sensors characteristics			
Location	Type	Range/Accuracy	Calibration
Velocity Penstock Valve Chamber 1	Acoustic	<1%	
Velocity Penstock Valve Chamber 2	Acoustic	<1%	
Pressure Penstock Valve Chamber 1	MPISGAN	500m /0.05%	-0.29 [m]
Pressure Penstock Valve Chamber 2	MPISGAN	500m /0.05%	-0.77 [m]
Midfell Surge Tunnel VST (damaged)	High freq.		
Holsufs Surge Shaft VSS	High freq.		
Air Vent 2			+1.3 [m]
Air Vent 3			-1.5 [m]
Air Vent 4			+0.1 [m]
Velocity Jokulsa Valve Chamber	Acoustic	2.5 %	
Pressure Halslon Plug		2.5 %	
Pressure Jokulsa Plug		2.5 %	-2 [m]
Jokulsa Surge Tunnel		Provides average measurement	
Ufsarlon Intake Collector		Provides average measurement	

6.1 Influence of leakage on the flow

Since the simplified leakage formulation (fig 2.10) does not take into account the full complexity of the phenomenon, it necessary to estimate proper leakage coefficient empirically by comparing to measurements. The 09.04.2008 trip was chosen as a base measurement and compared with calculations for 5 different leakage coefficients as shown in table 6.2. Due to well defined powerplant design data, the leakage coefficient is the only parameter used for calibration.

Table 6.2 Initial values for leakage test; 04.09.2008 case

Name	Value	Unit
Halslon Reservoir water level	606.5	[m a.s.l.]
Discharge to the station before trip	131.5	[m^3/s]
Discharge to the station after trip	22.18	[m^3/s]
Valve closing time	16	[s]
Leakage coefficient	0; 1; 2; 3; 4	10^{-7}[1/s]
Discharge in Jokulsa Tunnel before trip	Valve closed	

Fitting is evaluated on basis of the smallest difference between measurement and calculations. The time of extreme occurrence was not taken into account due to MST geometry simplifications which affect surge period.

The best fitting to measurement is obtained for k=2e-7 [1/s] (fig 6.6) with peak outflow from the system 9.8 [m3/s] as shown in figure 6.7.

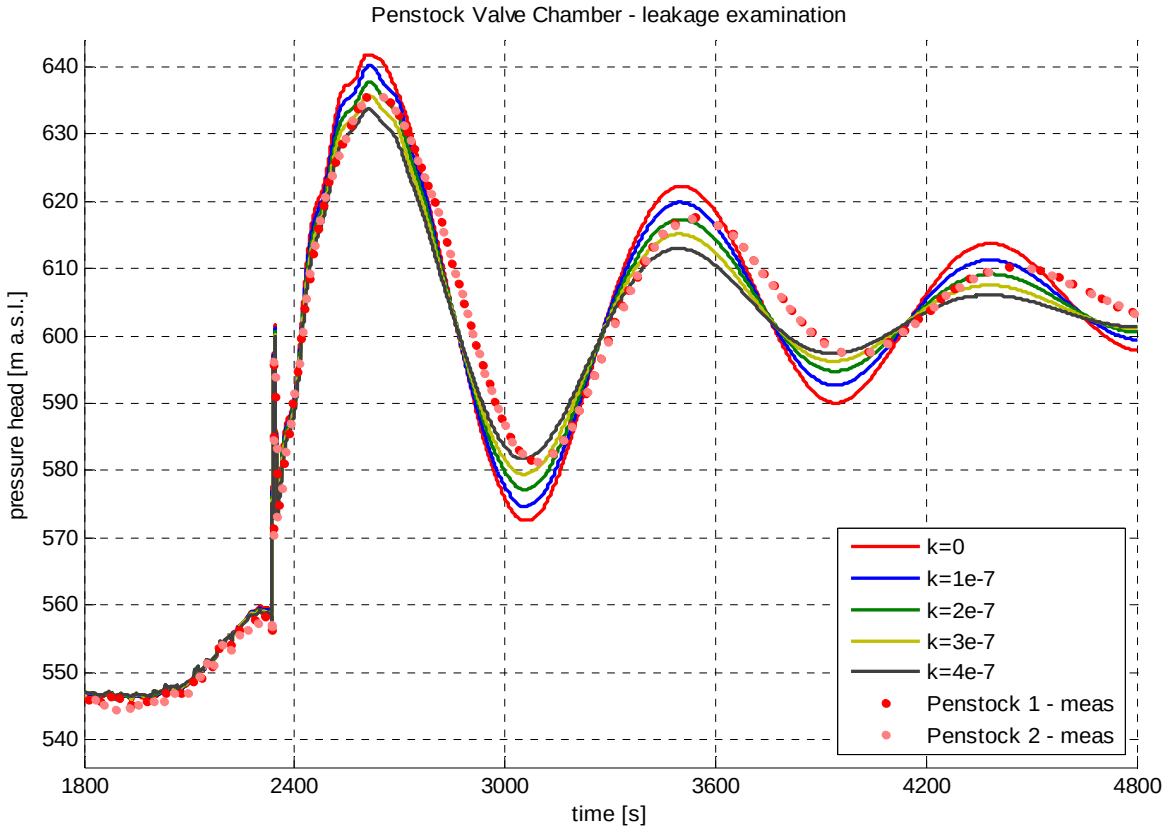

Figure 6.6 Fitting evaluation for case 09.04.2008 – Penstock Valve Chamber

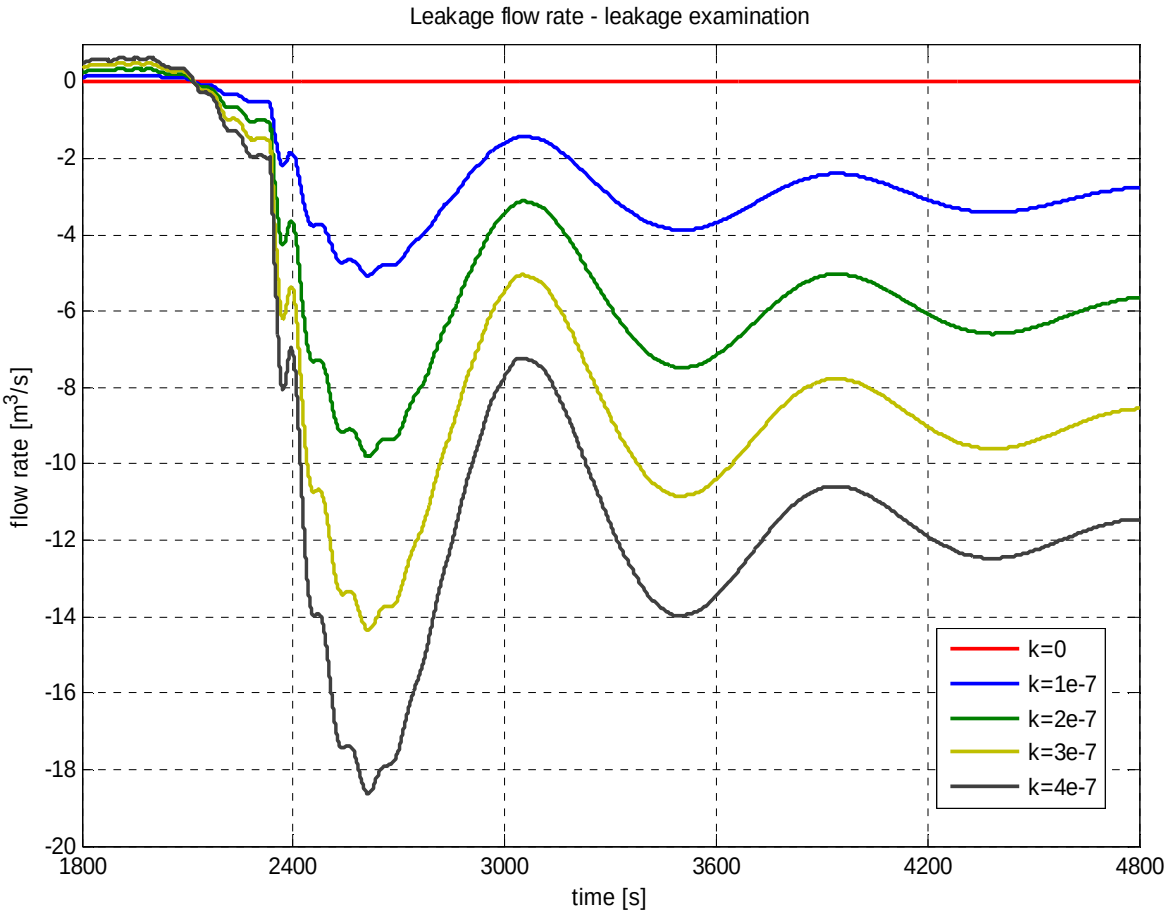

Figure 6.7 Outflow from the system due to leakage; case 09.04.2008

Particular characteristics shown in figure 6.7 oscillate around equilibrium. Decrease of leakage in time is expected due to rock saturation. It can be seen that leakage is a counter discharge against the main waterways flow, thus it acts as a damper reducing surge. Constant leakage coefficient introduces discharge error to the model in long simulation time.

Applied leakage has no influence on period because it does not change significantly the water volume in the system.

6.2 The power plant trip at 18.12.2010

Trip input discharge data were taken directly from the measurements and smoothed by Simple Moving Average of 5 values. Leakage is assumed to have an influence on the flow parameters, thus a leakage coefficient is $2\ 10^{-7}$[1/s] is applied.

The trip occurred due to the smelter failure and is the best measured case from all considered trips. The absolute time of the simulation is from 16:59:40 to 17:59:40.

Table 6.3 Initial values; 18.12.2010 case

Name	Value	Unit
Halslon Reservoir water level	616.6	[m a.s.l.]
Ufsarlon Pond water level	622.5	[m a.s.l.]
Jokulsa Tunnel discharge	12.1	[m^3/s]
Discharge to the station before trip	130	[m^3/s]
Discharge to the station after trip	10	[m^3/s]
Valve closing time	15	[s]
Ufsarlon Intake Gate opening	100%	

Due to presence of surge devices, the momentum of water within waterways is not destroyed quickly after valve closure and continues to flow. Since steady powerplant operation indicates no initial discharge to surge devices, the moving water from Headrace Tunnel has to pass its momentum to HSS and MST. Since it is not possible to move HSS and MST water mass instantaneously, the pressure at the bottom o surge devices has to increase to initiate mass movement. The characteristic pressure peak just after valve closure is shown in figure 6.9. Shape of the peak is dependent on valve closing time, initial powerplant discharge and geometry of surge device.

Water level in MST stops rising when the pressure in the tunnel at the surge chamber inlet is balanced by the pressure created by the head in the chamber. At this time the wl. in MST will be higher than in Halslon Reservoir (fig 6.8) and reversed flow will occur, setting up a long period oscillation. The oscillations are eventually damped out by friction in the tunnels.

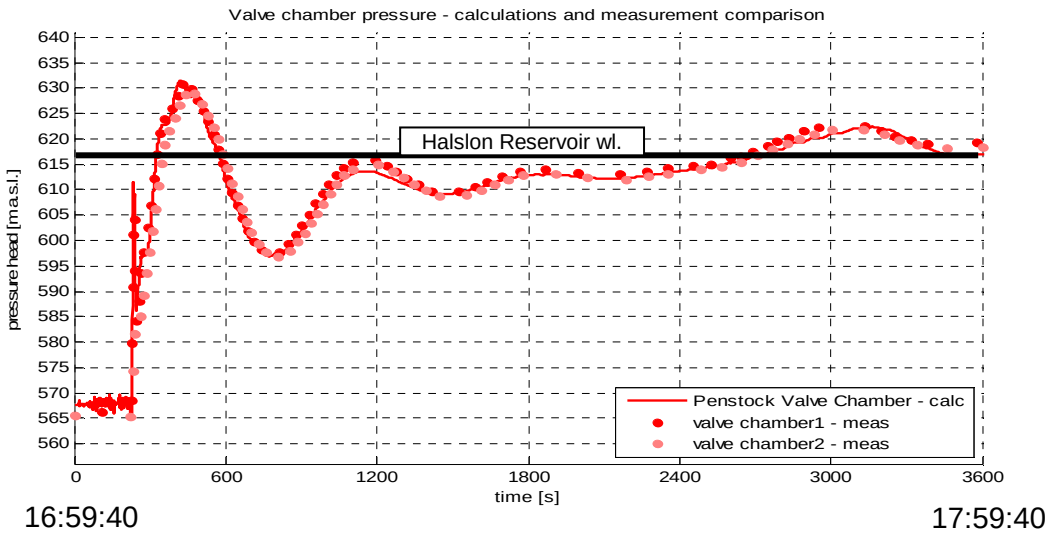

Figure 6.8 Penstock Valve Chamber pressure comparison; case 18.12.2010

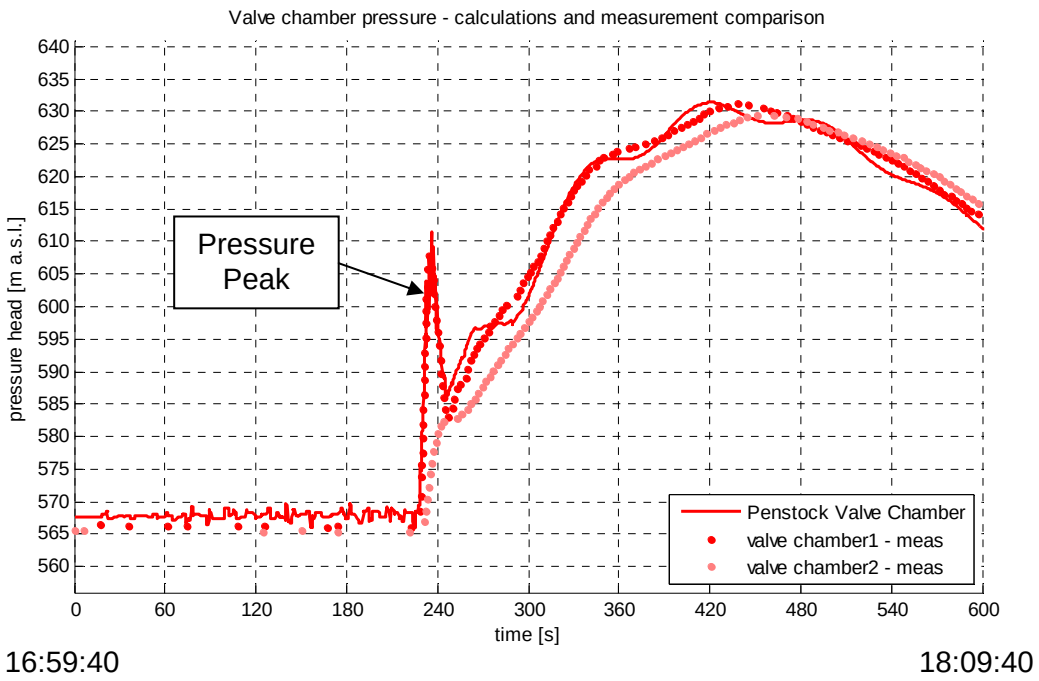

Figure 6.9 Penstock Valve Chamber pressure comparison; case 18.12.2010

PVC Pressure meters cannot detect waterhammer effect due to relatively low sampling time. Pressure waves can be detected by VST and VSS sensors.

The calculated Halslon Plug Pressure is taken directly from the solution at joint 7. Since the Pressure Jokulsa Plug Meter is situated upstream of the Jokulsa Valve Chamber it is necessary to calculate the corresponding pressure by subtracting Dissipater (eq. 2.20) head loss (hl_D) from pressure calculated at the joint.

$$P_{JokulsaPlug} = P_7 - hl_D(Q) \qquad 6.1$$

Here Q is Jokulsa Tunnel discharge. The plug pressure comparison is shown in figure 6.10.

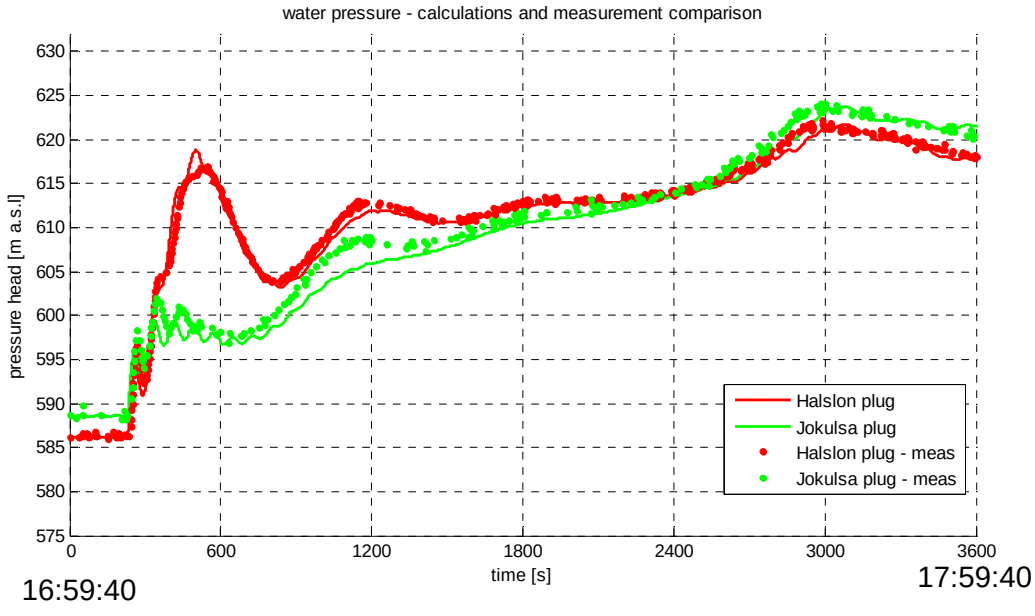

Figure 6.10 Plugs pressure comparison; case 18.12.2010

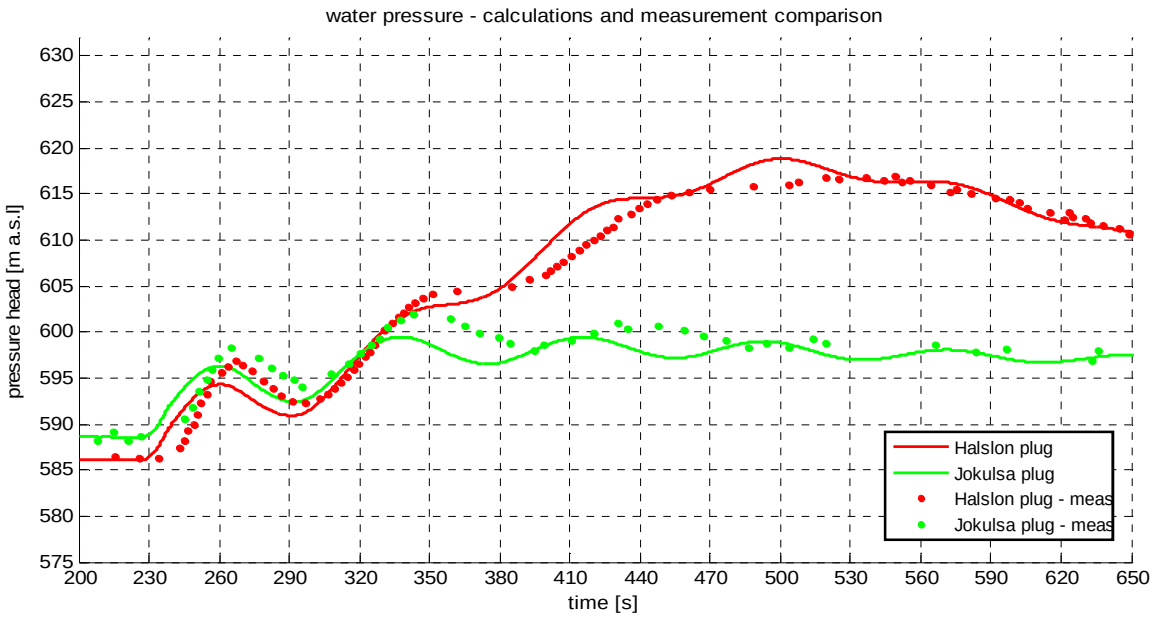

Figure 6.11 Plugs pressure comparison; case 18.12.2010

Superposition of different waves is clearly visible in figure 6.11. The additional oscillations are introduced by surge in MST and HSS.

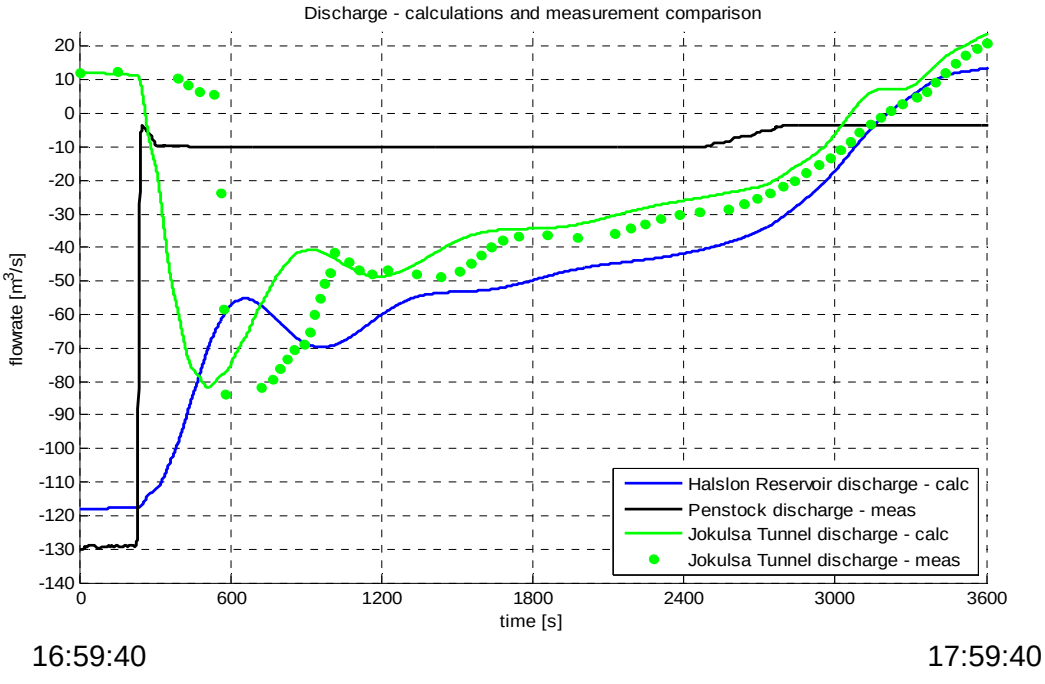

Figure 6.12 Jokulsa Tunnel Discharge comparison; case 18.12.2010

As shown in figure 6.2, the Jokulsa Tunnel Discharge meter is placed between 2 plug meters thus the surge time coincidence between Halslon Plug, Jokulsa Plug and Jokulsa Discharge meter should occur. The Jokulsa discharge measurement (fig 6.12) suggests that the surge starts about 300 [s] after the valve closure. Such significant time shift is not

indicated by the plug meters. Hence, comparison of figure 6.11 and 6.12 suggests a clock error of Jokulsa Tunnel Discharge meter.

The measurement noise shown in figure 6.13 can be caused by sensors and logger problems or trapped air which expands during the surge.

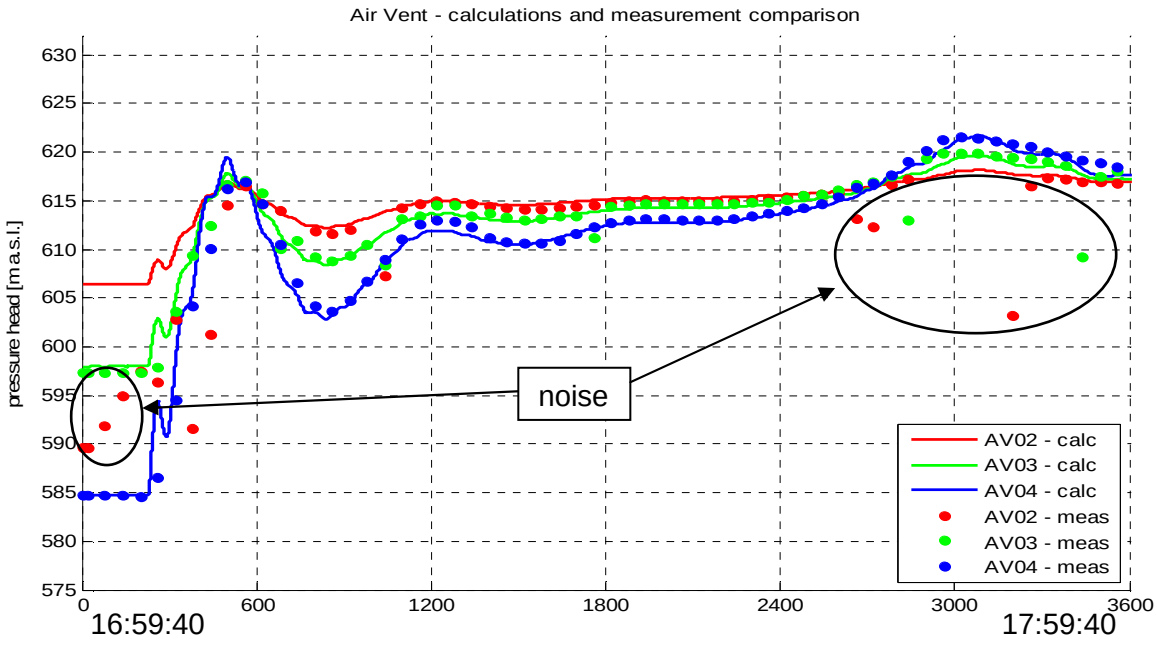

Figure 6.13 Air Vent pressure comparison; case 18.12.2010

Figure 6.14b shows UIC curve discrepancy between measurement and calculations due to simplifications of upper JT geometry. Oscillations indicated by water mass exchange between UIC and JST is marked. The discrepancy between measurement and calculations suggest to low headloss in UIC and JST.

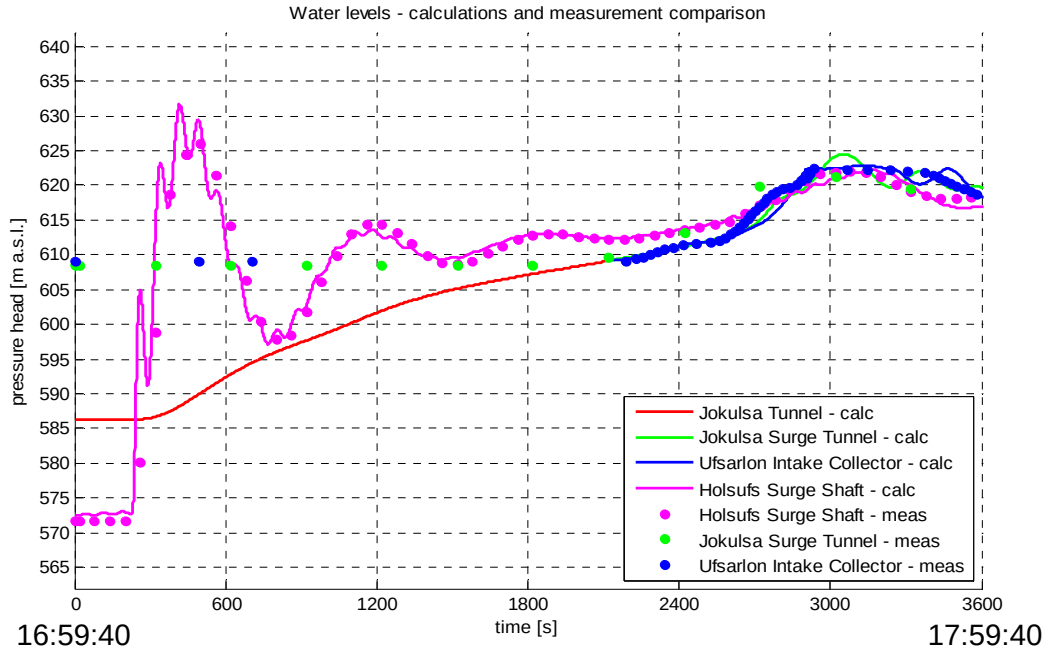

Figure 6.14a Water level comparison; case 18.12.2010

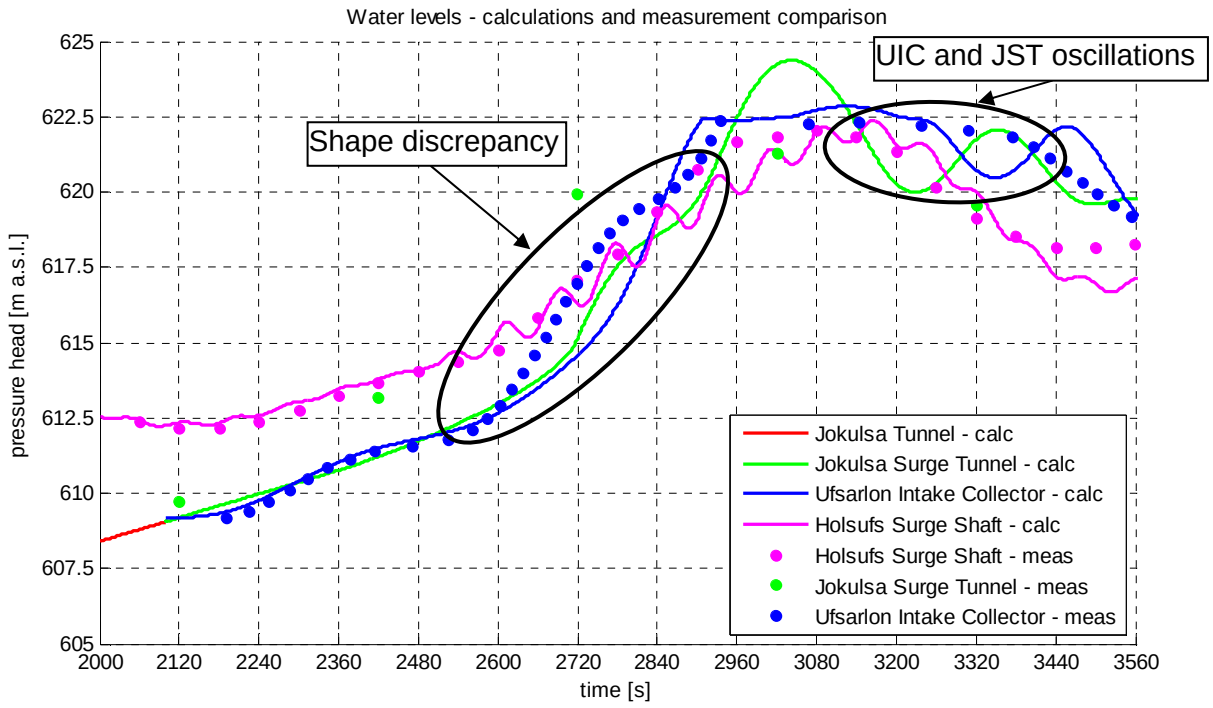

Figure 6.14bWater level comparison; case 18.12.2010

Maximal outflow from the system due to leakage (fig 6.16) is 6.4 [m^3/s] and is expected to occur 45 [min] after the trip.

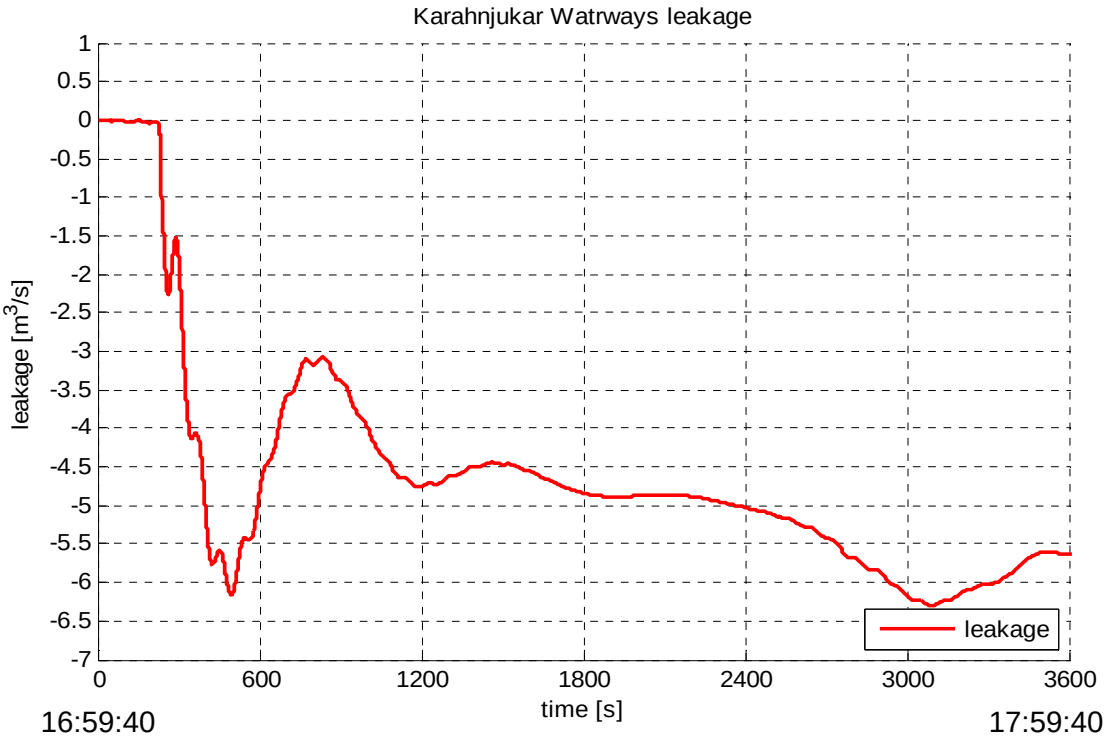

Figure 6.15 Outflow from the system due to leakage; case 18.12.2010

6.3 The power plant trip at 11.08.2009

The absolute time of the simulation is from 11:32:00 to 12:32:00.

Table 6.4 Initial values; 11.08.2009 case		
Name	Value	Unit
Halslon Reservoir water level	615.3	[m a.s.l.]
Ufsarlon Pond water level	624.07	[m a.s.l.]
Jokulsa Tunnel discharge	45.12	[m^3/s]
Discharge to the station before trip	106	[m^3/s]
Discharge to the station after trip	8.76	[m^3/s]
Valve closing time	15	[s]
Ufsarlon Intake Gate opening	100%	

The trip has typical surge pattern (fig 6.16a) due to pressurized JT flow. Oscillations around equilibrium line is clearly visible. The line is above HR wl. due to UP wl. 624.07 [m a.s.l.]; higher than HR wl.

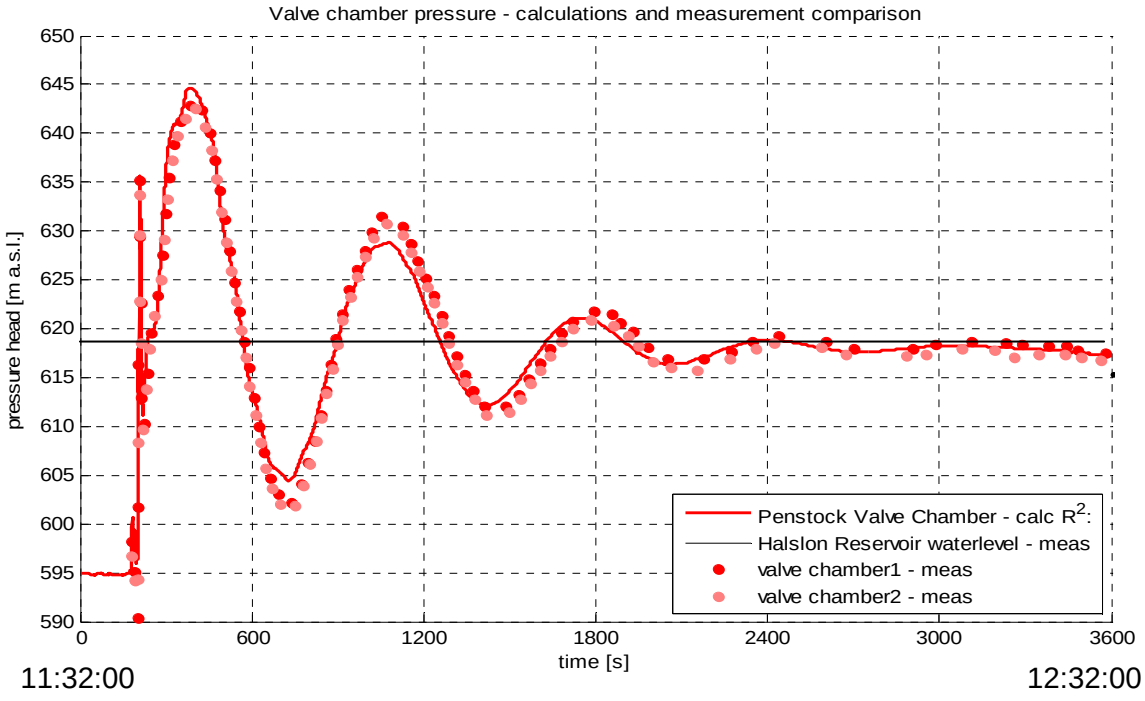

Figure 6.16a Penstock Valve Chamber pressure comparison; case 11.08.2009

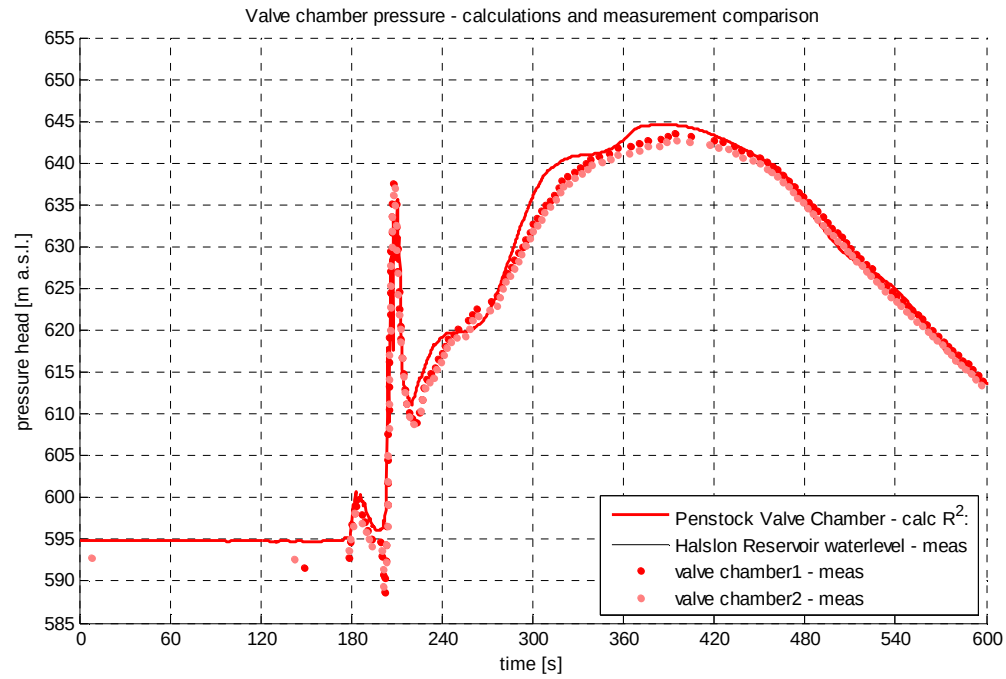

Figure 6.16b Penstock Valve Chamber pressure comparison; case 11.08.2009

Significant time shift between measurement and calculation is shown in figure 6.17. The discrepancy confirms the suspicion about Jokulsa Tunnel Discharge meter error observer in figure 6.12.

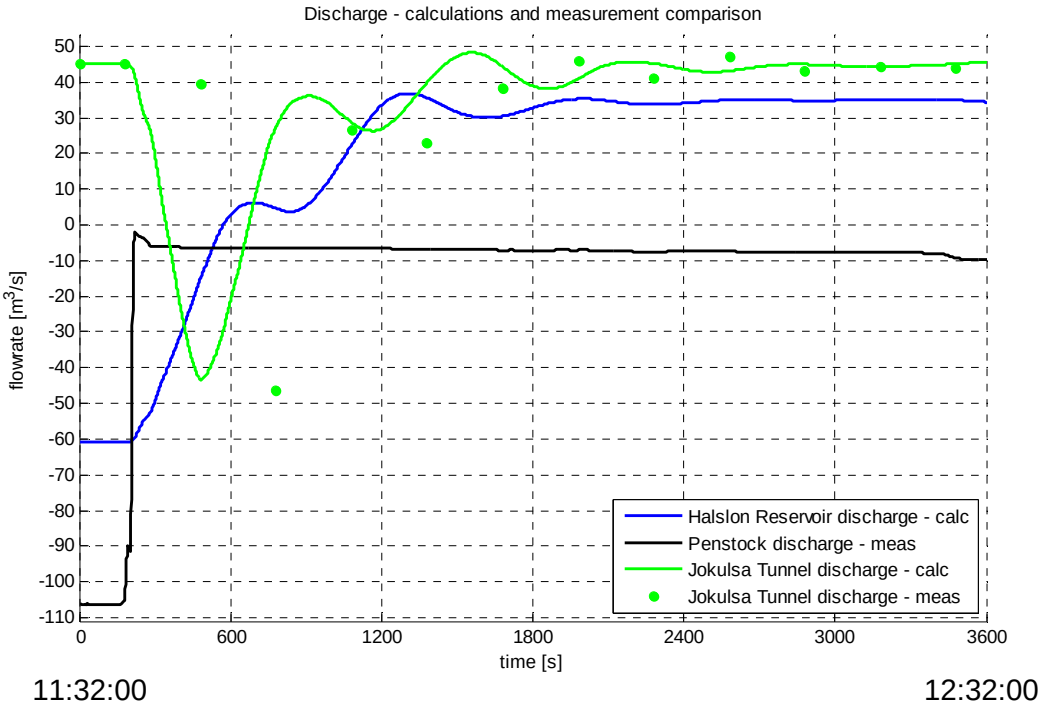

Figure 6.17 Jokulsa Tunnel Discharge comparison; case 11.08.2009

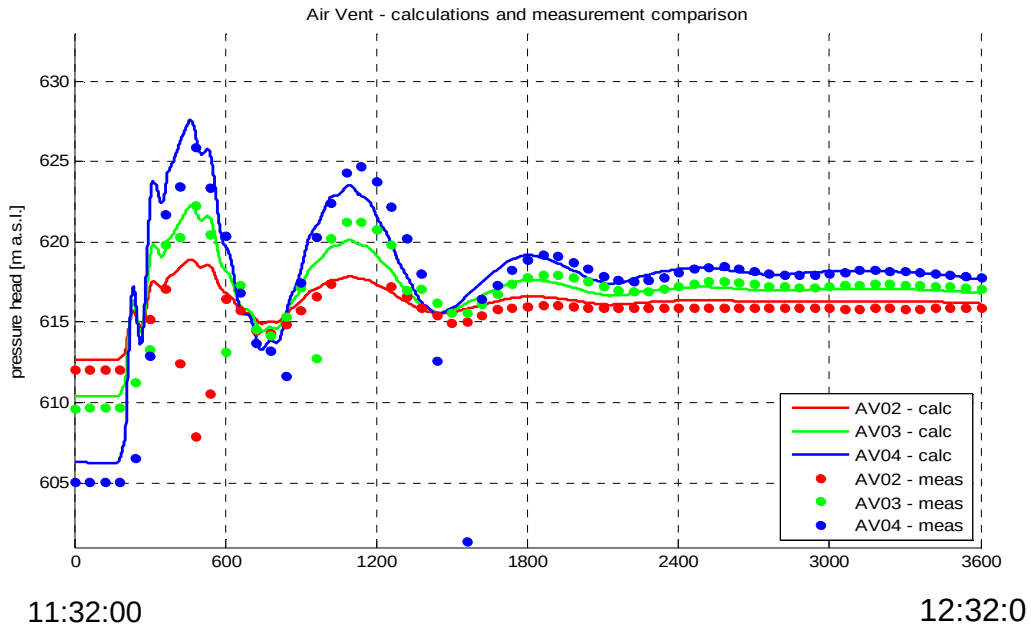

Figure 6.18 Air Vent pressure comparison; case 11.08.2009

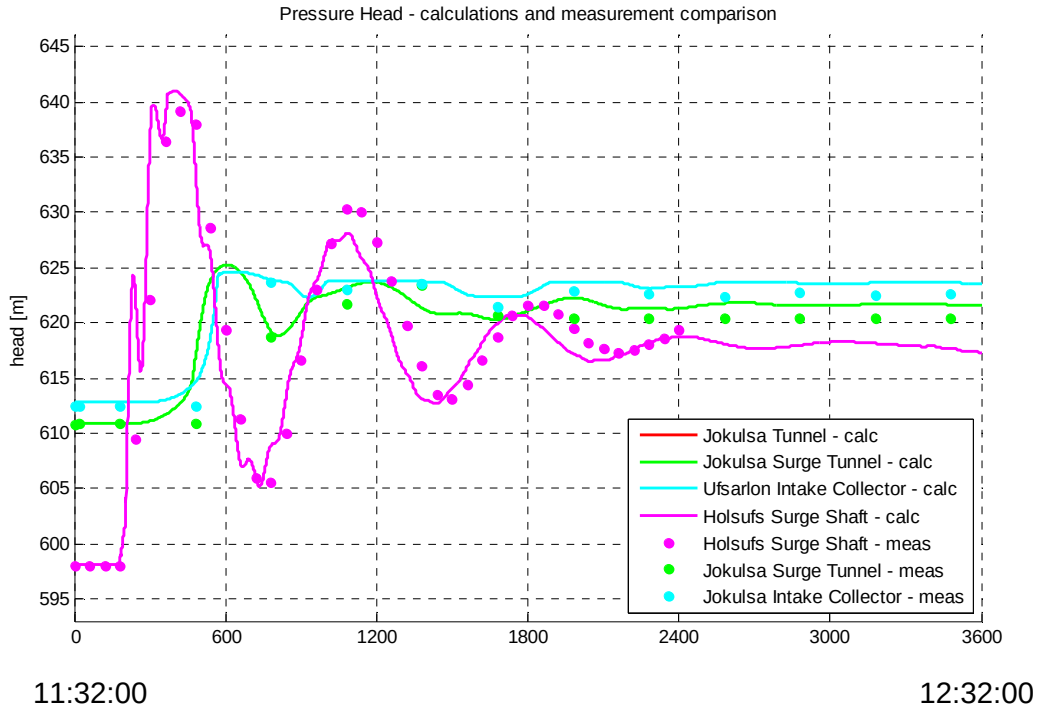

Figure 6.19 Water level comparison; case 11.08.2009

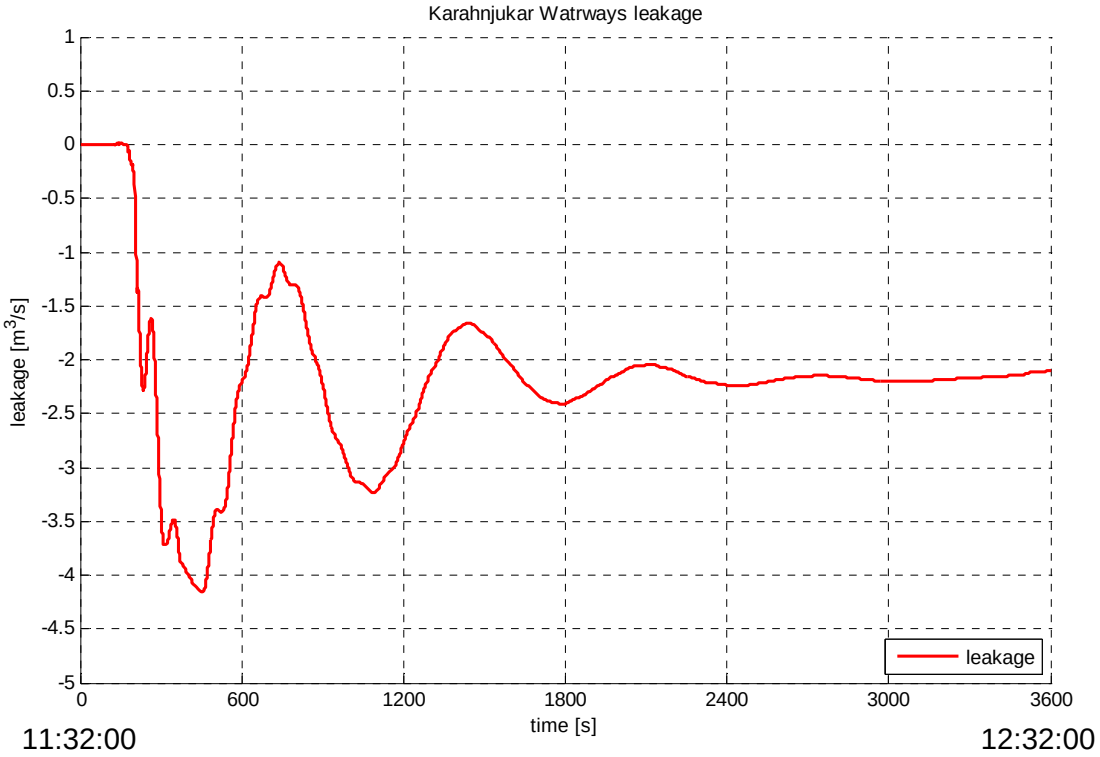

Figure 6.20 Outflow from the system due to leakage; case 11.08.2009

6.4 The power plant trip at 09.04.2008

The absolute time of the simulation is from 11:14:00 to 12:44:00.

Table 6.5 Initial values; 09.04.2008 case		
Name	Value	Unit
Halslon Reservoir water level	606.5	[m a.s.l.]
Jokulsa Tunnel discharge	Valve closed	
Discharge to the station before trip	131	[m3/s]
Discharge to the station after trip	13.2	[m3/s]
Valve closing time	15	[s]

Since the trip is with closed Jokulsa Tunnel, the surge oscillates around equilibrium HR wl. as shown in figure 6.21a.

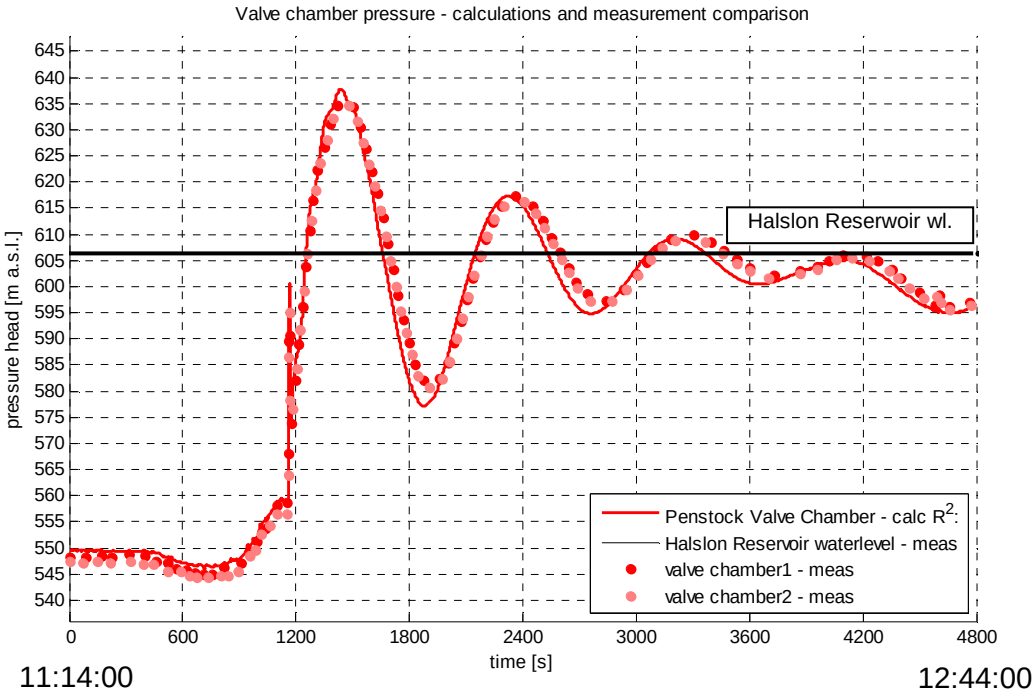

Figure 6.21a Penstock Valve Chamber pressure comparison; case 09.04.2008

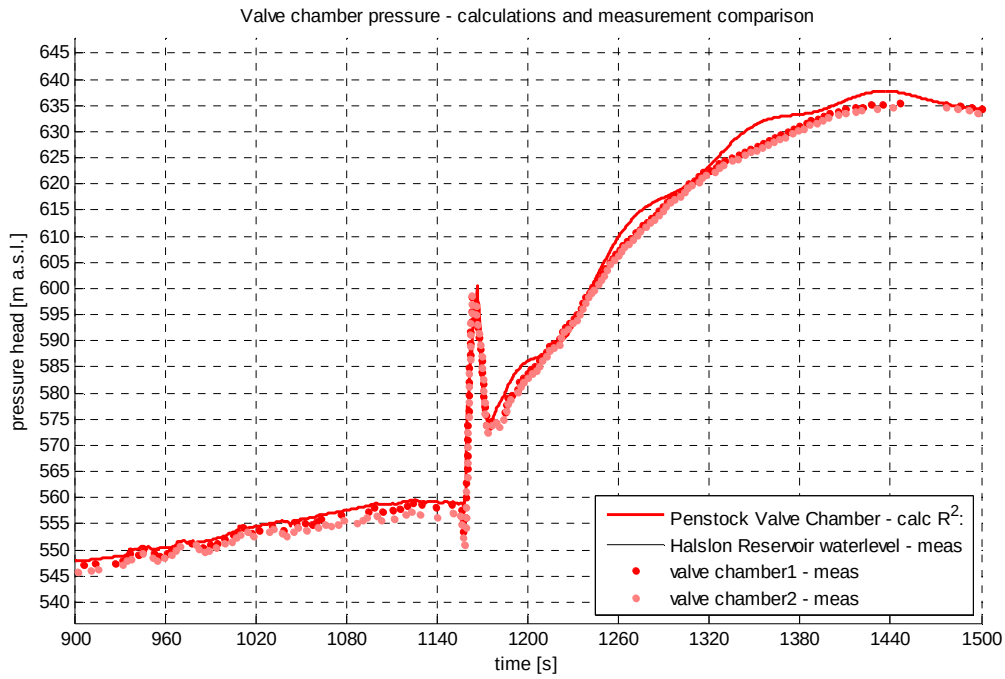

Figure 6.21b Penstock Valve Chamber pressure comparison; case 09.04.2008

Due to wrong TE distribution the Air Vent 1 is placed between TE nodes (app. A). Thus, model does not fit measurements in figure 6.22. The results should be interpolated between the nodes or TE distribution should be changed.

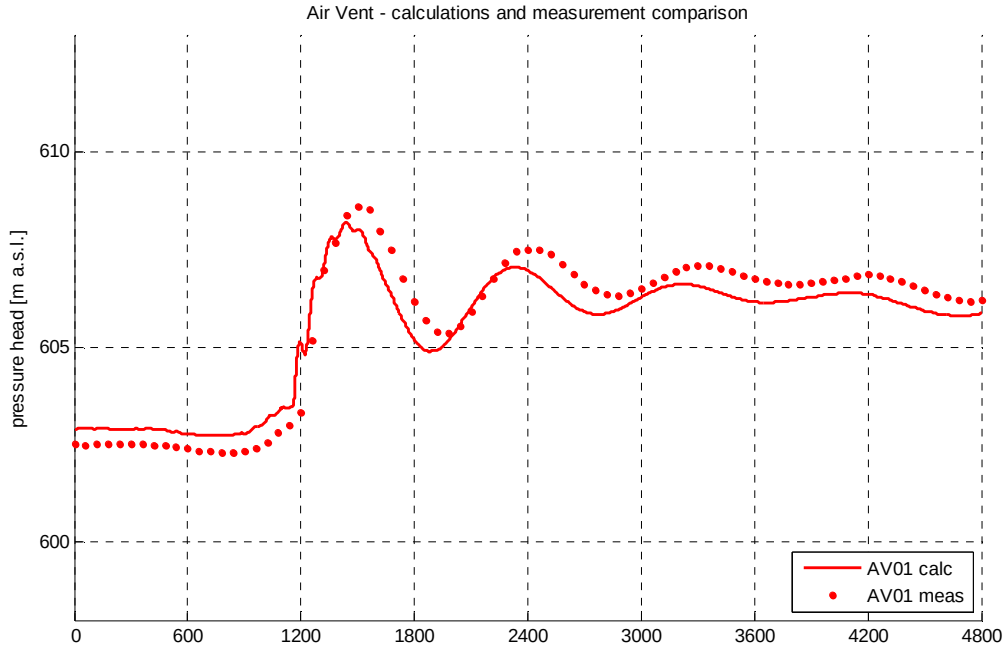

11:14:00 12:44:00

Figure 6.22 Air Vent pressure comparison; case 09.04.2008

Figure 6.23 Holsufs Surge Shaft water level comparison; case 09.04.2008

Due to a low water level in Halslon Reservoir and high powerplant discharge, the base leakage pressure ($P0_1$) is relatively low. Hence, maximum leakage discharge can be as high as 9 [m3/s]. Figure 6.24 shows discharge due to leakage and its significance when powerplant is shutdown. At the 1350 [s], the leakage comes up as a 10% of total flow from the reservoir.

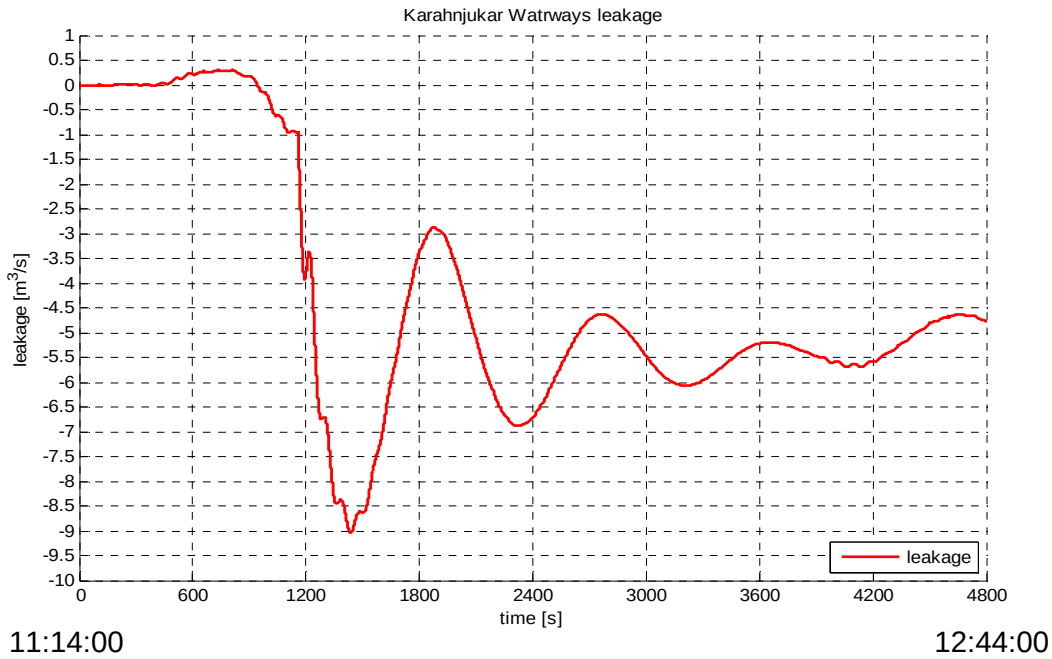

Figure 6.24 Outflow from the system due to leakage; case 09.04.2008

6.5 The power plant trip at 12.13.2007

The absolute time of the simulation is from 01:40:00 to 03:10:00.

Table 6.6 Initial values; 13.12.2007 case		
Name	Value	Unit
Halslon Reservoir water level	623.8	[m a.s.l.]
Jokulsa Tunnel discharge	Valve closed	
Discharge to the station before trip	67.2	[m3/s]
Discharge to the station after trip	7.3	[m3/s]
Valve closing time	15	[s]

Significant period difference between measurement and calculation is shown in figure 6.28. The oscillation pattern suggests local lack of water mass within MST (niches, D&B overbreak) due to simplified geometry. Further study on Surge Tunnel geometry is necessary.

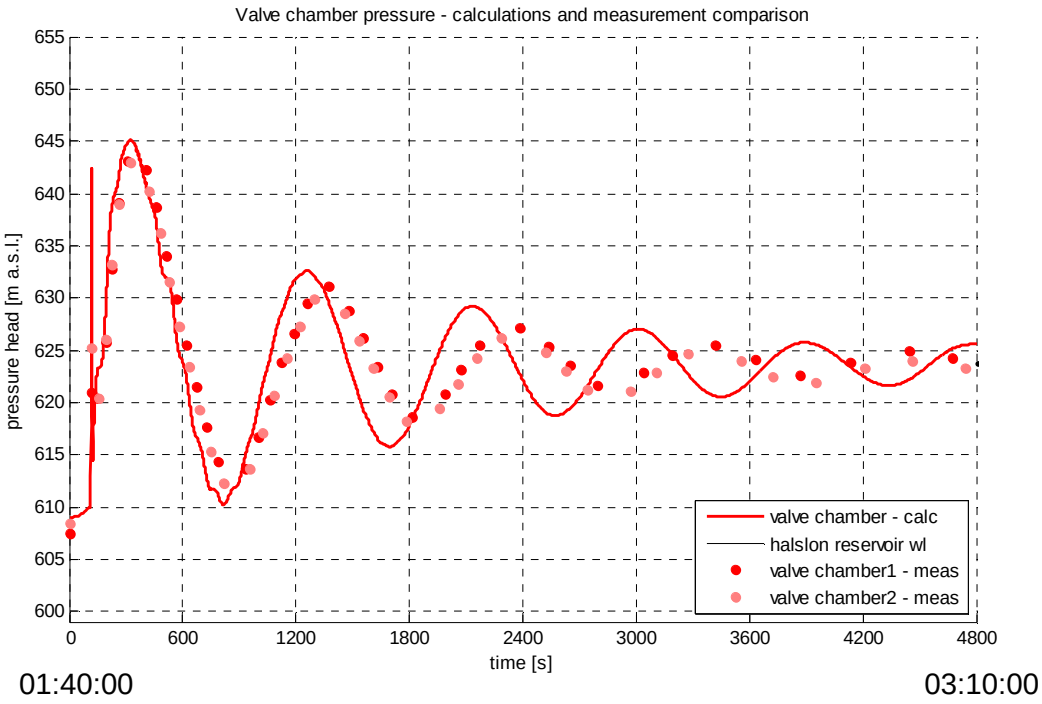

Figure 6.25a Penstock Valve Chamber pressure comparison; case 13.12.2007

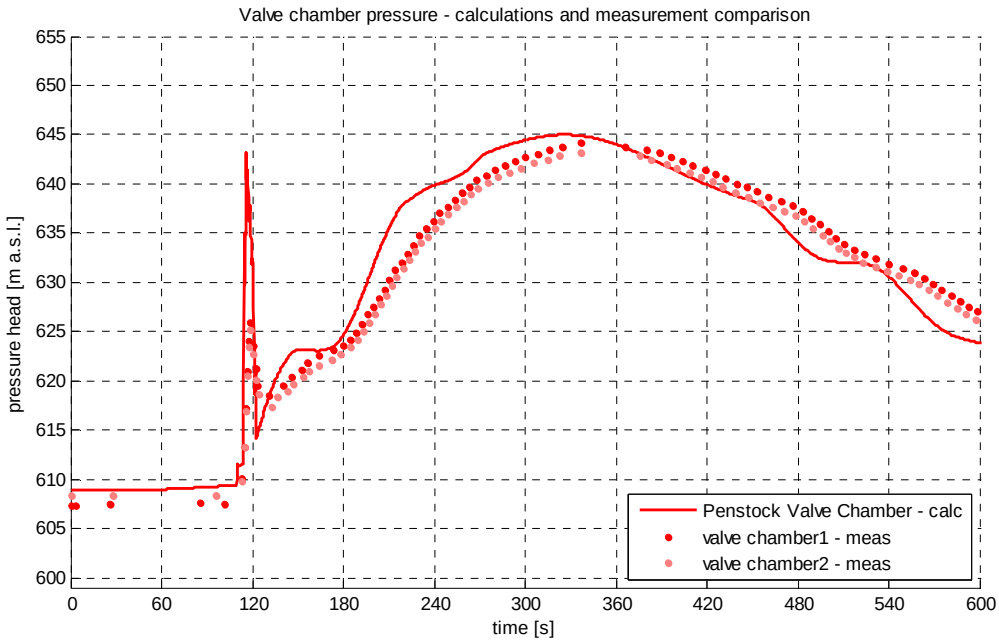

Figure 6.25b Penstock Valve Chamber pressure comparison; case 13.12.2007

Figure 6.26 shows significant discrepancy of Air Vents pressure measurement and calculations. Low damping for low flow rate is also clearly visible due to constant TE friction coefficients.

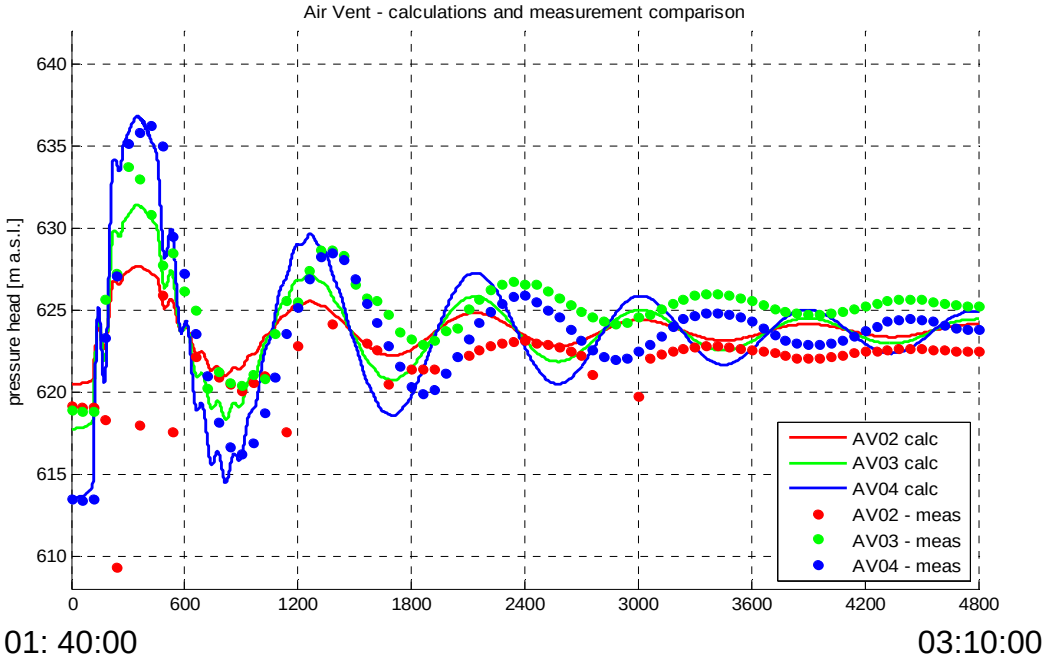

Figure 6.26 Air Vent pressure comparison; case 13.12.2007

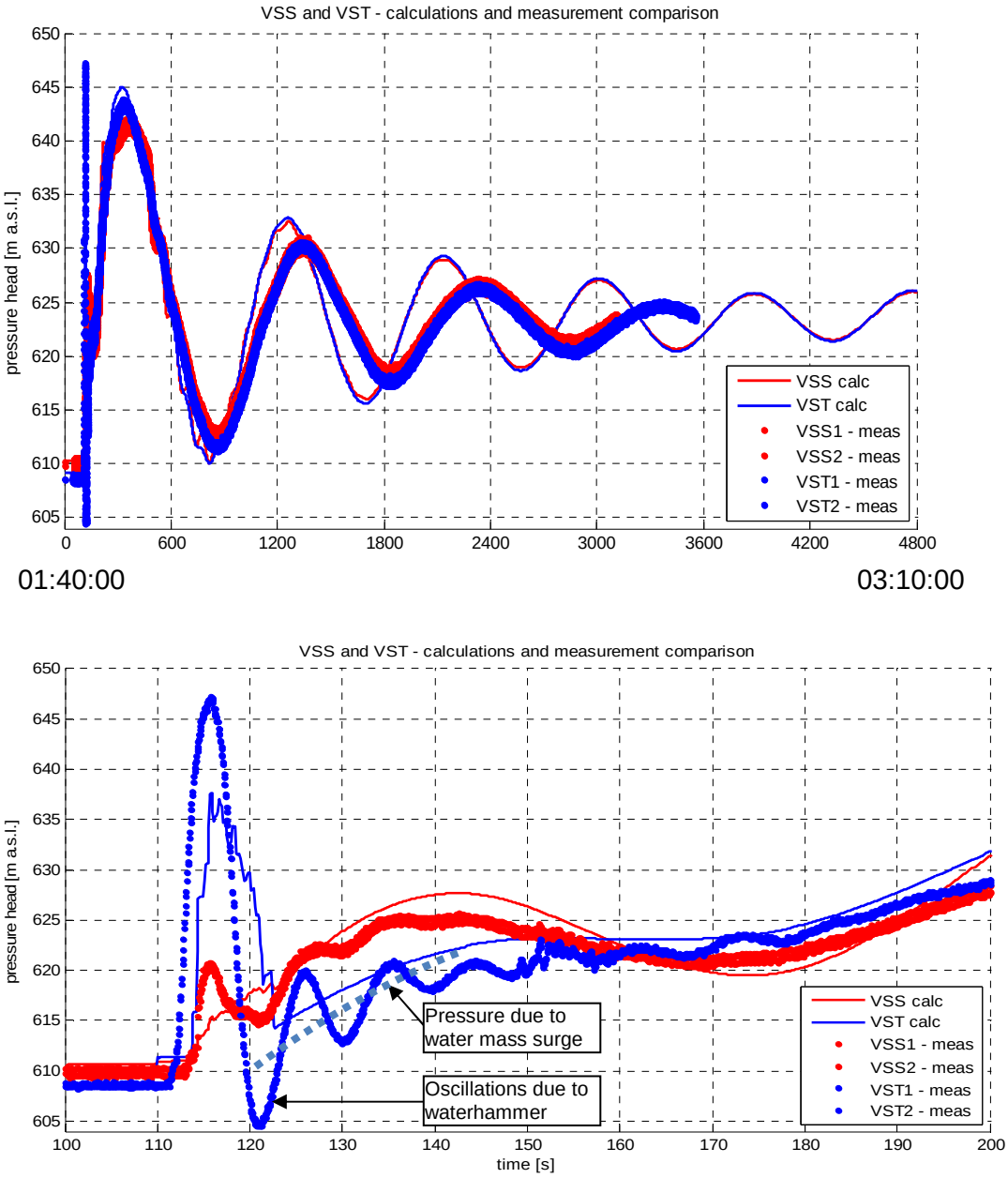

Figure 6.27 VSS and VST pressure comparison; case 13.12.2007

Waterhammer pressure vibrations are shown in figure 6.27. The pressure wave is totally damped in 70 [s] after valve closing. Since waterhammer effect is not included in TE, the model is capable to predict mass surge which is with good agreement with measurements. The chart suggest that Holsufs Surge Shaft is an effective surge device that reduces propagation of the waterhammer upstream of HST.

Figure 6.28 shows outflow from the system. The leakage is lower than in the previous cases (high powerplant discharge) due to small pressure differences between the initial flow and during the surge.

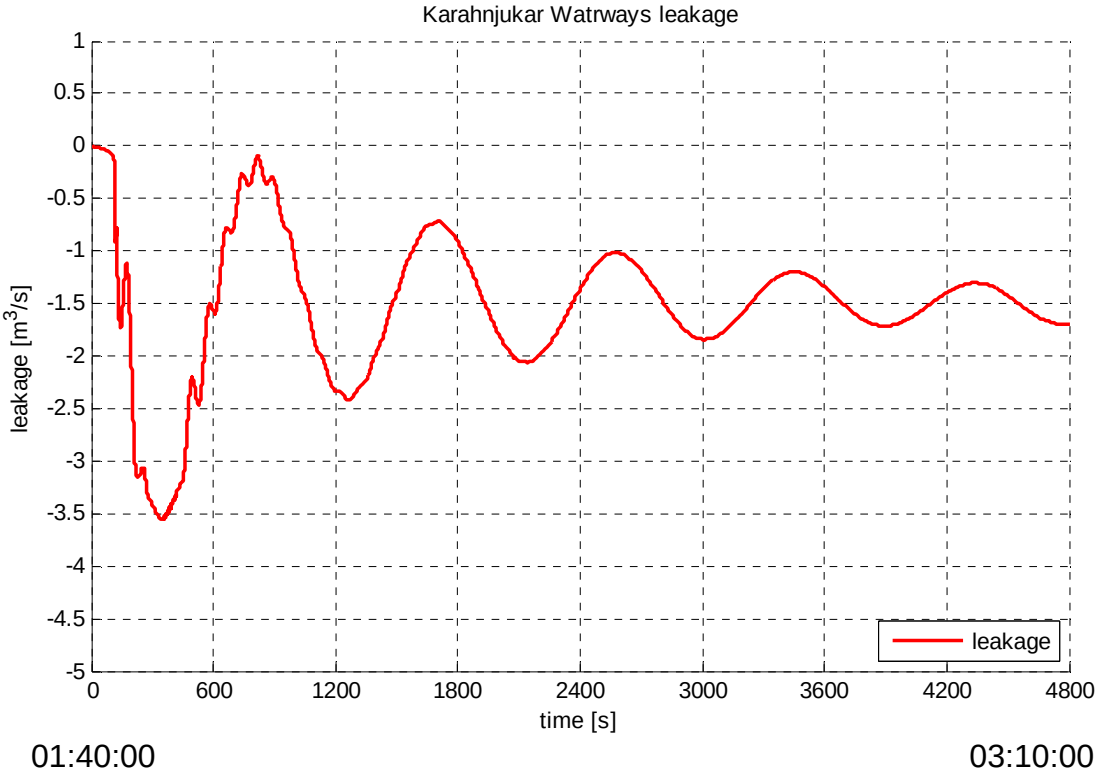

Figure 6.28Outflow from the system due to leakage; case 13.12.2007

7 IMPLEMENTATION OF TUNNEL ELEMENT METHOD IN POLAND

Energetic hydropotential of Poland is small due to low and unevenly distributed precipitation, high soil permeability, and low land inclination.

The possibilities of hydropower production in Poland are unevenly distributed. Most of the potential (about 68%) is within the Wisla River basin, then Dunajec, San, Bug, Odra, Bobr, and Warta as shown in figure 7.1.

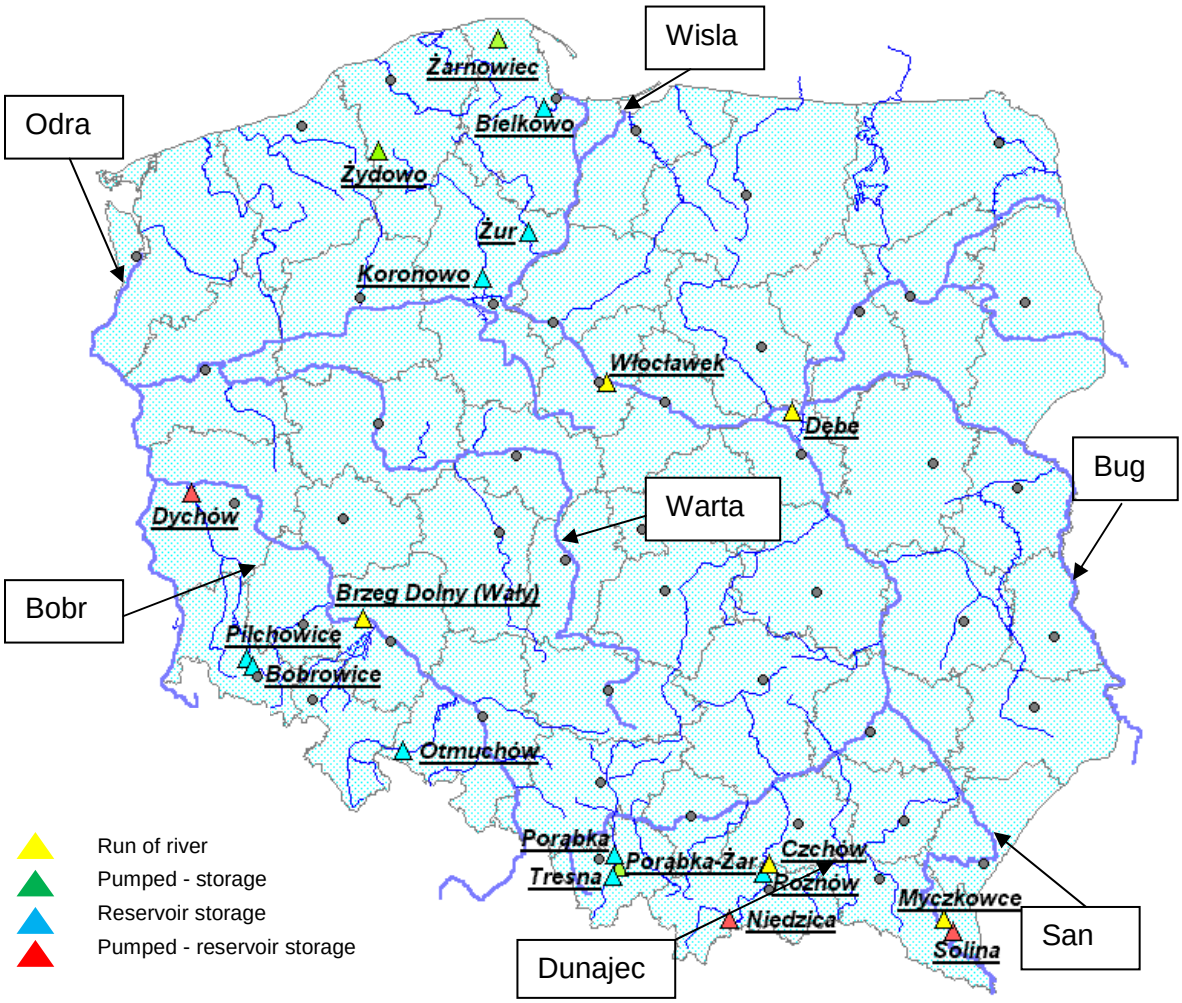

Figure 7.1 Hydropowerplants localization in Poland

Currently hydropower has a 1.5% share in the electricity production. 11% of the available resources are used in Poland. Almost 30% of the total hydroelectric potential is already harnessed. An increase of share of energy from renewable resources in the energetic budget of Poland to 7.5% in 2010 and 14% in 2020 is the main, strategic goal resulting from a “Strategy of renewable power industry development” elaborated by the Ministry of Environment.

Poland	
Gross theoretical hydropower potential (GWh/year)	25 000
Technically feasible hydropower potential (GWh/year)	12 000
Economically feasible hydropower potential (GWh/year)	7 000
Installed hydrocapacity (MW)	839
Hydro generation in 2008 (GWh/year)	2 042
% of total production by hydro in 2008 (average)	1.5
Hydro capacity under construction (MW)	~20
Planned hydro capacity (MW)	>406

Source: ”Hydropower and Dams”, World Atlas, 2009

10 largest HEP projects in Poland are shown in table 7.1. Pumped – Storage HEPs have the highest capacity.

Table 7.1 Largest hydroprojects in Poland

No.	Name/ location	River	First year of operation	Turbine power [MW]	Pump power [MW]	Head [m]
1	Zarnowiec	Piasnica	1983	716	800	117
2	Porabka-Zar	Sola	1979	500	540	432
3	Solina	San	1968	200	60	43
4	Wloclawek	Wisla	1970	160,2	-	8,8
5	Zydowo	Radew	1971	156	136	77,4
6	Niedzica	Dunajec	1997	92,8	89	42,2
7	Dychów	Bobr	1936/51*	79,5	30	29,8
8	Roznow	Dunajec	1942	50	-	26,5
9	Koronowo	Brda	1961	26	-	26
10	Tresna	Sola	1967	21	-	20,4

Tunnel Element model is constructed mainly for underground HEP with long tunnel systems and surge facilities. Since the mountain area of Poland is totally covered by national Parks and Natura 2000 Regions, underground HEP investment is limited. Poland considering only run of river projects. It limits further usage of the model to simple cases with short headrace and one surge facility.

Existing powerplants (fig. 7.1) do not include surge facilities.

Figure 7.2 Examples of Hydroelectric projects in Poland

1- Run of river - Brzeg dolny 9.72 [MW]
2- Pumped – Reservoir storage; Solina 200 [MW]
3- Pumped – storage; Zarnowiec 716 [MW]
4- Pumped – storage; Porabka-Zar 500 [MW]

8 OPERATING CURVES

Operating Curves are engineering charts expressing flow parameters as function of the powerplant initial operating conditions.

The Karahnjukar model can be used to produce Operating Curves for the following parameters during station trip:

1. Highest surge level in Holsufs Surge Shaft
2. Highest surge level in Midfell Surge Tunnel
3. Maximal discharge into Jokulsa Tunnel
4. Highest surge level in Jokulsa Tunnel
5. Highest surge level in Ufsarlon Intake Collector
6. Maximal backflow to Ufsarlon Pond

During a station trip the powerplant discharge has a typical profile as shown in figure 8.1

1. Steady operation
2. Valve closing in 10 [s]
3. No flow to powerplant (simulation time is 1 [h])

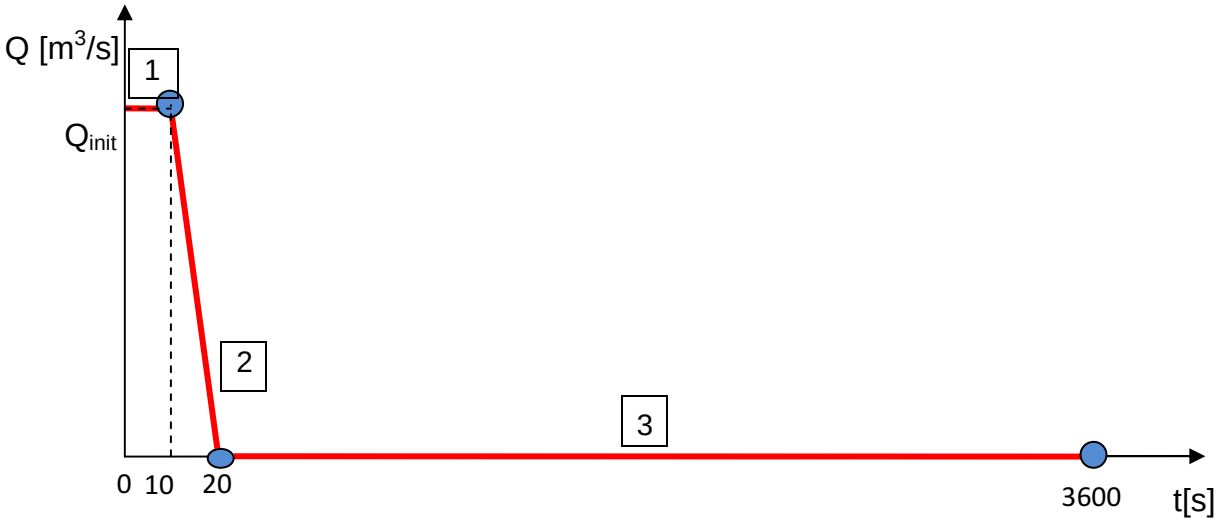

Figure 8.1 Powerplant discharge profile

Table 8.1 Operating Curves Initial Vector parameters				
	Unit	Start	End	Step
Halslon Reservoir water level	[m a.s.l.]	550	625	25
Jokulsa Tunnel Discharge	[m^3/s]	Closed	90	20
Powerplant Discharge	[m^3/s]	80	144	10
Leakage	[1/s]	$2\ 10^{-7}$		

Table 8.2 Jokulsa Discharge parameters		
Jokulsa Tunnel discharge [m3/s]	Ufsarlon Pond water level [m a.s.l.]	Radial Gate opening, elevation of lowest part [m a.s.l]
JVC closed	622	624.3
0	622.1	624.3
10	622.6	624.3
20	623	624.3
30	623.3	624.3
40	623.5	624.3
50	623.8	624.3
60	624	624.3
70	624.2	624.3
80	624.4	624.3
90	625	626.25

8.1 Highest surge level in Holsufs Surge Shaft

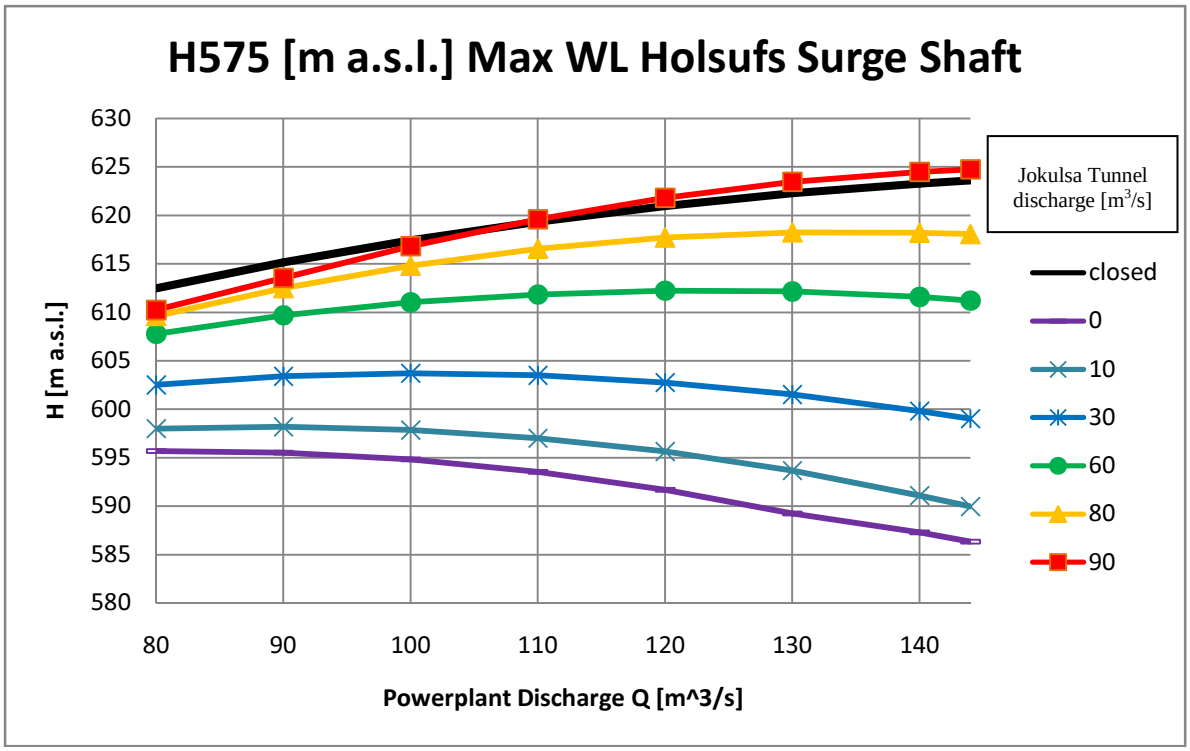

Figure 8.2 Maximal water level in Holsufs Surge Shaft; Halslon Reservoir 575[m a.s.l.]

Holsufs Surge Shaft Spill characteristics (fig 8.2) are nonlinear for Halslon Reservoir wl. 575 [m a.s.l.]. The most favorable surge characteristics are for open JVC and no JT discharge. The highest surge is expected for closed JVC. No overspill is expected during the powerplant operation with HR wl. 575 [m a.s.l.] . Maximal surge level decreases with increasing powerplant discharge due to HSS initial wl.; the highest powerplant discharge the lower HSS initial wl.

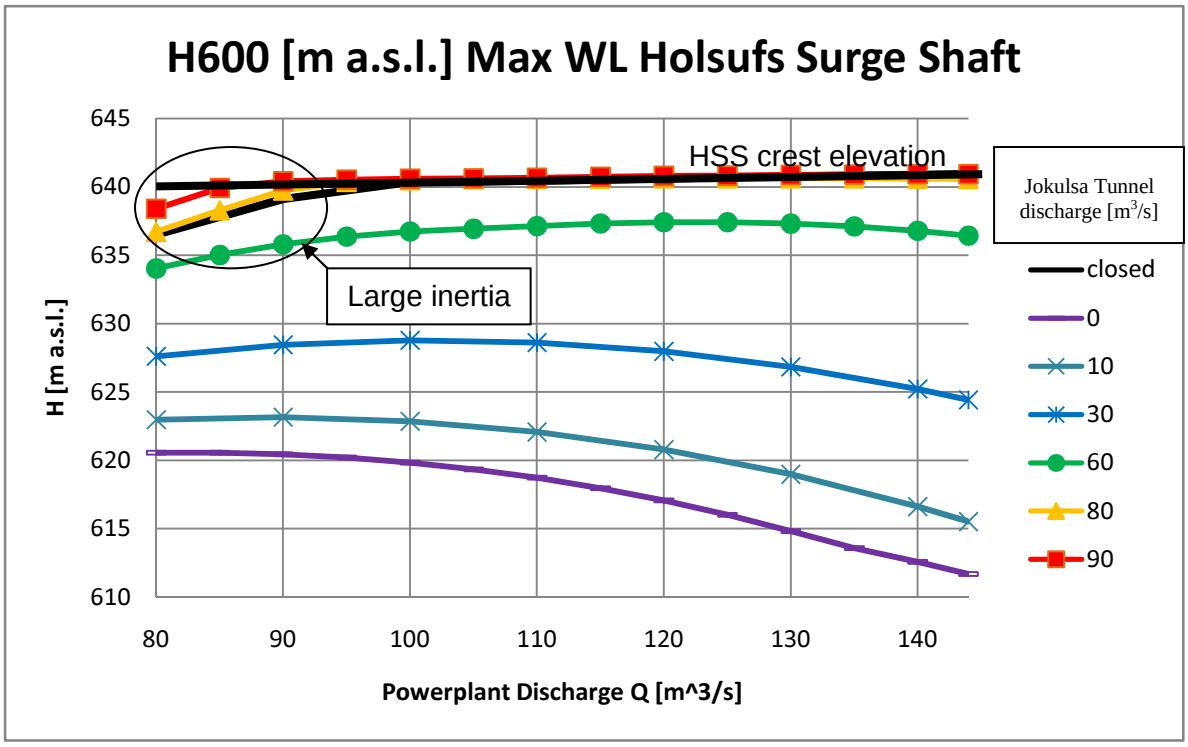

Figure 8.3 Maximal water level in Holsufs Surge Shaft; Halslon Reservoir 600 [m a.s.l.]

If Jokulsa Tunnel discharge is over 65 [m^3/s] it causes spill out as shown in figure 8.3. JT discharge above 80 [m^3/s] indicates higher surge than for JVC closed due to large JT inertia acting opposite to HRT backflow and chocking up the valve. Due to the inertia JT feeds HRT even for several seconds after the powerplant trip.

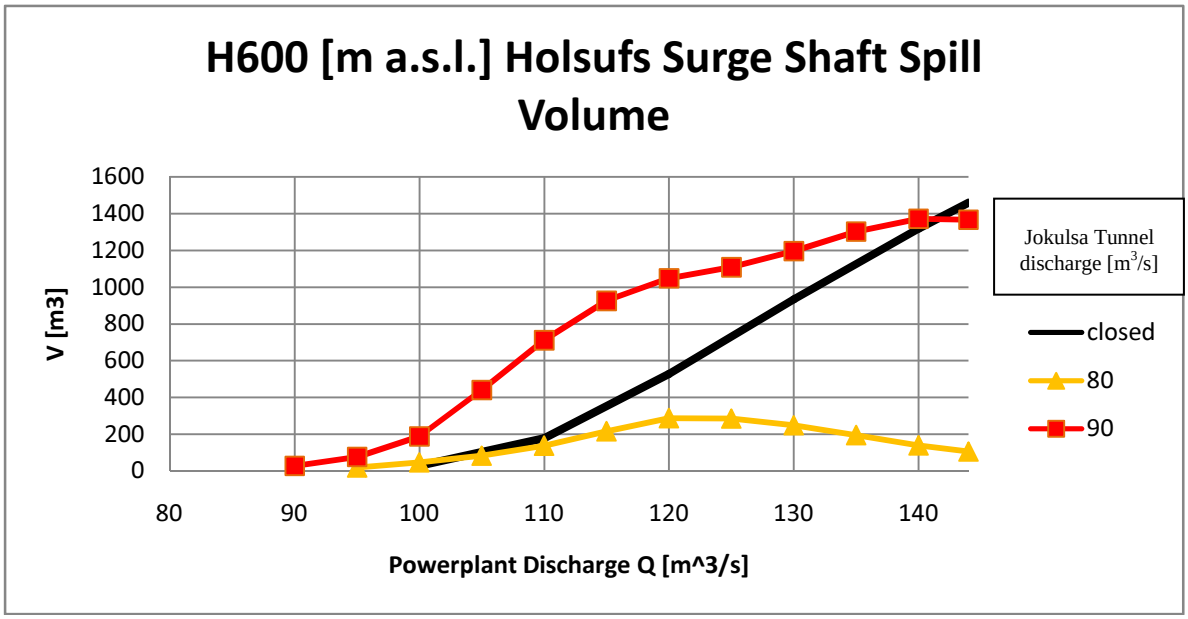

Figure 8.4 Maximal Holsufs Surge Shaft Spill Volume; Halslon Reservoir 600 [m a.s.l.]

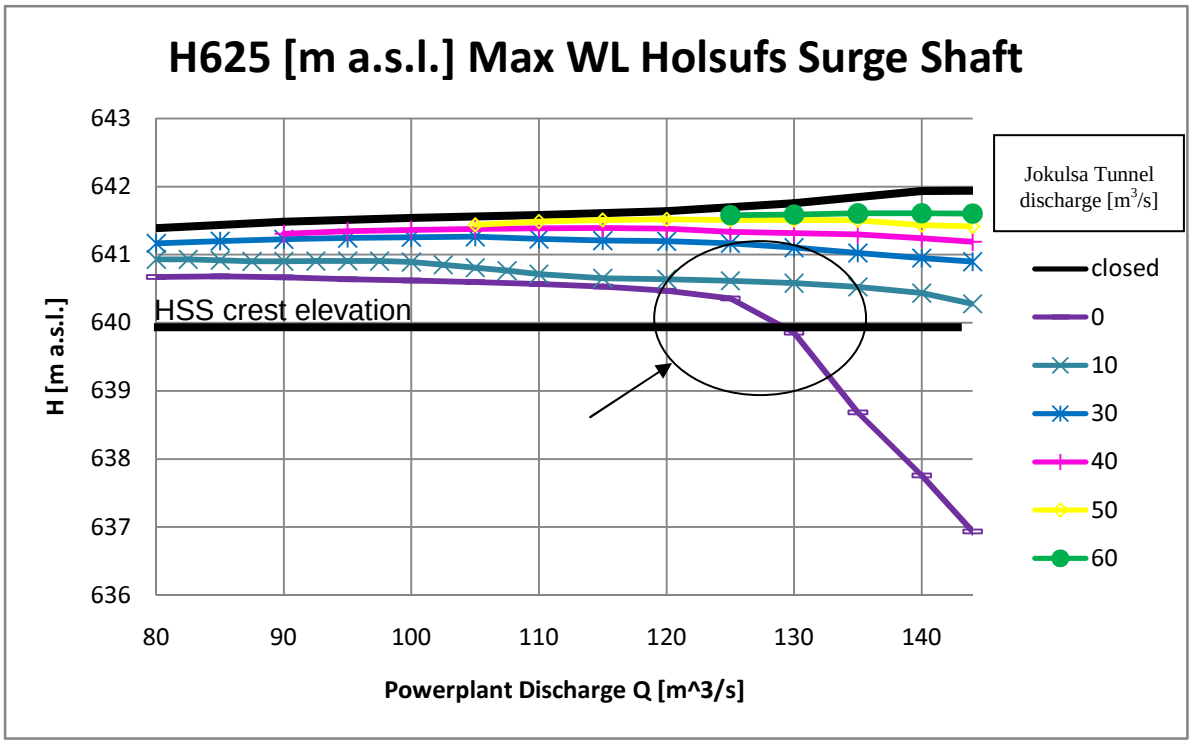

Figure 8.5 Maximal water level in Holsufs Surge Shaft; Halslon Reservoir 625 [m a.s.l.]

Overspill (fig 8.5) is expected for all JT discharge range for HR wl. 625 [m a.s.l.]. For no JT discharge, above powerplant discharge 125 [m^3/s], the curve bends down due to JT transient from fully pressurized to the free surface flow. The initial JT wl. for high powerplant discharge and no JT discharge is below 608 [m a.s.l.]. Hence there is relatively small inertia in JT acting against backflow due to surge, so JT can acts as additional surge tunnel reducing surge in MST and HSS. The maximum spill volume (fig 8.6) through HST is 8020 [m^3] and is close to the designed volume 10000 [m^3] [5].

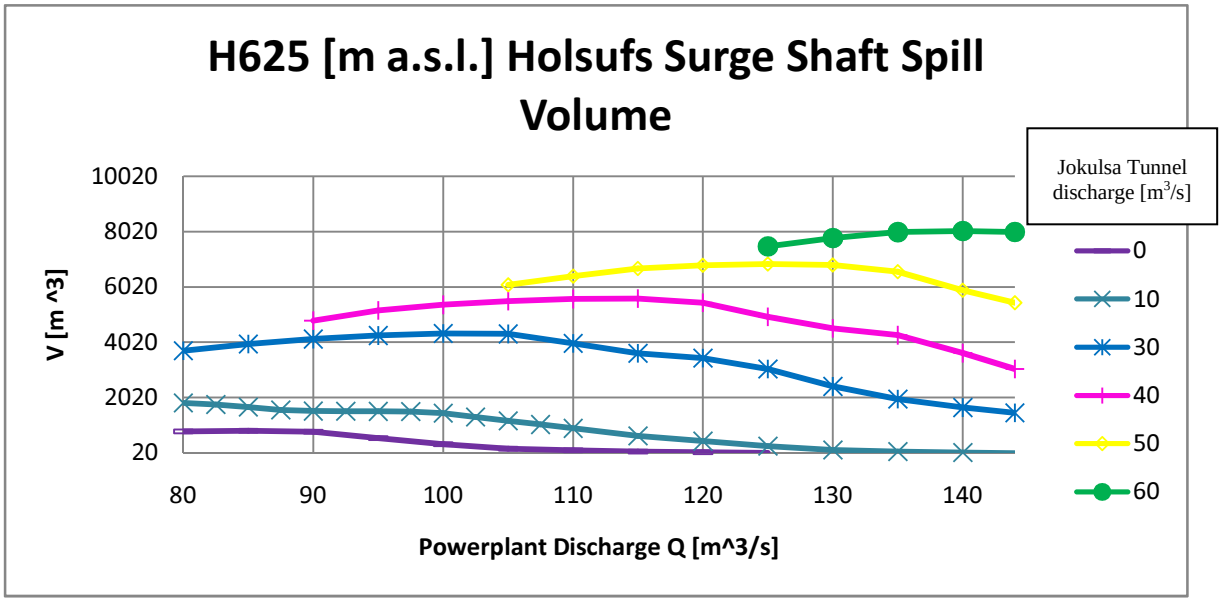

Figure 8.6 Maximal Holsufs Surge Shaft Spill Volume; Halslon Reservoir 625 [m a.s.l.]

8.2 Highest surge level in Midfell Surge Tunnel

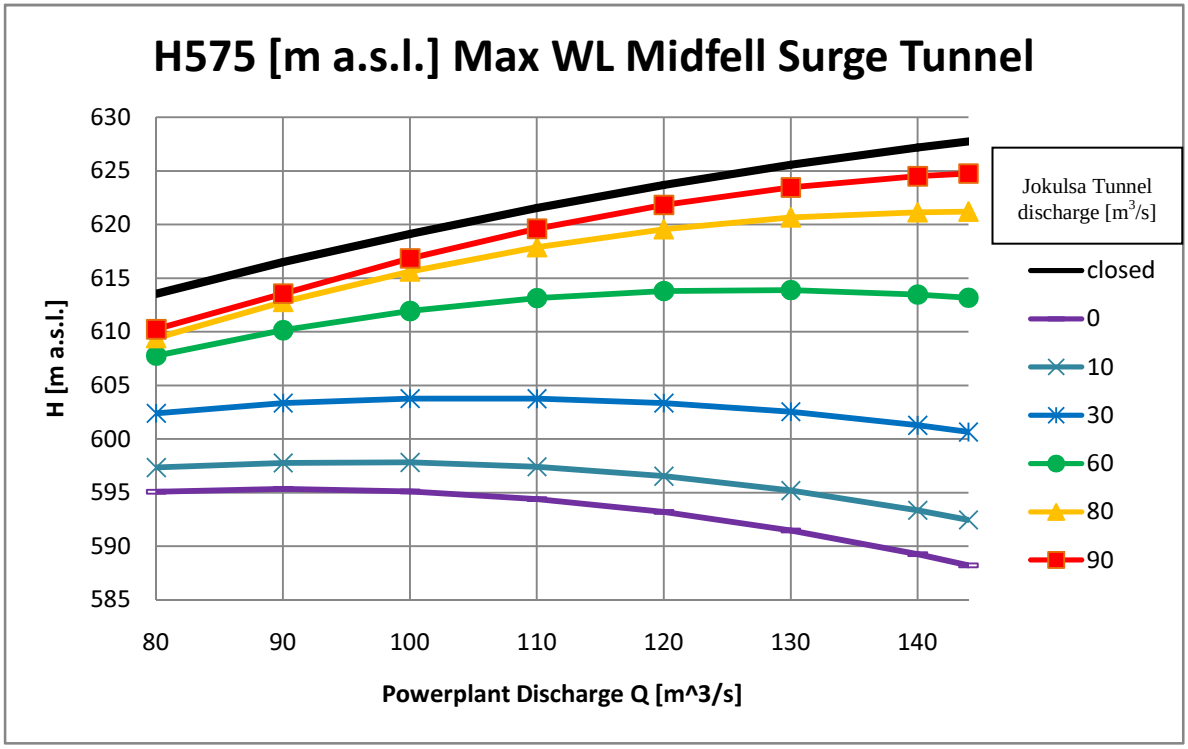

Figure 8.7Maximal water level in Midfell Surge Tunnel; Halslon Reservoir 575 [m a.s.l.]

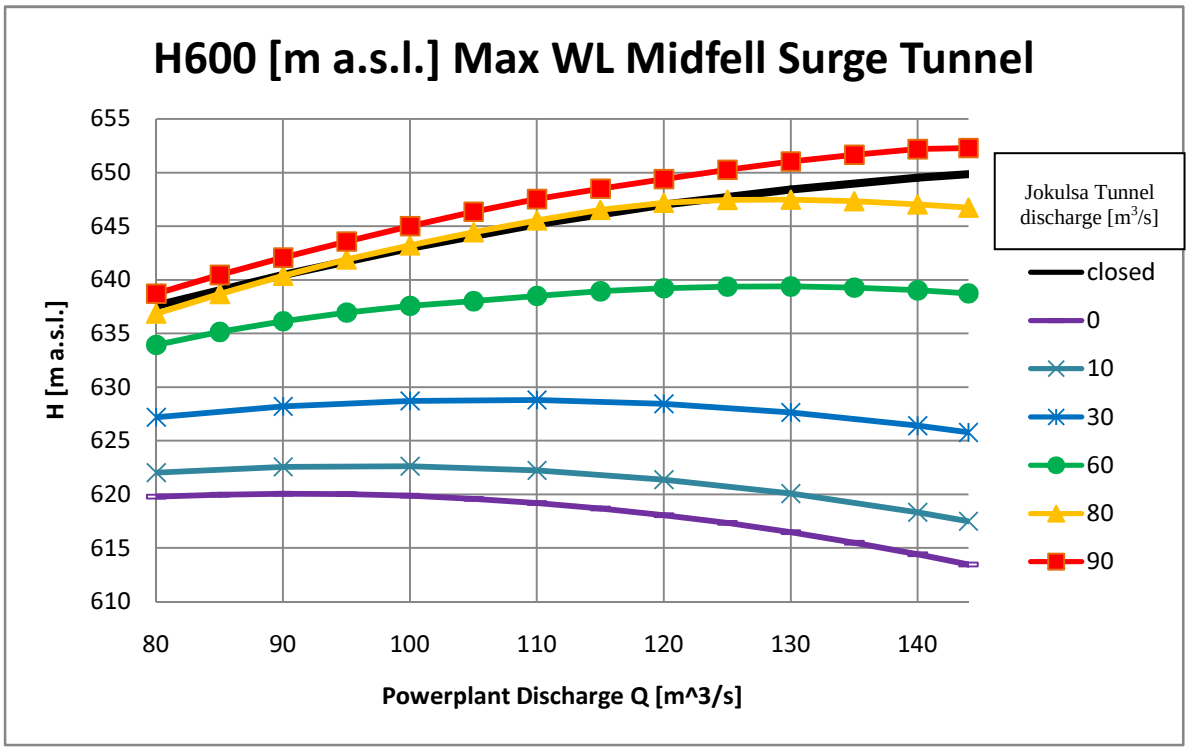

Figure 8.8 Maximal water level in Midfell Surge Tunnel; Halslon Reservoir 600 [m a.s.l.]

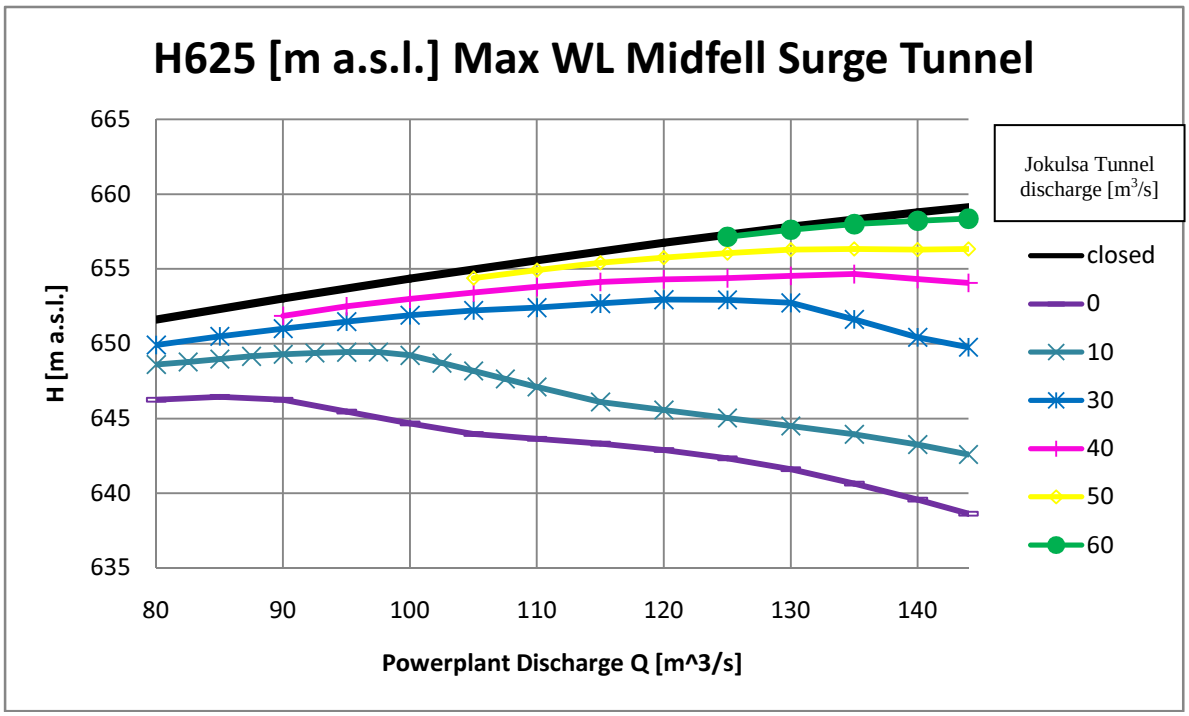

Figure 8.9 Maximal water level in Midfell Surge Tunnel; Halslon Reservoir 625 [m a.s.l.]

8.3 Maximum discharge into Jokulsa Tunnel

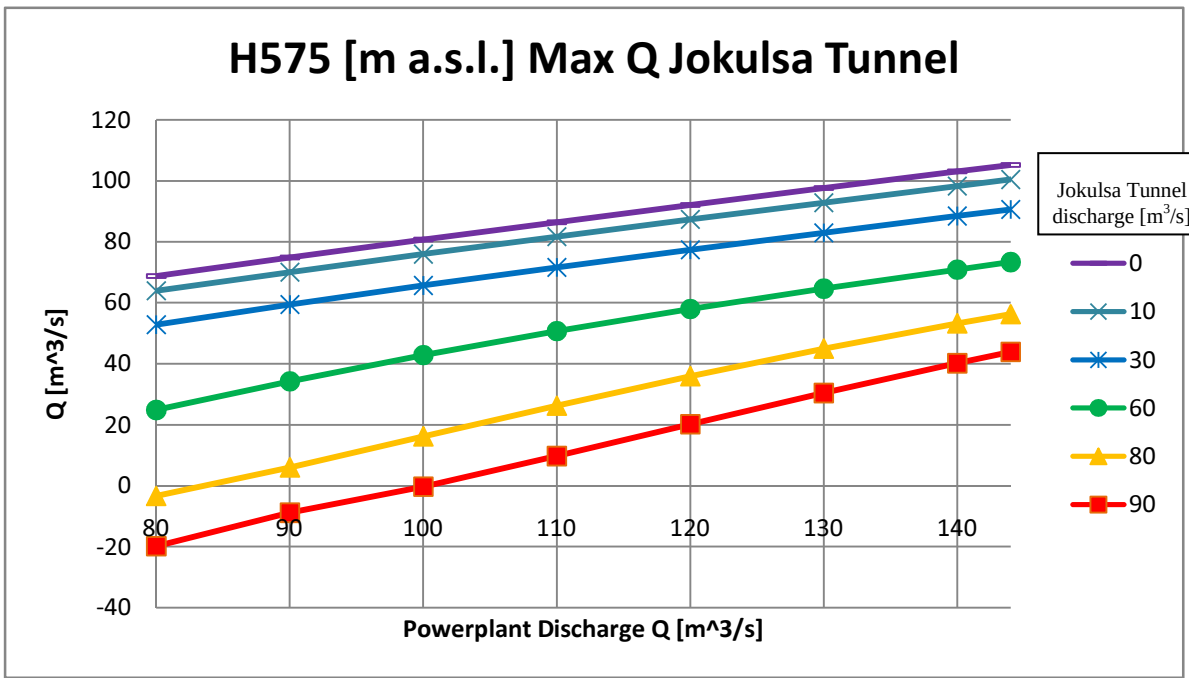

Figure 8.10 Maximal discharge to Jokulsa Tunnel; Halslon Reservoir 575 [m a.s.l.]

JT discharge characteristics (fig 8.10) are linear for HR wl. 575 [m a.s.l.]. The positive discharge value (vertical axis) indicates JT backflow. The backflow for JT discharge below 10 [m^3/s] and the powerplant discharge higher than 135 [m^3/s] is expected to exceed maximal flow for JT butterfly valve [6].

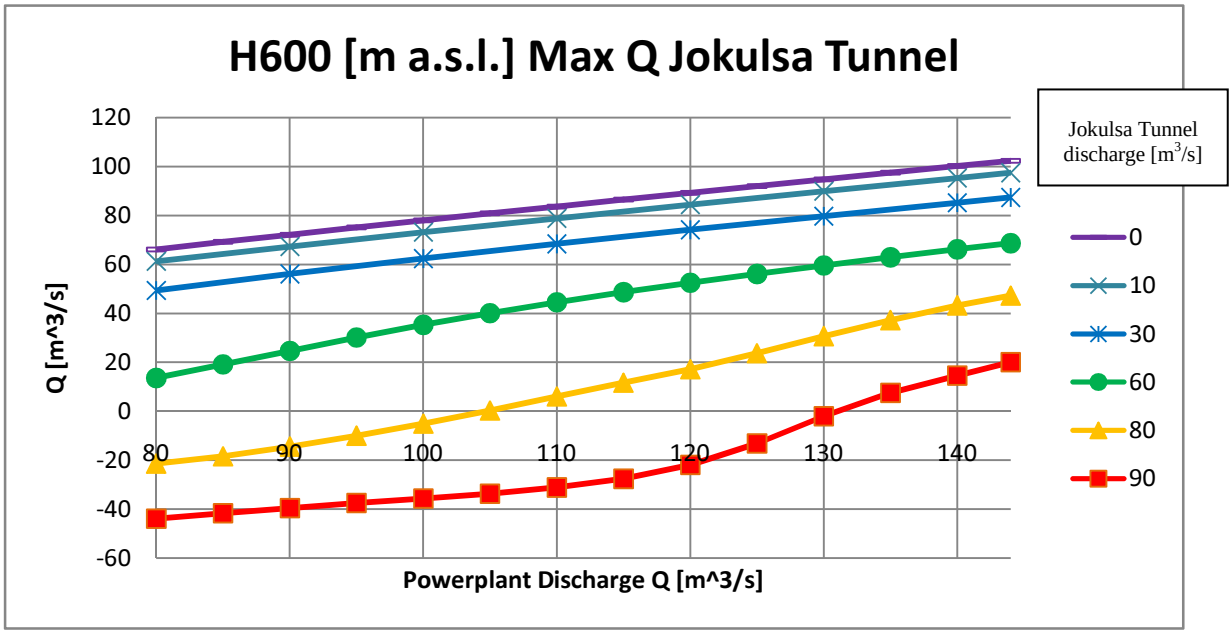

Figure 8.11 Maximal discharge to Jokulsa Tunnel; Halslon Reservoir 600 [m a.s.l.]

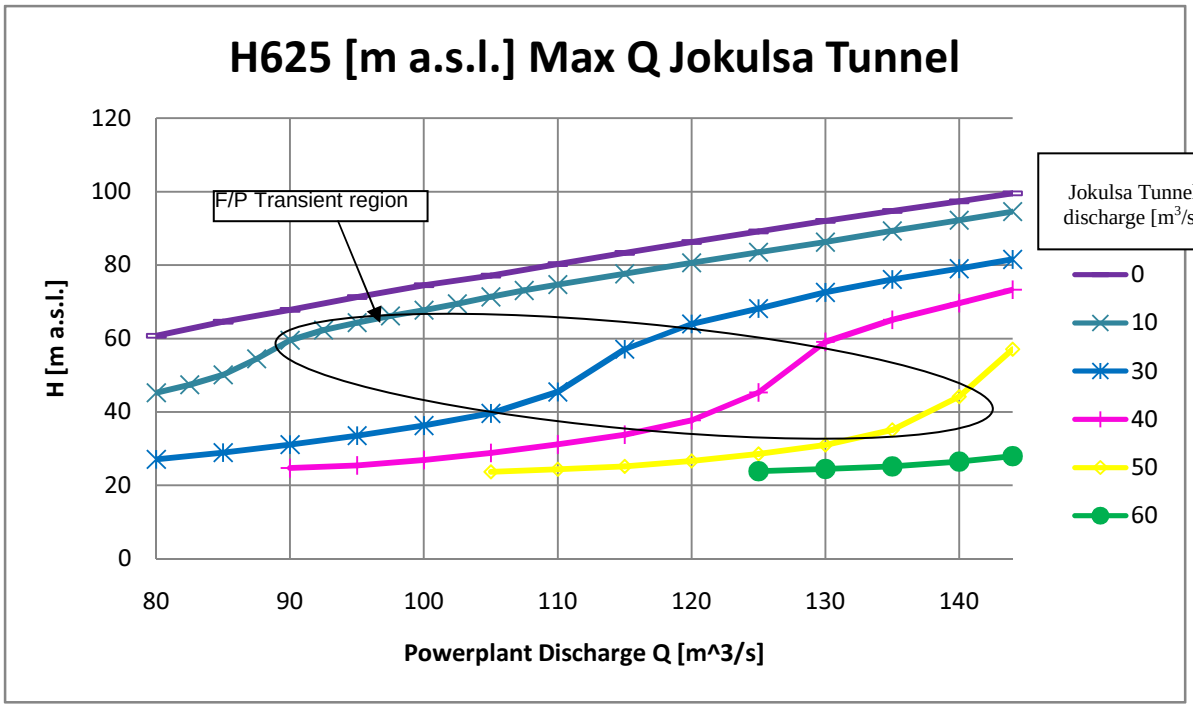

Figure 8.12 Maximal discharge to Jokulsa Tunnel; Halslon Reservoir 625 [m a.s.l.]

JT discharge characteristics are strongly nonlinear for HR wl. 625 [m a.s.l.] due to JT transient free surface/fully pressurized region marked in figure 8.12.

8.4 Highest surge level in Jokulsa Tunnel and Jokulsa Surge Tunnel

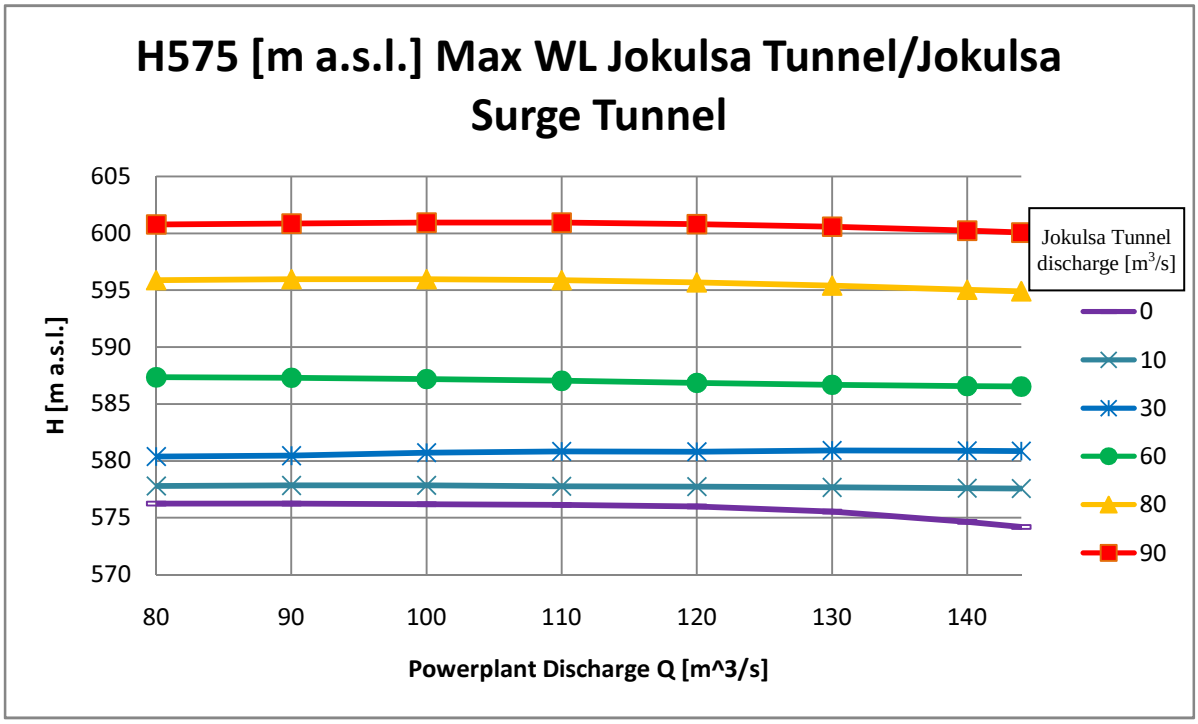

Figure 8.13 Maximal water level in Jokulsa Tunnel/Jokulsa Surge Tunnel; Halslon Reservoir 575 [m a.s.l.]

JT surge is almost independent from the powerplant discharge for HR wl. 575 [m a.s.l.] due to maximal JT wl. achieved for steady flow after the trip. Maximal surge level is expected for JT discharge 90 [m^3/s] as shown in figure 8.13.

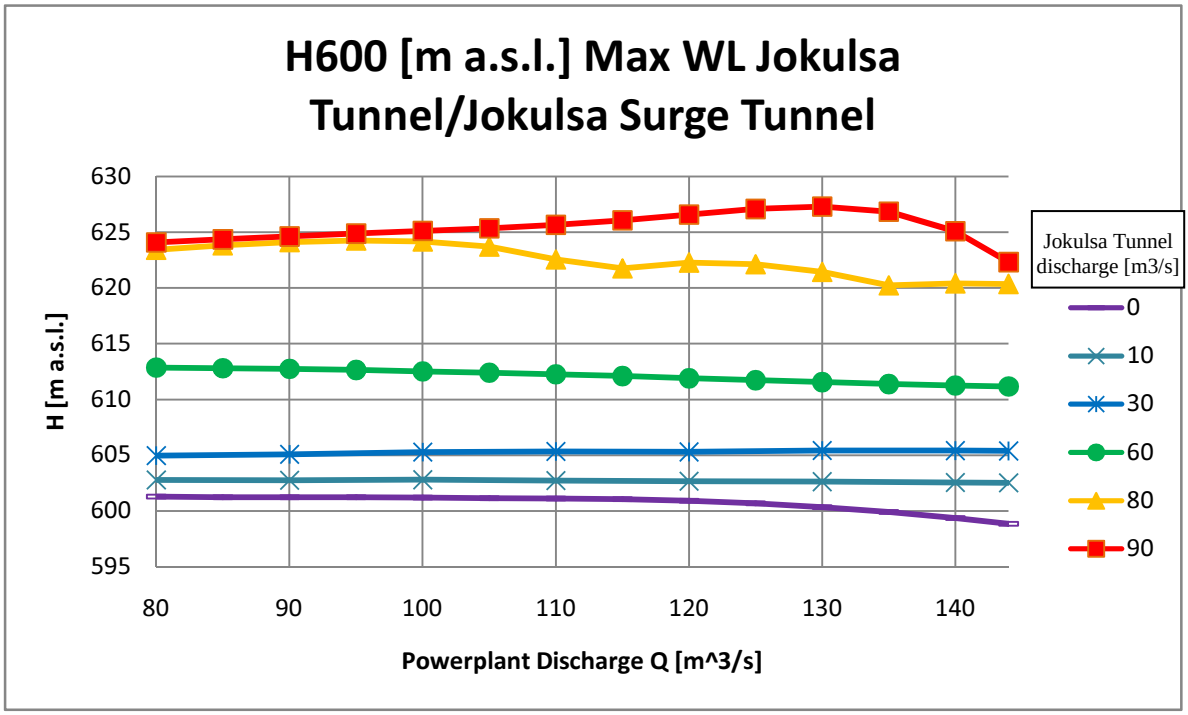

Figure 8.14 Maximal water level in JT/JST; Halslon Reservoir 610 [m a.s.l.]

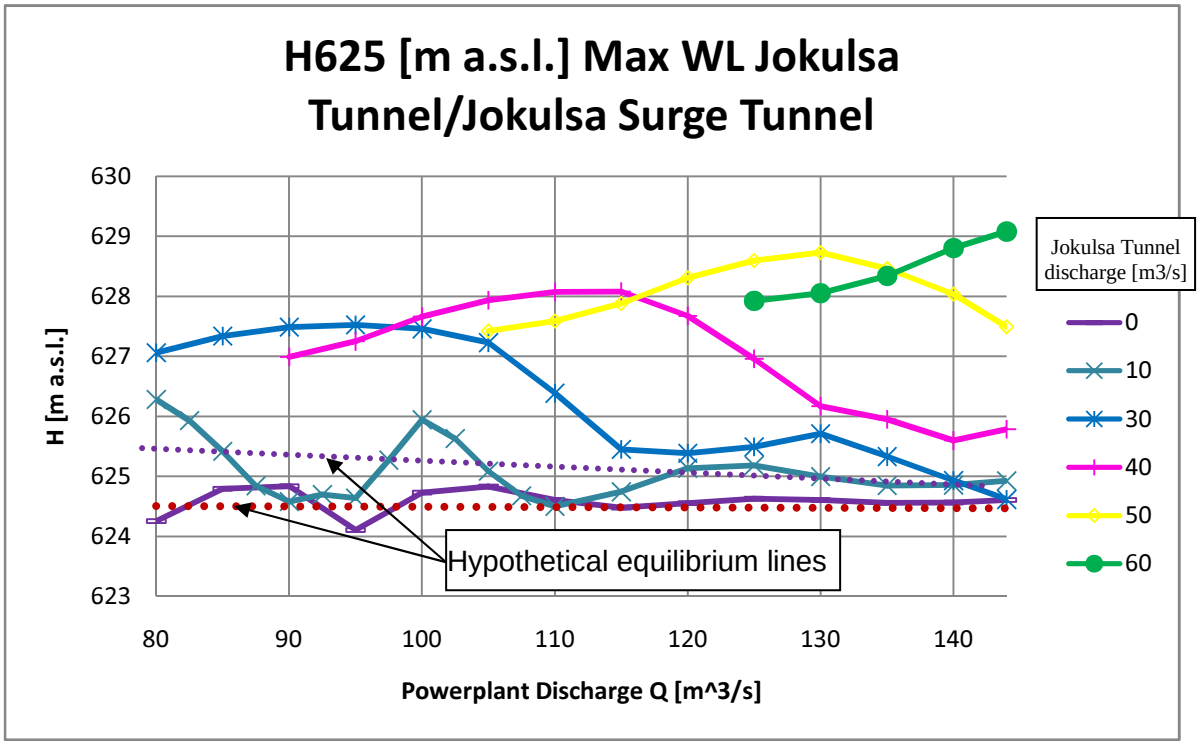

Figure 8.15 Maximal water level in JT/JST; Halslon Reservoir 625 [m a.s.l.]

JT surge characteristics shown in figure 8.15 are strongly nonlinear due to JT transient free surface/fully pressurized region. The model indicates unexpected deviation from the hypothetical equilibrium lines for JT discharge below 10 [m^3/s]. Since the initial JT wl. for the cases is slightly above 608 [m a.s.l.] – the worst defined region, the oscillations may occur due to model instability. This phenomenon should be further investigated.

8.5 Highest surge level in Ufsarlon Intake Collector

Since JT surge level does not exceed 608 [m a.s.l.] for HR wl. 575 [m a.s.l.], the UIC characteristics cannot be calculated for that case.

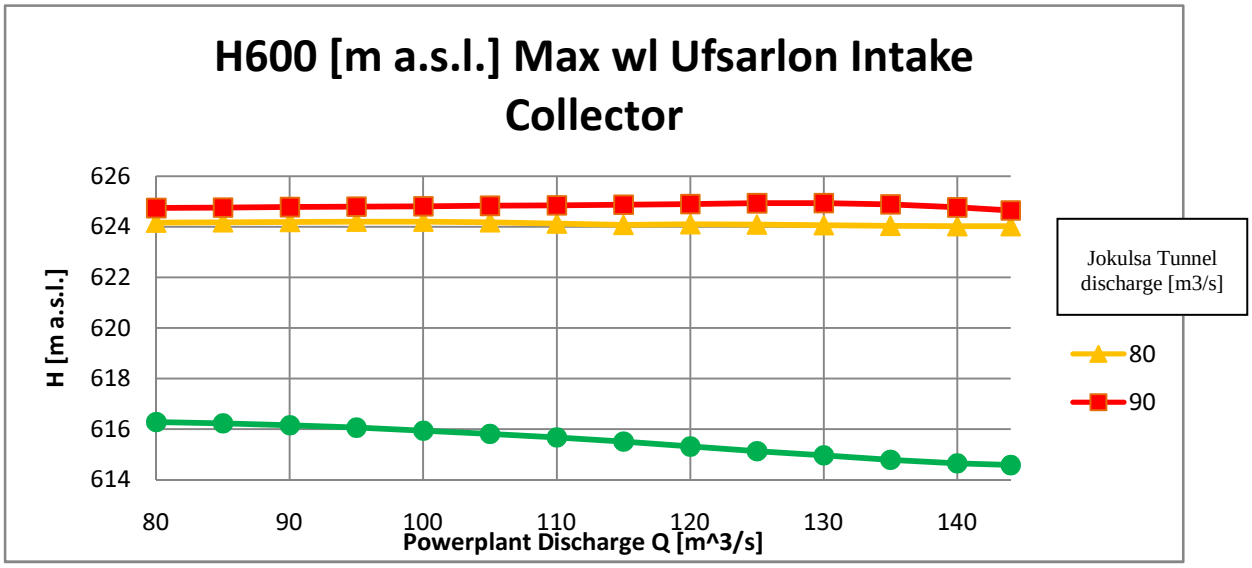

Figure 8.16 Maximal water level in UIC; Halslon Reservoir 600 [m a.s.l.]

UIC surge characteristics become linear for JT discharge above 60 [m^3/s] as shown in figure 8.16. The highest surge level is expected for JT discharge 90 [m^3/s]. UIC surge level increases with JT discharge and reaches maximal wl. for JT discharge 60 [m^3/s] as shown in figure 8.17.

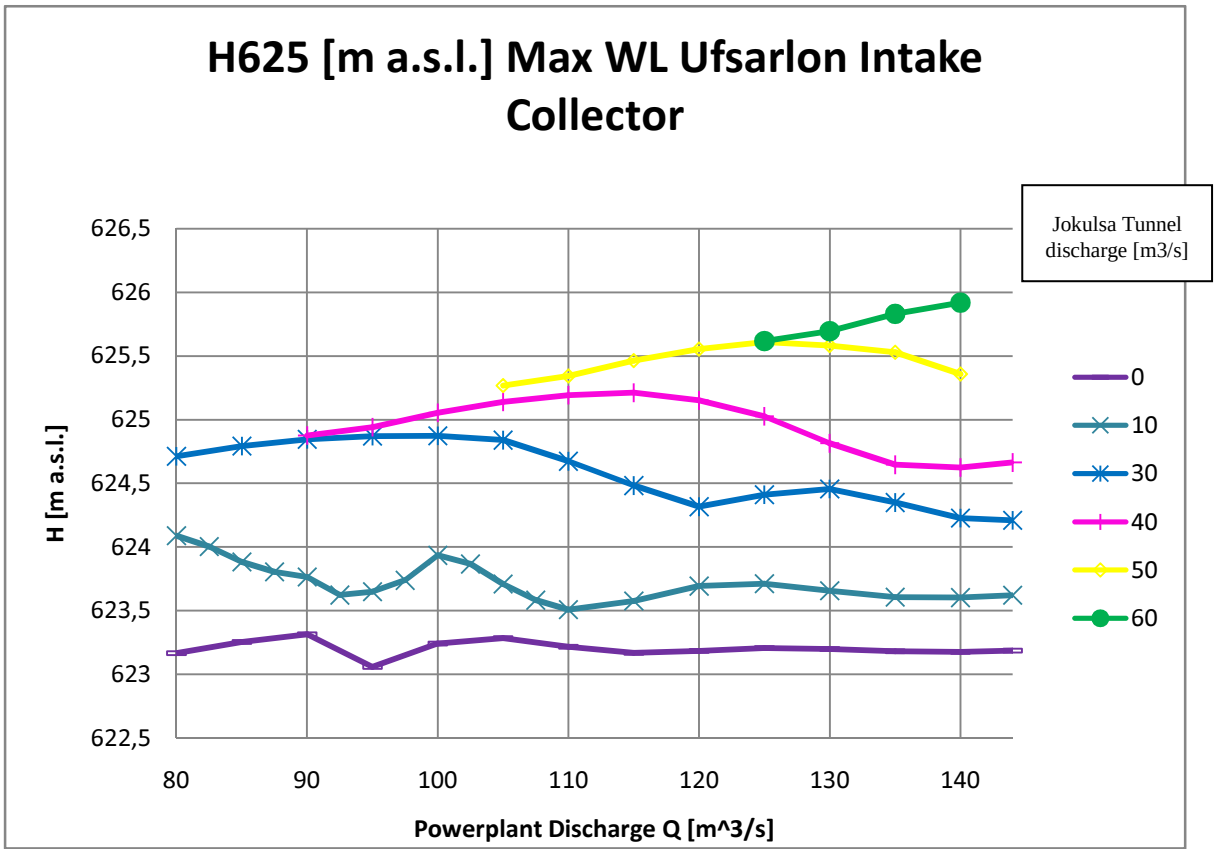

Figure 8.17Maximal water level in UIC; Halslon Reservoir 625 [m a.s.l.]

8.6 Maximal backflow to Ufsarlon Pond

According to chapter 3.7, backflow to Ufsarlon Pond can occur only when wl. in UIC exceeds UP wl. Figure 8.18 shows maximal backflow to UP which is expected for JT discharge 60 [m^3/s] and powerplant discharge 144 [m^3/s]. The UP backflow characteristics are similar to corresponding JT/JST surge and UIC wl. operation charts due to P/F transient determining flow pattern in upper JT.

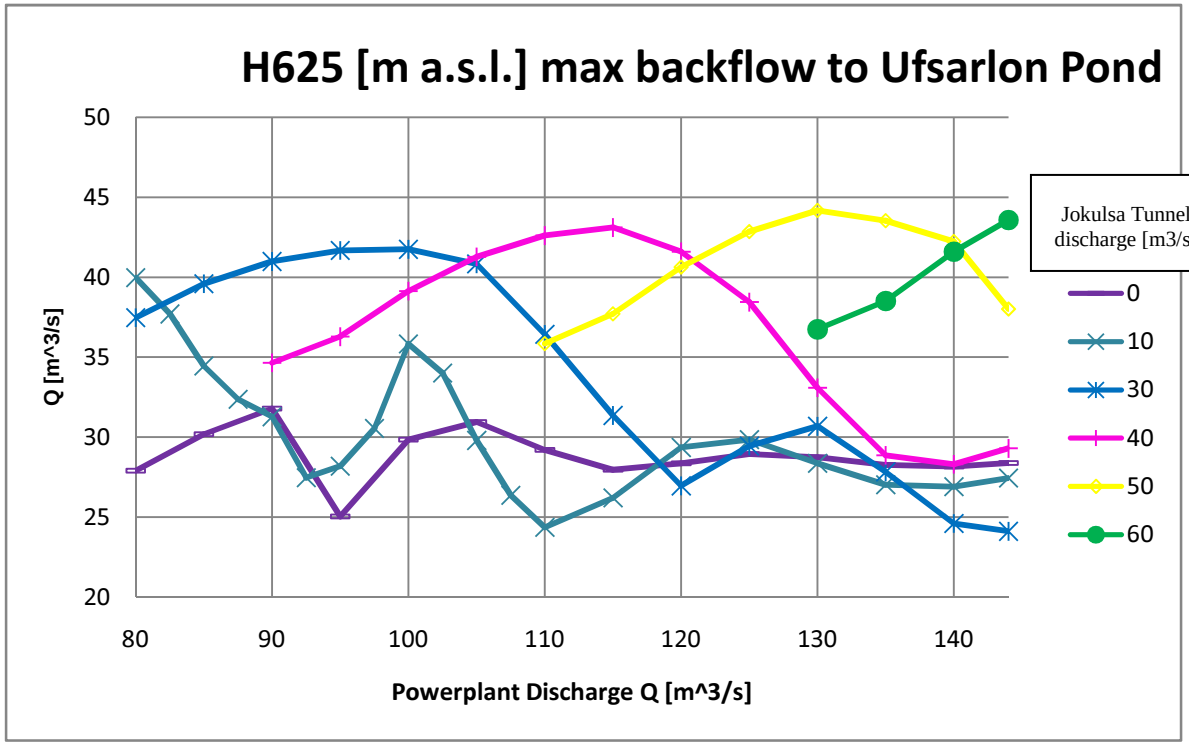

Figure 8.18 Maximal backflow to Ufsarlon Pond; Halslon Reservoir 625 [m a.s.l.]

9 CONCLUSIONS

The transient modeling method introduced here is an effective way of surge calculation. The method is capable of modeling vast amount of hydraulic waterway systems with specific phenomena occurring like overspill and throttling. It is possible to automate the process of equations system building using Guided User Interface.

Surge characteristics of Karahnjukar HEP are nonlinear due to complex geometry and various flow conditions. Geometry of Jokulsa Tunnel – Inverted Siphon – Jokulsa Surge Tunnel Junction and Free Surface/Fully Pressurized transient has significant influence on the flow in JST and UIC. That part is the most "nonlinear" section and needs further investigation.

Midfell Surge Tunnel geometry has significant influence on surge period due to big volume. On the other hand, Holsufs Surge Shaft has small influence on period but due to overspill it modifies significantly surge transient.

Since Tunnel Element method does not consider water compressibility and is based on simplified geometry, the accuracy of the results may be estimated as ±10%

Leakage from the tunnel system acts as a damper and has significant influence on transients, further studies on the phenomenon are recommended.

Since the model does not include waterhammer effect it is necessary to estimate its influence on surge characteristics.

TE method would be the most beneficial for Polish Oil and Gas industry.

10 FURTHER DEVELOPMENT

Program development:

- Improvement of tunnel elements distribution along waterways;
- Improvement of Jokulsa Tunnel – Inverted Siphon – Jokulsa Surge Tunnel junction formulation;
- Investigation of Midfell Surge Tunnel geometry;
- Introduction of variable geometry tunnel elements;
- Introduction of complex post process statistics – fitting, period, amplitude, damping;
- Application of waterhammer effect;
- GUI interface.

Further cases:

- Investigation of waterways leakage;
- Investigation of natural frequencies and dangerous operation;
- Response for variable discharge profile.

11 BIBLIOGRAPHY

1. Baumann A., “Internal Memo – Evaluation of the trip of units nos. 3, 4, 5 and 6 on December 13, 2007”, KEJV 2008
2. Baumann, A., Tomasson, G.G, “Free surface and pressurized flow regimes in a large water conveyance tunnel: The case of the Jökulsá Tunnel for the Kárahnjúkar HEP in Iceland” Hydro 2007 conference paper
3. Chaudhry M. H., “Applied Hydraulic Transients”, Litton Educational Publishing, Canada 1979
4. Hakonardottir K. M., “Karahnjukar waterways - roughness measurements and head loss calculations– Revised Report”, p. 47; Iceland 2009
5. Leifsson Þ. S., Kaelin J., “Karahnjukar Hydroelectric Project - Waterways Operation Manual, Revision 1”, Landsvirkjun, Iceland 2009
6. Leifsson Þ. S., Baumann A., “Asymmetric sudden enlargement energy dissipater in Jokulsa Tunnel of the Karahnjukar HEP in Iceland”, HYDRO 2010 conference paper
7. Lysne K. D., Glover B. “Hydraulic Design”, Norwegian University of Science and Technology, Norway 2003
8. Petry, B., Baumann, A., Tomasson, G.G., “Control of hydraulic transients in the power waterways of the Karahnjukar HEP in Iceland: Design challenges and solutions”, KEJV, Iceland 2006
9. Tomasson G. G., Baumann A., “Headrace tunnel KAR-14. Jökulsá tunnel KAR-21. Design Report on Hydraulic Transients. Revised report April 2007”, Landsvirkjun, Iceland 2007
10. Wylie E. B., V. L. Streeter, “Fluid Transients”, McGraw-Hill Inc, USA 1978
11. Matlab Manual – www.matlab.com
12. Shampine, L. F., Reichelt M. W., "The MATLAB ODE Suite," SIAM Journal on Scientific Computing 1997, Vol. 18 pp 1-22
13. Shampine, L. F., Reichelt M. W., Kierzenka J.A., "Solving Index-1 DAEs in MATLAB and Simulink," SIAM Review 1999, Vol. 41 pp 538-552

Appendix 1. Model formulation scheme

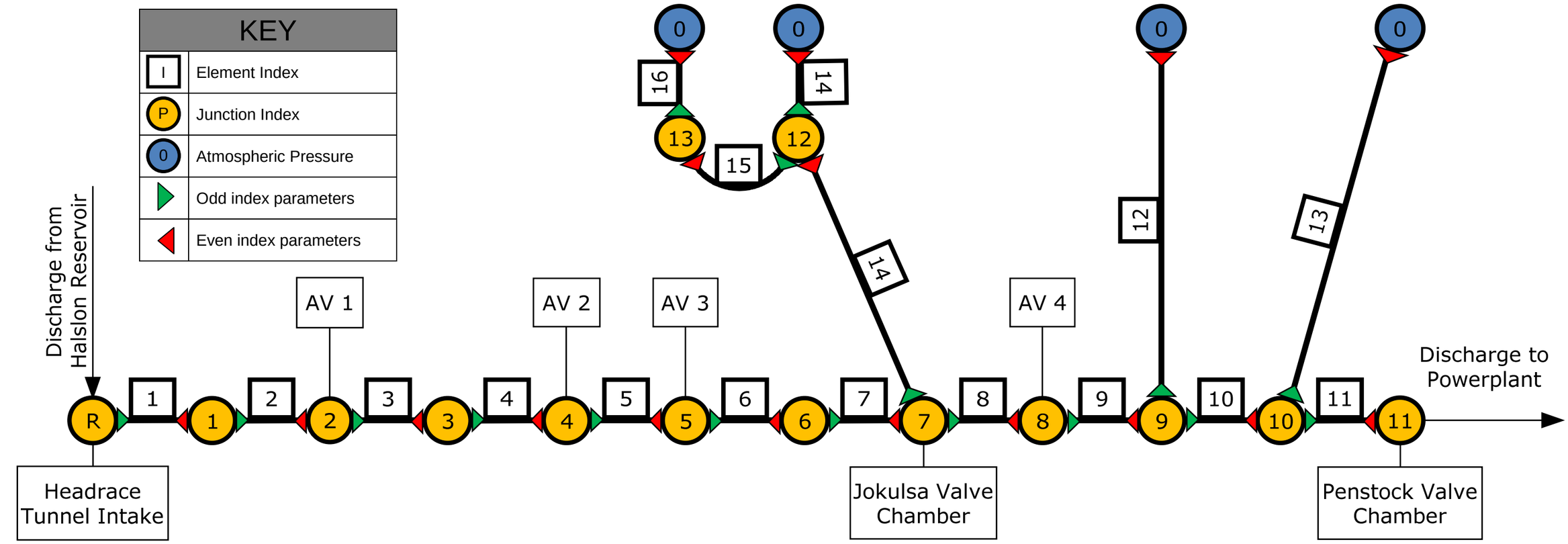

Element index	Elevation 1	Elevation 2	Length	Area	Specific friction coefficient	Local head loss coefficient	Element head loss	Equivalent Diameter	Section	Part	Comment
	El1	El2	L	A	k_f	k_l	hl	D			
	[m a.s.l]	[m a.s.l]	[m]	[m^2]	$\left[\frac{m}{m}\left(\frac{m^3}{s}\right)^{-2}\right]$	$\left[m\left(\frac{m^3}{s}\right)^{-2}\right]$	[m]	[m]			
1	528.1	529.6	1011.1	36.30	8.62E-08	0	1.81*	6.8	D&B 7.2 H.1-H.14	Headrace Tunnel	
2	529.6	523.3	1119.0	52.40	1.08E-07	0	2.50*	8.17	D&B 7.2 H.14-H.14-9	Headrace Tunnel	
3	523.3	493.8	5198.0	40.36	1.01E-07	0	10.89*	7.17	TBM3 7.2 H.14.9-H.16	Headrace Tunnel	
4	493.8	492.9	159.0	57.52	8.53E-08	0	0.28*	8.56	D&B 7.6 H.16-H.16-9	Headrace Tunnel	
5	492.9	507.9	6733.0	40.36	8.85E-08	0	12.35*	7.17	TBM3 7.2 H.16-9 H.21-9	Headrace Tunnel	
6	507.9	461.0	8946.0	40.36	9.21E-08	0	17.08*	7.17	TBM2 7.2 H.21-HA.2.9-0	Headrace Tunnel	
7	461.0	460.2	254.0	49.24	1.31E-07	0	0.69*	7.92	D&B 7.2 HA.2.9-0-H.J	Headrace Tunnel	
8	460.2	465.6	1075.0	57.52	8.27E-08	0	1.84*	8.56	D&B 7.6 H.J-H.30-1	Headrace Tunnel	
9	465.6	437.6	12161	44.98	6.18E-08	0	15.58*	7.57	TBM1 7.6 H.30-1-HSS 1.9	Headrace Tunnel	
10	437.6	430.2	2712.5	50.74	8.79E-08	0	4.94*	8.04	D&B 8 HSS 1.9 HS1.9-9	Headrace Tunnel	
11	430.2	429.8	182.45	41.83	8.79E-08	0	0.33*	7.3	D&B 8 HS1.9-9 - av(H.34, H.35)	Headrace Tunnel	
12	437.58	640	202.42	18.09	0	3.58E-03	74.27*	4.8	HSS	Holsufs Surge Shaft	
13	430.22	668.00	1668.45	variable	variable	variable	31.65*	variable	HST	Midfell Surge Tunnel	
14	460.18	608+ El1'(Q)	~10541.1	variable	variable	variable	10,6**	variable	JT	Jokulsa Tunnel	
15	608	607.85	2950.00	36.51	3.26E-07	0	7.8**	6.82	D&B 6 F.1 - F.30	Inverted Siphon	
16	607.85	630	22.15	variable	0	0	0	-	JIC	Intake Collector	
17	608+ El1'(Q)	637	~68.53	variable	0	0	0	-	JST	Jokulsa Surge Tunnel	

*Head loss calculated for flowrate Q=90 $\left[\frac{m^3}{s}\right]$; * *Head loss calculated for flowrate Q=90 $\left[\frac{m^3}{s}\right]$

Appendix 2. Upper Joulsa Tunnel Surge development for Halslon Reservoir 600 [m a.s.l.] and Jokulsa Tunnel Discharge 80 [m3/s]

Powerplant discharge 105 [m3/s]	Powerplant discharge 110 [m3/s]	Powerplant discharge 115 [m3/s]	Powerplant discharge 120 [m3/s]	Powerplant discharge 125 [m3/s]
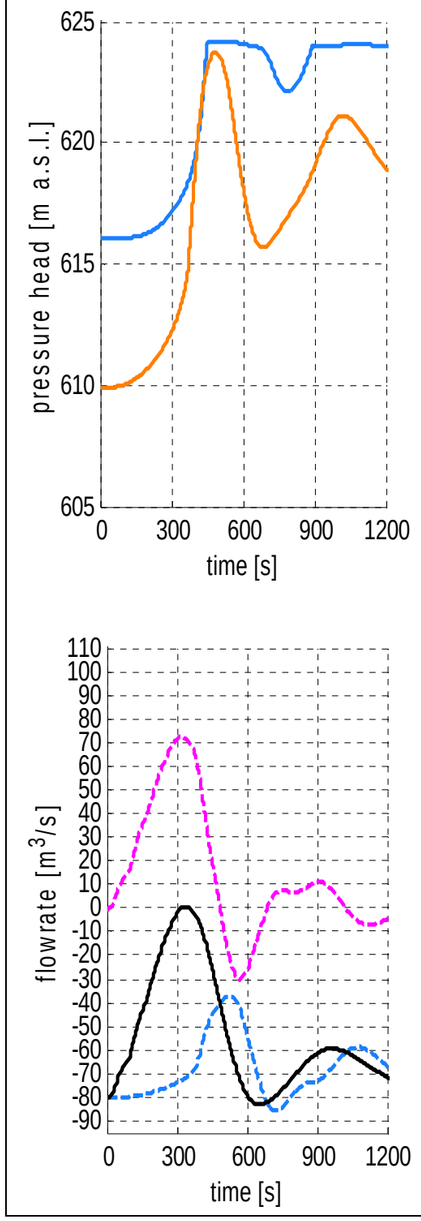	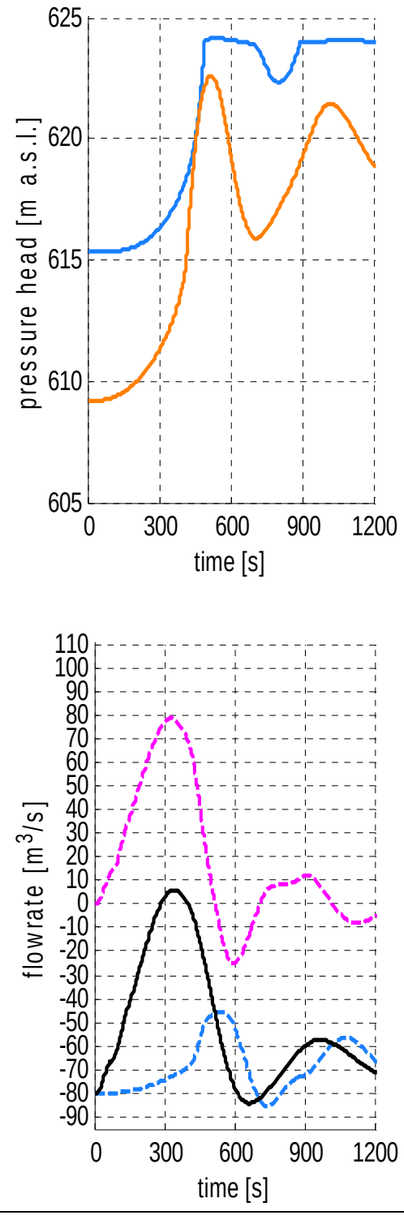	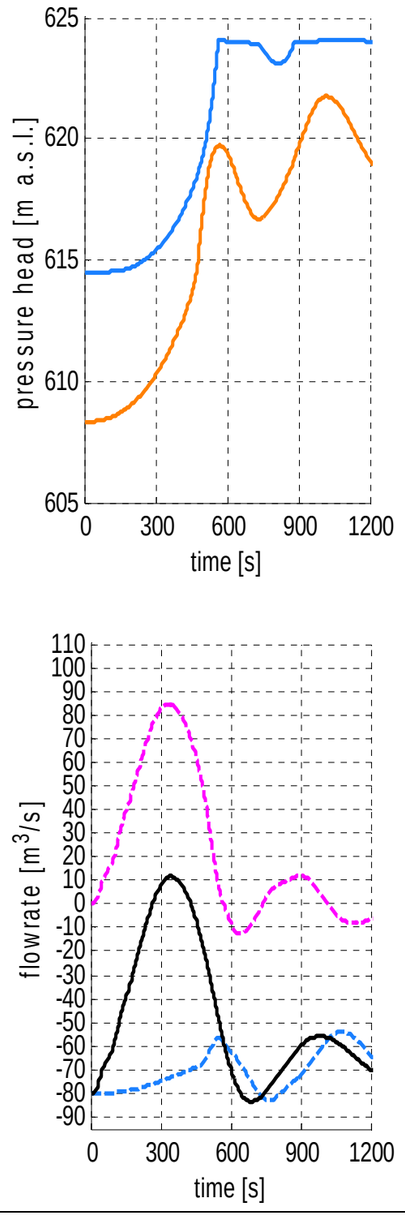	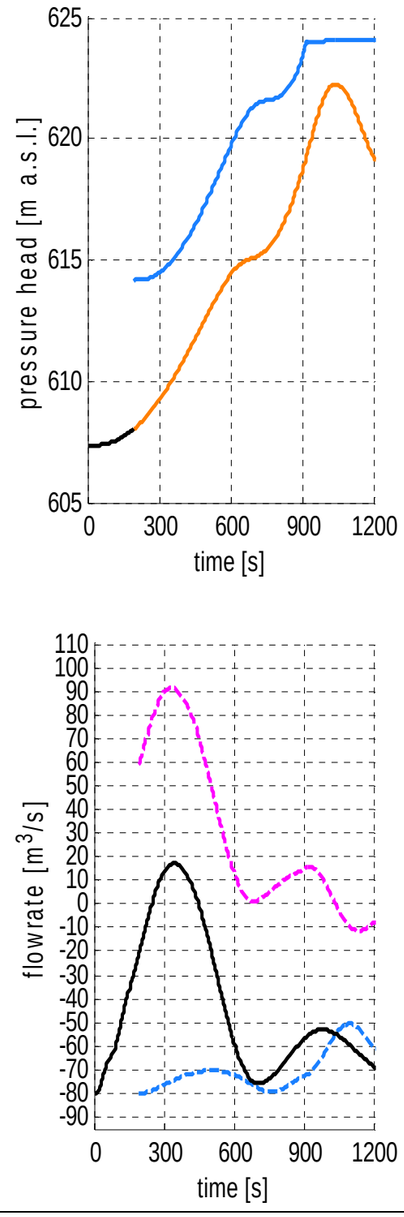	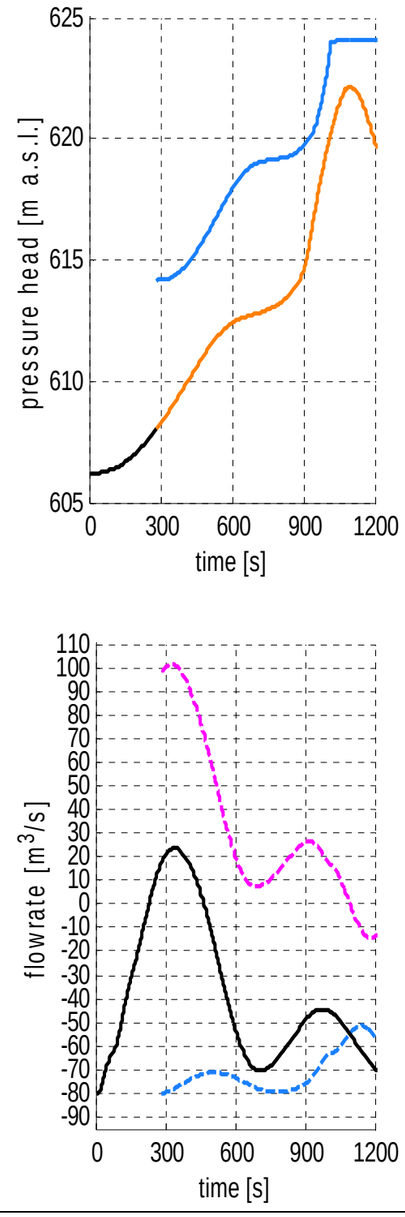

Appendix 3 Upper Joulsa Tunnel Surge development for Halslon Reservoir 625 [m a.s.l.] and Jokulsa Tunnel Discharge 10 [m3/s]

Powerplant discharge 80 [m3/s]	Powerplant discharge 85 [m3/s]	Powerplant discharge 90 [m3/s]	Powerplant discharge 95 [m3/s]	Powerplant discharge 100 [m3/s]